

OCEAN DRILLING PROGRAM

LEG 208 SCIENTIFIC PROSPECTUS

**EARLY CENOZOIC EXTREME CLIMATES:
THE WALVIS RIDGE TRANSECT**

Dr. James Zachos
Co-Chief Scientist
Earth Science Department
University of California, Santa Cruz
Santa Cruz CA 95064 USA

Dr. Dick Kroon
Co-Chief Scientist
Faculty of Earth Sciences
Vrije Universiteit Amsterdam
De Boelelaan 1085
1081 HV Amsterdam
The Netherlands

Dr. Jack Baldauf
Deputy Director of Science Operations
Ocean Drilling Program
Texas A&M University
1000 Discovery Drive
College Station TX 77845-9547
USA

Dr. Peter Blum
Leg Project Manager and Staff Scientist
Ocean Drilling Program
Texas A&M University
1000 Discovery Drive
College Station TX 77845-9547
USA

November 2002

PUBLISHER'S NOTES

Material in this publication may be copied without restraint for library, abstract service, educational, or personal research purposes; however, this source should be appropriately acknowledged.

Ocean Drilling Program Scientific Prospectus No. 108 (November 2002).

Distribution: Electronic copies of this series may be obtained from the ODP Publications homepage on the World Wide Web at <http://www-odp.tamu.edu/publications>.

This publication was prepared by the Ocean Drilling Program, Texas A&M University, as an account of work performed under the international Ocean Drilling Program, which is managed by Joint Oceanographic Institutions, Inc., under contract with the National Science Foundation. Funding for the program is provided by the following agencies:

Australia/Canada/Chinese Taipei/Korea Consortium for Ocean Drilling
Deutsche Forschungsgemeinschaft (Federal Republic of Germany)
European Science Foundation Consortium for Ocean Drilling (Belgium, Denmark, Finland, Iceland, Ireland, Italy, The Netherlands, Norway, Portugal, Spain, Sweden, and Switzerland)
Institut National des Sciences de l'Univers-Centre National de la Recherche Scientifique (INSU-CNRS; France)
Marine High-Technology Bureau of the State Science and Technology Commission of the People's Republic of China
National Science Foundation (United States)
Natural Environment Research Council (United Kingdom)
Ocean Research Institute of the University of Tokyo (Japan)

DISCLAIMER

Any opinions, findings, and conclusions or recommendations expressed in this publication are those of the author(s) and do not necessarily reflect the views of the National Science Foundation, the participating agencies, Joint Oceanographic Institutions, Inc., Texas A&M University, or Texas A&M Research Foundation.

This Scientific Prospectus is based on precruise JOIDES panel discussions and scientific input from the designated Co-chief Scientists on behalf of the drilling proponents. The operational plans within reflect JOIDES Planning Committee and thematic panel priorities. During the course of the cruise, actual site operations may indicate to the Co-chief Scientists and the Operations Manager that it would be scientifically or operationally advantageous to amend the plan detailed in this prospectus. It should be understood that any proposed changes to the plan presented here are contingent upon the approval of the Director of the Ocean Drilling Program in consultation with the Science and Operations Committees (successors to the Planning Committee) and the Pollution Prevention and Safety Panel.

ABSTRACT

During Ocean Drilling Program (ODP) Leg 208, we will drill a depth transect of five sites between 2500 and 4800 m water depth targeting early Cenozoic sediments on the northeastern flank of the Walvis Ridge. Previous drilling in this region (Deep Sea Drilling Project [DSDP] Leg 74) recovered pelagic oozes and chalk spanning both the Paleocene/Eocene and Eocene/Oligocene boundaries. Our drilling objective is to recover fully intact sequences spanning both of these “critical” intervals as well as the Cretaceous/Tertiary (K/T) boundary at the deep end-member sites. New multichannel seismic data (*Meteor* cruise M49/1) along with existing information from DSDP Leg 74 sites were used to identify site locations where continuous sequences of early Cenozoic sediment should be present. Double/triple advanced hydraulic piston coring and double extended core barrel coring, high-resolution physical property measurements, and construction of composite sections will be employed at each site to ensure 100% recovery of the sedimentary section. These composite sections will provide a detailed history of paleoceanographic variations associated with several prominent episodes of early Cenozoic climate change including the early Eocene Climatic Optimum (EECO), the Paleocene–Eocene Thermal Maximum (PETM, also known as LPTM), and the Early Oligocene Glacial Maximum (EOGM). In particular, the transect will enable characterization of depth-dependent changes in deepwater chemistry and circulation associated with these extreme climatic states. This will facilitate testing of the leading hypothesis for the cause of the PETM and carbon isotope excursion, the abrupt dissociation of as much as 2000 gigatons of marine methane hydrate. Numerical modeling demonstrates that the injection of such a large mass of carbon to the ocean/atmosphere should have triggered an abrupt (<10 k.y.) shoaling of the carbonate compensation depth and lysocline, followed by a gradual recovery. Sediment cores recovered during this leg will be used to constrain both the rate and scale of recovery, as well changes in other aspects of deep-sea chemistry. The Leg 208 transect will complement a transect drilled on the southern Shatsky Rise during ODP Leg 198.

INTRODUCTION

The Paleogene represents one of the more climatically dynamic periods in Earth history. Stable isotope-based reconstructions reveal a rather complex history of gradual and rapid warming and cooling (Miller et al., 1987; Miller and Katz, 1987; Stott and Kennet, 1990; Zachos et al., 1994, 2001). This includes a gradual 5-m.y.-long global warming trend that began in the late Paleocene and climaxed in the early Eocene in a 1- to 2-m.y.-long climatic optimum (early Eocene Climatic Optimum [EECO]), and a 12-m.y.-long steplike cooling trend that began in the early middle Eocene and culminated in the earliest Oligocene with the appearance of continental-scale ice sheets (Hambrey et al., 1991; Zachos et al., 1992). Among the more prominent events, however, is a brief but extreme greenhouse period known as the Paleocene–Eocene Thermal Maximum (PETM). This event occurred at ~55.0 Ma, midway through the Paleocene–Eocene warming trend, and was accompanied by major changes in ocean chemistry as inferred by shifts in carbon isotope patterns and in the distribution and preservation patterns of terrigenous and biogenic sediments on the seafloor (e.g., Bralower et al., 1995; Kennett and Stott, 1991; Robert and Kennett, 1997). In addition, this event was responsible for large-scale turnover of fauna and flora in the oceans and on land (e.g., Kelly et al., 1998; Koch et al., 1992, 1995; Thomas and Gooday, 1996; Thomas and Shackleton, 1996). Another notable transient is the earliest Oligocene Glacial Maximum (EOGM, also known as the Oi-1 Event), a brief but extreme glacial interval that occurred at ~33.4 Ma, coincident with the transition to permanent glacial conditions on Antarctica (e.g., Miller et al., 1987, 1991; Zachos et al., 1996). This

transient, like the PETM, has been linked to major changes in ocean chemistry and ecology (Barrera and Huber, 1991, 1993; Salamy and Zachos, 1999; Thomas and Ward, 1990; Thunell and Corliss, 1986).

Multiple hypotheses exist to explain the large-scale, long-term changes in Paleogene climate, though none have gained universal acceptance. In general, among the many factors, ocean gateways (continental geography) and greenhouse gas levels are recognized as the two key variables. Theoretical models have invoked either higher greenhouse gas levels or the absence of a circum-Antarctic current or some combination of the two to account for the EECO (Barron, 1985; Bice et al., 2000; Sloan and Barron, 1992; Sloan and Rea, 1996; Sloan et al., 1992, 1995). Similarly, the Oligocene glaciation has been attributed to both a reduction in greenhouse levels and the initiation of the Antarctic circumpolar current (e.g., Kennett and Shackleton, 1976; Mikolajewicz et al., 1993; Oglesby, 1991; Raymo et al., 1990; Rind and Chandler, 1991). The more abrupt transient excursions are more likely to have been forced by rapid changes in greenhouse gas levels because they transpire over short timescales (e.g., 10^3 – 10^4 yr) and, most importantly, are accompanied by geochemical and isotopic anomalies suggestive of major perturbations in the carbon and sulfur cycles (Dickens et al., 1995, 1997; Paytan et al., 1998; Pearson and Palmer, 2000; Schmitz et al., 1997; Stott and Kennet, 1990; Zachos et al., 1993).

Progress in characterizing Paleogene oceanography and climate history, particularly the transient events, has been hampered by the lack of high-quality, high-resolution multicored sequences. Most existing sites suffer from poor recovery and drilling disturbance, and few were multicored or drilled as part of depth transects. The few exceptions are sites recovered during recent Ocean Drilling Program (ODP) legs, including Sites 865, 999, 1001, 1051, and Bass River, New Jersey (Bralower et al., 1995, 1997; Miller et al., 1998; Norris and Röhl, 1999; Röhl et al., 2000). The high-resolution records produced from these sites have yielded a wealth of exciting, potentially important ideas about climate change that require additional data to be more fully explored. We currently lack the required sediment archives needed to characterize the changes in ocean circulation and chemistry that theoretically should have accompanied these climatic extremes. Gaining a more complete description of these events in a third dimension and at a higher temporal resolution is critical because such information is required for both formulating and testing hypotheses of what caused these events.

One of the more promising locations for recovering Paleogene sediments, including the PETM and EOGM, is Walvis Ridge in the South Atlantic Ocean. Walvis Ridge was the target of Deep Sea Drilling Project (DSDP) Leg 74, drilled in the summer of 1980, during which Sites 525–529 were drilled as a depth transect along the northern flank of the ridge from 2500 to 4100 m water depth (Moore, Rabinowitz, et al., 1984). Paleogene pelagic sediments characterized by moderate sedimentation rates (~8–15 m/m.y.) and superb magnetic stratigraphy were recovered at each site. However, because of the poor recovery (~50%) and coring disturbances, especially with the extended core barrel (XCB) in relatively unlithified sediments, only short segments of the sequences were recovered fully intact, thereby preventing attempts to conduct high-resolution investigations. Nevertheless, subsequent shore-based studies of these cores were instrumental in improving our understanding of Maastrichtian and Paleogene paleoceanography (e.g., carbonate compensation depth [CCD], carbon isotope stratigraphy, deep-sea temperature/ice volume) (e.g., Moore, Rabinowitz, et al., 1984, and papers within). In addition, a nearly complete PETM interval was recovered from the deepest hole at Site 527. Bottom-water and sea-surface temperature (SST) estimates obtained from analysis of Site 527 samples have provided critical constraints on the scale of this event (Thomas et al., 1999; Thomas and Shackleton, 1996). At the shallower sites, the PETM was not recovered because of core gaps (poor recovery).

During the winter of 2000, a seismic survey of the southeastern Walvis Ridge was undertaken by the *Meteor* (cruise M49/1). The survey extended from the location of the Leg 74 sites to areas located north

and northeast, a region where thicker sediment sequences were discovered (Fig. F1). The higher-fidelity multichannel seismic data generated during the survey allowed us to target a series of sites that will capture the PETM and other key intervals, possibly from penetration depths reachable by advanced hydraulic piston corer (APC), at least at the three shallowest sites. The sites have been positioned at depths that will provide a paleodepth range of 2200 m. This paleodepth transect will provide critical constraints on several aspects of the PETM event, as well as the EOGM, a lower-priority target. Advances in coring technology and drilling strategies (i.e., multihole composite sections) should allow for 100% recovery of sequences that were only partially recovered during Leg 74. In addition, recent advances in data acquisition and chronostratigraphy will enable high-precision correlation and dating of these sediments.

BACKGROUND

Geologic Setting

Walvis Ridge is a northeast-southwest-trending aseismic ridge that effectively divides the eastern South Atlantic Ocean into two basins, the Angola Basin to the north and the Cape Basin to the south (Figs. F2, F3). It consists of a series of interconnected crustal blocks that slope gradually toward the northwest and more steeply toward the southeast. Magnetic and gravity anomalies indicate the ridge was formed by hotspot volcanism near the mid-ocean ridge as the basin gradually widened (Rabinowitz and Simpson, 1984). The subsidence history of Walvis Ridge has been determined using simple thermal subsidence models (Moore, Rabinowitz, et al., 1984).

Plagic sediments drape most of the ridge and generally increase in thickness toward the continental margin (Moore, Rabinowitz, et al., 1984). In the vicinity of the proposed target area on the southeast portion of the ridge, sediment thickness varies from ~300 m on the deeper portions of the ridge to ~500 m near the summit, a pattern that is clearly expressed in acoustic reflectors (Fig. F4). The sediments are primarily calcareous oozes and chalks that range in age from Campanian to Holocene (Fig. F5). The Neogene sequences are dominated by nannofossil and foraminifer-nannofossil oozes with relatively high carbonate contents, in excess of 90%. Turbidites and occasional slumps are present in some areas. The underlying Paleogene sediments are dominated by nannofossil and foraminifer nannofossil chalks. Carbonate contents are also high, in excess of 80% through most of the Paleocene, Eocene, and Oligocene with the exception of several short carbonate-poor intervals at the deeper sites (i.e., Site 527; upper Paleocene, upper Eocene, and early-middle Miocene). Most of these carbonate-poor layers represent episodes of CCD shoaling. A few thin chert layers are present below the upper Paleocene of the shallowest sites (525 and 528) and in the lower Eocene of Site 529. Slump deposits of various scales are present in the upper Paleocene at Site 529 as well. In most sections, calcareous microfossil preservation varies from good to excellent. The natural remanent magnetization of the Walvis Ridge sediments appears to be strong and stable. As a result, the quality of the magnetic polarity records are excellent, particularly over the Upper Cretaceous and lower Paleocene (Chave, 1984).

Stratigraphic Evolution

Sediment accumulation rates on Walvis Ridge are quite variable in both space and time. On average, the highest rates (~8–13 m/m.y.) occur in the Quaternary, Paleocene, and Maastrichtian. Hiatuses are a common feature of the Neogene at most sites. For example, most of the Pleistocene is missing at shallow sites (Sites 525 and 526), whereas the lower and middle Miocene is absent at several of the deeper sites. Most of the Neogene hiatuses appear to be erosional in nature, although dissolution clearly contributed in

some cases (i.e., lower–middle Miocene at Site 527). Hiatuses are also present in the upper Eocene and upper Oligocene. In contrast, at middepths (Site 529), most of the Paleogene is present but the middle–upper Miocene is either condensed or absent. In the deepest section (Site 527), the middle–upper Eocene is relatively condensed and the Oligocene and Miocene is highly condensed and/or absent. Nevertheless, it appears that for most of the early Paleogene, deposition was more or less continuous over much of the rise. This continuity in sediment accumulation is reflected to some extent in the parallel trends in the low-resolution carbon isotope stratigraphies for four of the Leg 74 sites (Fig. F6) (Shackleton and Hall, 1984).

Cyclical variations in sedimentation are evident in various lithologic/physical properties indices, particularly in the more expanded Maastrichtian and Paleocene sequences. Spectral analysis of sediment color banding reveals the presence of a strong precessional beat in upper Maastrichtian and lower Paleocene sediments at Sites 525 and 528 (Herbert et al., 1995; Herbert and D'Hondt, 1990). Similar color cycles are present in some cores from the upper Paleocene, lower Eocene, and Oligocene as well, although no attempt has been made to document their frequency because of the poor condition of the cores.

SCIENTIFIC OBJECTIVES

Early Cenozoic “greenhouse” climates have been identified as a high-priority interest of U.S. and International global change programs. Moreover, the ODP Extreme Climates Program Planning Group has also ranked the Paleocene–Eocene as a high-priority objective. Here, we outline questions specific to the nature and causes of these warm episodes that can be addressed by drilling in the southeast Atlantic. We also discuss in greater detail some other aspects of Paleogene paleoceanography that are relevant to this proposal.

Early Eocene Climatic Optimum

The EECO represents the most recent episode of sustained global warmth. For 1–2 m.y. of the early Eocene, global climate was very warm and ice free (Fig. F7). In the oceans, paleontologic and isotopic proxies indicate that the high-latitude seas and bottom waters were as much as 8°C warmer than present (Miller et al., 1987; Shackleton and Boersma, 1981; Zachos et al., 1994; Stott and Kennett, 1990). On land, the biogeographic ranges of subtropical to temperate fauna and flora extended well into polar latitudes (Axelrod, 1984; Estes and Hutchison, 1980; Wolfe, 1980) and polar ice sheets were small or nonexistent.

Several critical issues concerning the EECO need to be addressed. The first concerns the nature of climate variability during this period. At present, not a single marine record details paleoceanographic/climatic variability of this interval on orbital timescales. As a result, we do not know the approximate duration of the EECO, nor how stable climate was during this period. The second issue concerns the origin of the EECO. Empirical and theoretical geochemical studies suggest that greenhouse gas levels were significantly higher, possibly six times the preindustrial level at the peak of the EECO (Berner et al., 1983; Pearson and Palmer, 2000). These estimates are supported to some extent by climate modeling in which the observed EECO meridional thermal gradients could only be attained in simulations with greenhouse gas levels six to eight times those at present (Sloan and Rea, 1996) and by a new boron isotope–based pH record that indicates unusually low levels for the Eocene ocean, consistent with high pCO₂ (Pearson and Palmer, 2000). The third issue concerns the underlying mechanism for greenhouse gas changes: why did CO₂ levels increase in the early Eocene? Were mantle outgassing rates higher than suggested by geochemical models? Regardless, several lines of evidence now indicate that the EECO was indeed a

“greenhouse” climate and that other factors such as continental geography and oceanic gateways played a subordinate role in sustaining this extreme global warmth.

Paleocene-Eocene Thermal Maximum

In terms of the rate and degree of warming, the PETM is unprecedented in Earth history. Isotope records suggest that at 55 Ma the deep-sea and high-latitude oceans warmed by 4° and 8°C, respectively, in a period of <10 k.y. (Fig. F8). This period of extreme warmth, which lasted <150 k.y., triggered profound changes in global precipitation and continental weathering patterns (e.g., Gibson et al., 1993; Kaiho et al., 1996; Robert and Kennett, 1994). The PETM also affected biota on a global scale, triggering both rapid turnover of benthic and planktonic organisms in the ocean (Kelly et al., 1996; Thomas and Shackleton, 1996; Thomas and Ward, 1990) and a sudden radiation of mammals on land (Clyde and Gingerich, 1998; Koch et al., 1992; Rea et al., 1990).

Several mechanisms have been proposed for the PETM, including massive outgassing associated with rifted margin volcanism (Eldholm and Thomas, 1993) and sudden dissociation of methane hydrates stored on continental shelves and slopes (Dickens et al., 1995, 1997). Both hypotheses were inspired, in part, by marine and terrestrial carbon isotope records that show an abrupt 3‰–4‰ decrease in the ocean/atmosphere carbon reservoirs in <10 k.y. (Bralower et al., 1995, 1997; Kennett and Stott, 1991; Koch et al., 1992, 1995). Such a large and rapid carbon isotope excursion (CIE) requires a sudden injection of a large volume of isotopically depleted carbon into the ocean/atmosphere system. In terms of fluxes and isotopic mass balances, the hydrate dissociation model is clearly more plausible. If estimates are correct, only a fraction of the total reservoir of methane hydrate stored on continental margins is sufficient to generate the observed isotopic excursion. In principle, with warming of deep waters, shelf and slope hydrates could become unstable, triggering a catastrophic release of CH₄ and immediate greenhouse warming.

A massive methane dissociation event should have profound effects on ocean chemistry. Dickens et al., (1997) used a box model to simulate the effects on ocean carbonate chemistry of releasing roughly 1.1×10^3 gigatons of methane (immediately oxidized to carbon dioxide) directly into the atmosphere. The amount of carbon added to the system was determined from mass balance calculations assuming a $\delta^{13}\text{C}$ of –60‰ for bacterially produced methane. This exercise found several notable effects including a dramatic increase in weathering rates on land, a reduction in ocean pH, and a shoaling of the CCD and lysocline, all within several thousands of years (Fig. F9). The effects on the ocean were greatest in areas proximal to sources of deep water where the excess CO₂ reentered the deep ocean via convective processes. The CCD is eventually restored, although not to its original position, as the system appears to initially overcompensate before returning to a steady-state level. This is consistent with the PETM low carbonate or clay layers in deep-sea sites (Fig. F10).

The clathrate and other models can be tested with deep-sea drilling. A series of paleodepth transects in each of the major ocean basins would allow for characterization of the lysocline/CCD changes during this event. The initial shoaling should be expressed as a dissolution interval or hiatus in deeper sites coincident with the benthic foraminifer extinction and carbon isotope excursion. The model-predicted overshoot should be preserved as well. Existing PETM sequences show a reduction in carbonate content to varying degrees coincident with the excursion. However, without vertically offset sites, it is not yet possible to quantify the extent to which the reduction in carbonate content reflects changes in microfossil preservation or the depth range over which the carbonate changes occurred. With a series of well-placed vertical depth transects, it should be possible to separate the effects of preservation from those of

production. Walvis Ridge appears to be well suited for this, as rates of sedimentation were fairly high and continuous through the late Paleocene–early Eocene over most of the ridge.

An interesting new development is the emergence of evidence of additional biotic events and CIEs. Faunal and isotope data from Hole 690B (Thomas et al., 2000) point toward other times with conditions potentially similar to but not as extreme as those of the PETM. If this second event has a similar origin as the first, we would expect a similar but smaller-scale response in ocean carbonate chemistry. Moreover, drilling at Blake Nose shows similar repetitions of the climatological and sedimentological conditions of the Paleocene/Eocene (P/E) boundary in the rock record. A long-term gamma ray record from Site 1051 shows a series of major peaks that represent a reduction in the carbonate content and/or increased terrigenous flux augmenting the clay content. Cyclicity of clay fluxes on the timescale of ~2 m.y. most likely reflects on climate cycles, although the precise nature of the climatic changes is unknown. One of the gamma ray maxima coincides with the carbon isotope event and peaks again near the top of Chron C24r (Norris et al., 1998). These cycles persist throughout the early Eocene, indicating that this warm greenhouse period was not stable. The long-term periodicity in these records most likely reflects on a long-period orbital cycle (2 m.y.). The role of orbital forcing in driving these and other early Paleogene climate changes still needs to be evaluated.

Middle Eocene to Early Oligocene Cooling and Glaciation(s)

The primary transition from “greenhouse” to “ice-house” conditions occurred during the middle Eocene to early Oligocene. Although this encompasses 18 m.y., stable isotopic records reveal a steplike procession, with much of the change occurring in just a few relatively brief steps in the earliest–middle Eocene (~52 Ma) and earliest Oligocene (Fig. F11) (EOGM; ~33.4 Ma) (e.g., Miller et al., 1987; Kennett and Stott, 1991; Zachos et al., 1996). The first event marks the onset of ephemeral glacial activity (Browning et al., 1996; Hambrey et al., 1991), whereas the second and larger of the two steps, EOGM, represents the first appearance of permanent ice sheets on Antarctica (Barrera and Huber, 1991; Zachos et al., 1992). Furthermore, the highest-resolution deep-sea isotope records of this transition indicate that the final transition may have been modulated by orbital forcing (Diester-Haass and Zahn, 1996).

In principle, this climatic transition should have had a dramatic effect on ocean/atmospheric circulation patterns and continental weathering rates and, hence, ocean chemistry. For example, reconstructions of bottom-water isotope patterns hint at a brief pulse of a proto-North Atlantic Deep Water (NADW) coincident with the EOGM (Miller et al., 1991; Zachos et al., 1996). Also, carbonate sediment patterns suggest a significant deepening of the CCD at the Eocene/Oligocene (E/O) boundary (Peterson and Backman, 1990; van Andel, 1975). The latter is consistent with a sudden lowering of sea level and/or an increasing chemical weathering of continents, both of which would increase the flux of dissolved ions to the deep sea. However, the CCD on regional scales is also sensitive to changes in the rates and patterns of carbonate production patterns. A depth transect is required to separate these potential effects and more tightly constrain rates of change.

Oceanic Recovery from the Cretaceous–Tertiary Mass Extinction

The Cretaceous–Tertiary (K-T) impact and mass extinction caused a number of long-term changes in oceanic properties. These include (1) a drastic decrease in the organic flux to deep water, as indicated by decreased carbon isotopic gradients (Hsü et al., 1982; D’Hondt et al., 1998; Stott and Kennett, 1989; Zachos et al., 1989) and lower barium accumulation rates, and (2) a drastic decrease in deep-sea carbonate accumulation (D’Hondt and Keller, 1991; Zachos and Arthur, 1986), and, at least in the South Atlantic,

enhanced 100-k.y. oscillations in deep-sea sedimentation (D'Hondt et al., 1996). All of these long-term changes were sustained for a million years or more. The final recovery from several of these changes is poorly constrained. For example, although we know that deep-sea carbonate accumulation did not recover for >2 m.y. after the mass extinction (Zachos and Arthur, 1986), the final recovery of deep-sea carbonate accumulation has only been identified at a single Caribbean site (ODP Site 1001), where it appears that carbonate accumulation did not recover for 4 m.y. after the K-T event (D'Hondt et al., 1998). Poor core recovery has precluded successful identification of this final recovery in previously drilled South Atlantic sites. However, the improved recovery made possible by modern ODP techniques should allow its successful identification at the proposed drill sites.

Documenting the timing of these recoveries and their relationships to other paleoceanographic properties would provide a critical test of the coupling between oceans, climate, and biota. The K-T mass extinction effectively changed the state of the global ecosystem. However, there is little reason to believe that any physical consequences of the K-T impact could have lingered for more than a few thousand years. Consequently, the Maastrichtian through Paleocene record of deep-sea sediments provides an ideal opportunity for testing the sensitivity of the global environment to biological disaster. For example, the long-term decrease in deep-sea carbonate accumulation might have changed oceanic alkalinity and atmospheric CO₂ concentrations. If so, the interval of decreased carbonate accumulation should be marked by changes in various paleoceanographic proxies, such as increased foraminiferal preservation and migration of the lysocline or CCD. Similarly, the 100-k.y. oscillations in early Paleocene deep-sea sediments may have resulted from a decreased ability of post-extinction biota to buffer seasonal and Milankovitch-scale climate change (D'Hondt et al., 1996). If so, these oscillations should correspond to similar oscillations in various paleoceanographic proxies, such as carbon isotopic differences between planktonic and benthic foraminifers.

Paleogene Deepwater Circulation and Chemical Gradients

In principle, changes in either the meridional thermal gradient or precipitation patterns can dramatically alter the mode of ocean circulation, thermohaline or otherwise (Broecker, 1997). Warming of polar regions coupled with increased precipitation, for example, would tend to lower the density of high-latitude surface waters, thereby inhibiting sinking. This, in turn, might be balanced by increased convection elsewhere, possibly in subtropical regions where high rates of evaporation raise seawater salinity and density. Given the extreme thermal gradients and precipitation patterns, it is likely that deep convection during the PETM, and possibly during the EECO, was not occurring at high latitudes. If true, there should be some obvious evidence for this in deepwater chemical gradients as inferred from stable carbon isotopes and the distribution of carbonates on the seafloor.

A shift in the source of waters bathing Walvis Ridge should be reflected in carbon isotope, carbonate dissolution, and benthic assemblage patterns, as well as in other isotopes with short residence times (i.e., Nd). Several studies have shown that through much of the late Paleocene and early Eocene the most negative deep-ocean carbon isotope values were consistently recorded by benthic foraminifers from the Pacific Ocean (Kennett and Stott, 1990; Corfield and Norris, 1996; Corfield and Cartlidge, 1992; Pak and Miller, 1992). Although this pattern is of the same sign as modern, the gradient is much smaller, indicating that Pacific deep waters were only slightly more aged than Atlantic deep waters. As such, one would predict a similar CCD in the two basins. Low-resolution records of carbonate accumulation on Walvis Ridge for the Cenozoic show features suggestive of large-scale changes in the CCD at the P/E and E/O boundaries, although these "events" are not well defined (Moore, Rabinowitz, et al., 1984).

PROPOSED DRILL SITES

Proposed Sites WALV-8A, WALV-8B, and WALV-8C

A suite of three proposed sites, WALV-8A through WALV-8C (2530–2557 m water depth) has been positioned in the vicinity of DSDP Site 525 (Figs. F12, F13, F14; Table T1). This area represents the shallowest segment of the planned Walvis Ridge drilling transect. Total sediment thickness at these sites ranges from 460 to 490 ms two-way traveltime (TWT) (multichannel profile GeoB01-031), and the basal sediments are likely Campanian (Fig. F5). At Site 525 a major unconformity was encountered across the E/O boundary. We believe that sequences to the northeast of Site 525, along seismic reflection line GeoB01-031, may offer a more complete Paleogene sequence. The new seismic lines show a series of reflectors (Me, E₁, and K/T) that can be traced from Site 525 to WALV-8A, WALV-8B, and WALV-8C and indicate the E/O unconformity (E₁) to fade out laterally away from Site 525 (Figs. F12, F13). The E/O unconformity at Site 525 is seen in seismic line GeoB01-031 as a zone of hard and truncated reflectors. This zone is not seen at proposed Sites WALV-8A through WALV-8C. The next prominent reflector is the Cretaceous/Tertiary (K/T) boundary (500–570 ms TWT at Site 525), just above the basement reflectors. Correlating reflectors from Site 525 to the Sites WALV-8A through WALV-8C suggests the Paleogene sequence is most complete at Sites WALV-8A and WALV-8B. Total sediment thickness at these two locations is estimated to be 620 and 530 ms TWT. The E/O and P/E boundaries are shallowest at Site WALV-8C, <280 and 370 ms TWT, compared to 400 and 480 ms TWT at Site WALV-8A. Subbottom depths of the target reflectors at proposed Site WALV-8A are considerably deeper than is desirable for our planned work. Therefore, proposed Site WALV-8B is the primary site, and Sites WALV-8A and WALV-8C serve as alternates.

Proposed Sites WALV-9A and WALV-9B

Proposed Sites WALV-9A and WALV-9B (2979–3083 m water depth) are located in an area proximal to DSDP Site 529 in the upper segment of the planned Walvis Ridge drilling transect (Fig. F14). A total of 417 m of sediment was recovered at Site 529 by rotary drilling (Fig. F5). The sequence, which was poorly recovered, ranged from Pleistocene to late Maastrichtian in age. Based on Site 529, the EOGM, EECO, and PETM target intervals are expected at 189–208, 246–265, and 265–274.5 meters below seafloor (mbsf). Slumps were reported at this site in the upper Paleocene (293.5–312.5 mbsf), in the Oligocene–Miocene NN1 Zone (75–122.5 mbsf), and in the lower Pleistocene.

Site WALV-9A has been positioned on seismic lines GeoB01-055 and GeoB01-048, immediately northwest of DSDP Site 529 at a water depth of 2979 m (i.e., 66 m shallower than Site 529). The site is located on a topographic high that is underlain by a package of expanded sediment sequences. Seismic profile GeoB01-055 clearly shows a southward thinning of acoustic units and the presence of sediment slumps between 22:30 and 00:15 (i.e., immediately south of Site WALV-9A). An erosional channel is seen immediately northeast of the site on crossing line GeoB01-048, and a progressive thinning of acoustic units is seen to the southwest. Site WALV-9A therefore appears ideally located for obtaining expanded sediment sections in an area that remained unaffected by local erosion. Proposed Site WALV-9B is located along line GeoB01-048 (shotpoint 3854). It is located in an area where the Neogene sediment has been eroded and where the Paleogene is more accessible. As such, proposed Site WALV-9B has a higher priority for drilling, but approval for drilling by the Pollution Prevention and Safety Panel (PPSP) is still pending at the time of production of this prospectus.

Proposed Sites WALV-10A, WALV-10B, WALV-10C, and WALV-10D

These proposed sites (3719–3961 m water depth) are in the vicinity of DSDP Site 528 in the central segment of the Walvis Ridge drilling transect. A total of 474 m of Pleistocene through upper Maastrichtian sediment was retrieved at Site 528 (Fig. F14). The Paleogene was rotary drilled throughout with an average recovery rate of 60%. We suspect that the P/E boundary was lost in a core gap. Based on the Site 528 stratigraphy, our target intervals are at 217–236 mbsf (Eocene–Oligocene transition), 293–312 mbsf (EECO), and 312–321 mbsf (PETM). No hiatuses, slumps, or other sedimentary disturbances are reported for these intervals. We have tentatively labeled several prominent reflectors (Me, P-E, and K/T), which can be traced across all sites.

Positioning of sites was based on line GeoB01-059 and crossing lines GeoB01-062, GeoB01-064, and GeoB01-066. Site WALV-10A is a reoccupation of DSDP Site 528, with the goal of retrieving a more complete sediment sequence than was possible using rotary core barrel (RCB) drilling that was employed at the DSDP site. The site is at an isolated topographic high that is bounded by erosional channels in the southwest and northeast. Proposed Sites WALV-10B through WALV-10C are located along line GeoB01-059, on a gently northwest-dipping slope that shows parallel subbottom reflectors indicating undisturbed acoustic units. Total sediment thickness at these sites varies between 460 and 490 ms TWT (Table T1). At the deepest proposed Site WALV-10D, part of the Neogene is missing (due to slumping?), making it a more attractive target for accessing the Paleogene.

Proposed Sites WALV-11A, WALV-11B, WALV-11C, and WALV-11D

This is part of the deep segment of the Walvis Ridge drilling transect, in 4313–4526 m water depth, around the location of DSDP Site 527 (Fig. F15). The sediment column at Site 527 consists of a 360-m-thick Pleistocene to middle Maastrichtian sequence. A single but major regional unconformity spans the middle Miocene to the lower Oligocene and is responsible for a pronounced reflector (O-M unconformity) that is recognized in all profiles. A second prominent reflector marks the K/T boundary. From the Site 527 stratigraphic record we expect the EOGM, EECO, and PETM target intervals to be at 113.5–132.5, 180–189.5, and 189.5–199 mbsf. We have selected four possible locations where these reflectors can be recognized.

Proposed Site WALV-11B, the primary site, is located to the southwest of DSDP Site 527 and should yield a Paleocene–Eocene interval similar to, or more expanded than, that at Site 527. Along seismic line GeoB01-039, a series of undulating, diverting, and truncated reflectors is seen at 100 ms TWT at Site 527, around the subbottom depth where the middle Miocene to early Oligocene hiatus has been reported. Offsetting the drill site to the southwest where this acoustic pattern is not present appears desirable. Total sediment thickness at Site WALV-11B is 360 ms. Also along this line to the northeast of Site 527 is Site WALV-11C, with a total sediment thickness of 340 ms TWT (Table T1). Proposed Site WALV-11A is essentially a reoccupation of DSDP Site 527 on seismic line GeoB01-039. The intention is to retrieve a more complete sediment sequence than was possible using hydraulic piston corer drilling that was employed at the DSDP site. Site WALV-11D is positioned at the northern end of the sedimentary wedge that forms the slope along which the Walvis Ridge drilling transect is located. Total sediment thickness at Site WALV-11D is 300 ms TWT. Subbottom reflectors shoal at the site because of a progressive northwestward thinning of the uppermost acoustic units at the northern end of the wedge. From comparing acoustic units with those that were drilled at Site 527 it appears reasonable to infer that Paleogene sequences are near the sediment surface at proposed Site WALV-11D. The site appears to be

unaffected by sediment slumping, which is indicated to the southeast along seismic line GeoB01-038 (14:30 to >18:00) and may offer a suitable alternate should slumping be a problem at Site WALV-11B.

Proposed Sites WALV-12A, WALV-12B, and WALV-12C

Proposed Sites WALV-12A through WALV-12C (4726–4768 m water depth) are designated to be the deep end-member of the drilling transect. Site WALV-12A is located on line GeoB01-035 in a perched basin that is filled with ~280 ms TWT of sediment. Sites WALV-12B (shotpoint 3349) and WALV-12C along line GeoB01-036 are located on a sedimentary ridge and a southeast-dipping slope (Fig. F16). Sediment thickness at these sites is 240 and 300 ms TWT. Here, identification of reflectors is tenuous given the lack of previous drilling in this area. Nonetheless, we expect the Neogene to be mostly clay and condensed. In contrast, the Paleogene should be relatively carbonate rich. One prominent reflector is most likely the K/T boundary contact. This deep site will be critical for establishing a possible overdeepening of the CCD following the PETM as the ocean carbon balance was restored through weathering feedbacks and carbonate deposition.

Proposed Site WALV-13B

Proposed Site WALV-13B (3768 m water depth) is an alternate site located northeast of the main Walvis Ridge transect area, half-way between Frio Ridge in the northeast and the transect at the central Walvis Ridge. Time permitting, this site will be targeted for an expanded Paleogene sequence. Site WALV-13B is located on line GeoB01-029b, common depth point 2890, on the flank of a narrow valley incision. It appears conceivable that the incision was cut into the sediment cover by a sediment slide that went down the narrow valley immediately southwest of the incision. As such, the Neogene cover may be thin or absent here. Total sediment thickness at the flank of the incision is 480 ms TWT. The K/T boundary is estimated to lie at 316 mbsf.

SITE SURVEY

A high-resolution seismic site survey of Walvis Ridge was completed during *Meteor* cruise M49/1 (4 January–10 February 2001) (Figs. F1, F2, F3). The purpose of the M49/1 seismic survey was to optimize target sites so as to avoid sediment slumps, hiatuses, and condensed stratigraphic sections that were penetrated at some of the existing DSDP sites. To this end, a seismic survey was conducted that included existing sites. The survey grid focused on a region to the north and east of the Leg 74 Sites, away from a large channel that dissects the ridge to the southwest. Because of extensive downslope sediment transport throughout the region, the survey targeted several isolated bathymetric highs where the effects of downslope sediment transport appear to be minimal. All survey data were submitted to the Lamont-Doherty Earth Observatory data bank during summer 2001. A list of the survey lines across the proposed Leg 208 sites is given in Table T1.

OPERATIONAL STRATEGIES

The primary objective of Leg 208 drilling is to recover sediments representing each of the target intervals over a paleowater depth range of 2 km. The recovered sequences should be stratigraphically continuous and have sedimentation rates sufficient to resolve at least 41-k.y. orbital cycles. In addition, the sediments should be relatively un lithified to allow for easy extraction of calcareous microfossils for

geochemical analyses. Preservation need not be perfect, but good enough so that relative changes in isotopic and trace metal ratios are preserved.

Coring Strategies

To meet the objectives listed above, we have designed a transect with 5 primary and 12 alternate sites (Tables T1, T2). Several of the existing Paleocene–Eocene sections recovered from the Atlantic are riddled with unconformities. Some unconformities are clearly erosional (nondepositional) in nature, whereas others may be due to intense dissolution. Evidence suggests that the unconformities around the primary target, the P/E boundary, on Walvis Ridge, are highly localized. The new site survey data demonstrate that more expanded (and possibly continuous) sequences can be recovered nearby. We have tried to maximize our opportunities to recover the P/E boundary and other key target intervals by selecting sites that appear to have a relatively thick Paleogene sequences. We also have included at least one proximal alternate site for each of the primary sites, which will give us flexibility to move to a new site should we discover a local unconformity at the P/E boundary.

At present, the primary sites for Leg 208 are WALV-8B, 9A, 10C, 11B, and 12A (WALV-9A will most likely be replaced by WALV-9B once it is approved by the PPSP). They span a water depth range from 2557 to 4726 m. The primary stratigraphic targets for Sites WALV-8B and WALV-9A include expanded PETM and EOGM intervals in upper Paleocene to lower Oligocene chalks and oozes (Fig. F5). We are avoiding areas proximal to DSDP Site 525, where the upper Eocene and lower Oligocene are absent, and Site 529, where several slumps are present. Proposed Site WALV-10C, located to the north of Site 528 (Fig. F14) at an intermediate depth of 3842 m, offers a potentially more expanded upper Paleocene to upper Oligocene section. The deepest site, WALV-12B, is located well north of DSDP Site 527. Proposed Site WALV-11B is located near Site 527 but at slightly shallower water depth of 4375 m. The primary target is a complete Paleogene sequence that includes the PETM and EOGM excursions, as well as the K/T boundary. Drilling will proceed to lower Paleocene sediments at three sites (WALV-8B, WALV-9A, and WALV-10C) and the upper Maastrichtian at two (WALV-11B and WALV-12A).

Each site will be double APC and/or XCB cored. Third holes will be drilled if it can be established through near–real time stratigraphic correlation that primary target horizons fall within coring gaps in the first two holes. Multiple hole coring is intended to fill coring gaps from one hole with recovered sequences from another hole.

The current time estimate for coring is ~33 days, with ~6 days available for logging. Total transit time is estimated to be ~18 days (Table T2).

Core Logging Strategy

An important part of the shipboard measurements at each site will be the near–real time construction of a composite depth scale from hole-to-hole correlation of cores and spliced sections representing complete stratigraphic intervals. The primary splice is used for later sampling, and an alternate spliced section, as complete as possible, will be used for ODP archiving and also for additional sampling if warranted. Composite sections will be constructed using core logging data (magnetic susceptibility, natural gamma radiation, color reflectance, and gamma ray density). Two dedicated stratigraphic correlators will operate the whole-core multisensor track (MST), retrieve the relevant data from the database, and correlate cores from multiple holes by vertical whole-core depth shifting. The MST sampling program will be set to optimize measurement time (within constraints of adequate data quality and depth resolution) for the overall time available. In typical operations, ~60–90 min will be available to process

one core (~10 m), which will also set the core processing rate for all other laboratory stations. Correlation should occur as rapidly as possible such that the stratigraphic correlator can inform the driller (or core technician) at what depth the drill string should be placed for shooting cores in the third hole based on the correlation of the cores from the first two holes.

After MST measurements are completed, the cores will be split. Working halves will be available for moisture and density sampling and other physical properties measurements. The archive halves will undergo digital imaging with the new digital imaging system, visual core description, diffuse color reflectance measurements with the automated Minolta CM2002, and natural remanent magnetization analysis in the paleomagnetism laboratory. The imaging and color reflectance devices will be operated by the lithostratigraphy (sedimentology) group.

Sampling Strategies

Sample Allocation Committee

For each drilling leg, a sample allocation committee (SAC) is constituted, comprised of the Co-Chief Scientists, the ODP Staff Scientist, and the ODP Curator. During the leg, the Curator's authority and responsibilities to the SAC may be ceded to the shipboard Curatorial Representative.

Because the SAC best understands the scientific needs of their leg, this group establishes a leg-specific sampling strategy and makes decisions on leg-specific sample requests received before the leg sails, during the leg, and within (but not after) the 1-yr postcruise moratorium. The sampling strategy outlined here was agreed upon by the Leg 208 SAC in September 2002.

Shipboard Sampling

Samples for routine shipboard analyses of ephemeral properties and for measurements essential to safety monitoring and initial shipboard interpretations will be taken during the cruise by the shipboard participants. Samples for shipboard analyses are taken by the appropriate laboratory representatives. Shipboard samples include the following:

Catwalk Samples:

- Vacutainer samples of free gas,
- Headspace samples for organic geochemistry,
- Interstitial water samples for inorganic geochemistry, and
- Core catcher samples for biostratigraphic analyses.

Working-Half Core Samples:

- 10-cm³ samples for moisture and density determination (~1/section),
- 6-cm³ samples for carbonate concentration (coulometry) (~1/section), and
- 2-cm³ samples for x-ray diffraction (XRD) and/or inductively coupled plasma–mass spectrometry (ICP-MS) as needed.

In addition, individual sample requests for intervals recovered in only one hole, such as some of the deeper XCB intervals, will be sampled on the ship with the approval of the SAC. Some of the samples for SAC-approved pilot studies may also be taken during the cruise. All scientific shipboard party members will participate in the sampling effort, regardless of their personal sampling plan.

Postcruise Sampling of Critical Intervals and Stratigraphic Splices

Whenever possible, samples for postcruise research will be taken from the splice constructed by hole-to-hole correlation of cores during the cruise. Such sampling will maximize integration and impact of scientific results. Because it takes a few days to complete the composite depth section and splice (and more time to prepare adequate sampling templates), high-resolution sampling will not be possible during the cruise. This is also true for low- and high-resolution sampling of “critical intervals,” which include the K/T, P/E, and E/O boundaries. All sampling for postcruise research, except for special cases mentioned above, will therefore be deferred to one or more postcruise sampling party(ies) ~4–5 months postcruise in Bremen, Germany.

Sample Requests

It is the cruise participants’ responsibility to read and understand the ODP Sample Distribution, Data Distribution, and Publications Policy, which can be found at <http://www-odp.tamu.edu/publications/policy.html>.

Sample requests can be submitted by shipboard and shore-based participants at any time. Participants are asked to submit a request no later than 3 months precruise. Requests received precruise may have precedence over competing requests made during the cruise. All precruise requests will be posted on the ODP web page and the URL will be made available to the Leg 208 participants only. The SAC encourages participants to contact each other and coordinate sample requests and proposed work before the cruise to minimize this effort during the precious time available during the cruise. A draft sampling plan will be prepared at the early in the cruise by the scientific party, under the leadership of the SAC, and refined during the cruise based on the actual coring results. The final sampling plan will be highly integrated, ensuring that essential work will be completed on all intervals and that duplication of efforts will be avoided.

Downhole Logging Strategies

Downhole logging will provide physical and chemical proxy data for interpreting some of the fundamental questions Leg 208 is addressing. Where core recovery is poor, downhole logs may present the most reliable source of information; where core recovery is good, log data can be correlated with core data to produce more detailed and emphatic results. All sites deeper than 300 mbsf and all sites using XCB coring in the lower interval will be logged with the two standard logging tool strings, the triple combination (triple combo) and the Formation MicroScanner (FMS)/sonic string. The Well Seismic Tool (WST) will be deployed at a minimum of two sites. The characteristics of these logging tools are summarized below (additional information can be found at <http://www.ldeo.columbia.edu/BRG>).

The triple combo tool string includes the Dual Induction Tool (DIT), which measures indirect resistivity at three invasion depths, the Accelerator Porosity Sonde (APS), which measures porosity from epithermal neutron measurements, and the Hostile Environment Litho-Density Sonde (HLDS), which measures bulk density from Compton scattering and provides an indication of general lithology from the photoelectric effect. Commonly, the Hostile Environment Gamma Ray Sonde (HNGS) is added to this tool string. Following its past successes, the LDEO Multi-Sensor Spectral Gamma Ray Tool (MGT) will be added to the triple combo tool string, providing a vertical resolution three times higher than the standard gamma ray sonde. Density measurements will be crucial for calculating acoustic impedance values, and neutron porosity data will be particularly valuable for identifying intervals of high-porosity radiolarian ooze. The downhole natural gamma radiation and density values will be correlated with comparable analyses from

the MST, which will enable the precise depth matching of cored sections. MGT logs will be useful for cyclostratigraphic analysis of Upper Cretaceous and lower Cenozoic sequences.

The FMS/sonic tool string includes the Formation MicroScanner, which measures resistivity at centimeter resolution on four pads moving along the borehole, the General Purpose Inclinometer Tool (GPIT), and the Dipole Sonic Imager (DSI), which measures compressional and shear wave velocity, as well as cross-dipole and Stoneley waveforms. Chert horizons likely to present in some intervals at Leg 208 sites show up exceptionally well as resistive stripes on FMS images.

The WST is a single-axis checkshot tool used for zero-offset vertical seismic profiles (VSPs). It consists of a single geophone that is used to record acoustic waves generated by a water or air gun located near the sea surface. Downhole sonic data in conjunction with the density results, and checkshot surveys where necessary, allow generation of a velocity profile, a time/depth model, and synthetic seismograms. These results will be compared with the regional seismic sections to interpret the origin and geological significance of the major reflectors at a regional scale. WST checkshot surveys should be measured at 30- to 50-m spacing.

REFERENCES

- Axelrod, D.I., 1984. An interpretation of Cretaceous and Tertiary biota in polar regions. *Palaeogeogr., Palaeoclimatol., Palaeoecol.*, 45:105–147.
- Barrera, E., and Huber, B.T., 1991. Paleogene and early Neogene oceanography of the southern Indian Ocean: Leg 119 foraminifer stable isotope results. In Barron, J., Larsen, B., et al., *Proc. ODP, Sci. Results*, 119: College Station, TX (Ocean Drilling Program), 693–717.
- Barrera, E., and Huber, B.T., 1993. Eocene to Oligocene oceanography and temperatures in the Antarctic Indian Ocean. In Kennett, J.P., and Warnke, D.A., (Eds.), *The Antarctic Paleoenvironment: A Perspective on Global Change*. Antarct. Res. Ser., 49–65.
- Barron, E.J., 1985, Explanations for the Tertiary global cooling trend. *Palaeogeogr., Palaeoclimatol., Palaeoecol.*, 50:729–739.
- Berner, R.A., Lasaga, A.C., and Garrels, R.M., 1983. The carbonate-silicate geochemical cycle and its effect on atmospheric carbon dioxide over the past 100 million years. *Am. J. Sci.*, 283:641–683.
- Bice, K.L., Scotese, C.R., Seidov, D., and Barron, E.J., 2000. Quantifying the role of geographic change in Cenozoic ocean heat transport using uncoupled atmosphere and ocean models. *Palaeogeogr., Palaeoclimatol., Palaeoecol.*, 161:295–310.
- Bralower, T.J., Thomas, D.J., Zachos, J.C., Hirschmann, M.M., Röhl, U., Sigurdsson, H., Thomas, E., and Whitney, D.L., 1997. High-resolution records of the late Paleocene thermal maximum and circum-Caribbean volcanism: is there a causal link? *Geology*, 25:963–966.
- Bralower, T.J., Zachos, J.C., Thomas, E., Parrow, M., Paull, C.K., Kelly, D.C., Premoli Silva, I., Sliter, W.V., and Lohmann, K.C., 1995. Late Paleocene to Eocene paleoceanography of the equatorial Pacific Ocean: stable isotopes recorded at Ocean Drilling Program Site 865, Allison Guyot. *Paleoceanography*, 10:841–865.
- Broecker, W.S., 1997. Thermohaline circulation, the Achilles heel of our climate system: will man-made CO₂ upset the current balance? *Science*, 278:1582–1588.
- Browning, J.V., Miller, K.G., and Pak, D.K., 1996. Global implications of lower to middle Eocene sequence boundaries on the New Jersey Coastal Plain—the Ice-house cometh. *Geology*, 24:639–642.
- Cande, S.C., and Kent, D.V., 1992. A new geomagnetic polarity time scale for the Late Cretaceous and Cenozoic. *J. Geophys. Res.*, 97:13917–13951.
- Chave, A.D., 1984. Lower Paleocene–Upper Cretaceous magnetostratigraphy, Sites 525, 527, 528, and 529, Deep Sea Drilling Project Leg 74. In Moore, T.C., Jr., Rabinowitz, P.D., et al., *Init. Repts. DSDP*, 74: Washington (U.S. Govt. Printing Office), 525–532.
- Clyde, W.C., and Gingerich, P.D., 1998. Mammalian community response to the Latest Paleocene Thermal Maximum: an isotaphonomic study in the northern Big-horn Basin, Wyoming. *Geology*, 26:1011–1014.
- Corfield, R., and Cartlidge, J., 1992. Oceanographic and climatic implications of the Palaeocene carbon isotope maximum. *Terra Nova*, 4:443–455.

- Corfield, R., and Norris, R., 1996. Deep water circulation in the Paleocene ocean. *In* Knox, R.W., Corfield, R.M., and Dunay, R.E. (Eds.), *Correlation of the Early Paleogene in Northwest Europe*. Spec. Publ.—Geol. Soc. London, 101:443–456.
- D’Hondt, S., Donaghay, P., Zachos, J.C., Luttenberg, D., and Lindinger, M., 1998. Organic carbon fluxes and ecological recovery from the Cretaceous–Tertiary mass extinction. *Science*, 282:276–279.
- D’Hondt, S., and Keller, G., 1991. Some patterns of planktic foraminiferal assemblage turnover at the Cretaceous/Tertiary boundary. *Mar. Micropaleontol.*, 17:77–118.
- D’Hondt, S., King, J., and Gibson, C., 1996. Oscillatory marine response to the Cretaceous–Tertiary impact. *Geology*, 24:611–614.
- Dickens, G.R., 2000. Methane oxidation during the late Palaeocene Thermal Maximum. *Bull. Soc. Geol. France*, 171:37–49.
- Dickens, G.R., Castillo, M.M., and Walker, J.G.C., 1997. A blast of gas in the latest Paleocene: simulating first-order effects of massive dissociation of oceanic methane hydrate. *Geology*, 25:259–262.
- Dickens, G.R., O’Neil, J.R., Rea, D.K., and Owen, R.M., 1995. Dissociation of oceanic methane hydrate as a cause of the carbon isotope excursion at the end of the Paleocene. *Paleoceanography*, 10:965–971.
- Diester-Haass, L., and Zahn, R., 2001. Paleoproductivity increase at the Eocene–Oligocene climatic transition: ODP/DSDP Sites 763 and 592. *Palaeogeogr., Palaeoclimatol., Palaeoecol.*, 172:153–170.
- Eldholm, O., and Thomas, E., 1993. Environmental impact of volcanic margin formation. *Earth Planet. Sci. Lett.*, 117:319–329.
- Estes, R., and Hutchinson, J.H., 1980. Eocene lower vertebrates from Ellesmere Island, Canadian Arctic archipelago. *Palaeogeogr., Palaeoclimatol., Palaeoecol.*, 30:325–347.
- Gibson, T.G., Bybell, L.M., and Owens, J.P., 1993. Latest Paleocene lithologic and biotic events in neritic deposits of southwestern New Jersey. *Paleoceanography*, 8:495–514.
- Hambrey, M.J., Ehrmann, W.U., and Larsen, B., 1991. Cenozoic glacial record of the Prydz Bay continental shelf, East Antarctica. *In* Barron, J., Larsen, B., et al., *Proc. ODP, Sci. Results*, 119: College Station, TX (Ocean Drilling Program), 77–132.
- Herbert, T.D., and D’Hondt, S.L., 1990. Precessional climate cyclicity in Late Cretaceous–early Tertiary marine sediments: a high resolution chronometer of Cretaceous–Tertiary boundary events. *Earth Planet. Sci. Lett.*, 99:263–275.
- Herbert, T.D., Premoli Silva, I., Erba, E., and Fischer, A.G., 1995. Orbital chronology of Cretaceous–Paleogene marine strata. *In* Kent, W.A.B. (Ed.), *Geochronology, Time Scales, and Global Stratigraphic Correlation*. Spec. Publ.—SEPM, 81–93.
- Hsü, K.J., He, Q., McKenzie, J.A., Weissert, H., Perch-Nielsen, C., Oberhansli, H., Kelts, K., LaBrecque, J., Tauxe, L., Krahenbuhl, U., Percival, S.F., Wright, R., Karpoff, A.M., Petersen, N., Tucker, P., Poore, R.Z., Gombos, A.M., Posciotto, K., Carman, M.F., and Schreiber, E., 1982. Mass mortality and its environmental and evolutionary consequences. *Science*, 216:249–256.
- Kaiho, K., Arinobu, T., Isihwatar, R., Morgans, H.E.G., Okada, H., Takeda, N., Tazaki, K., Zhou, G., Kajiwara, Y., Matsumoto, R., Hirai, A., Niitsuma, N., and Wada, H.,

1996. Latest Paleocene benthic foraminiferal extinction and environmental changes at Tawanui, New Zealand. *Paleoceanography*, 11:447–465.
- Kelly, D.C., Bralower, T.J., and Zachos, J.C., 1998. Evolutionary consequences of the Latest Paleocene Thermal Maximum for tropical planktonic foraminifera. *Palaeogeogr., Palaeoclimatol., Palaeoecol.*, 141:139–161.
- Kelly, D.C., Bralower, T.J., Zachos, J.C., Premoli Silva, I., and Thomas, E., 1996. Rapid diversification of planktonic foraminifera in the tropical Pacific (ODP Site 865) during the late Paleocene Thermal Maximum. *Geology*, 24:423–426.
- Kennett, J.P., and Shackleton, N.J., 1976. Oxygen isotopic evidence for the development of the psychrosphere 38 Myr ago. *Nature*, 260:513–515.
- Kennett, J.P., and Stott, L.D., 1990. Proteus and Proto-oceanus: ancestral Paleogene oceans as revealed from Antarctic stable isotopic results: ODP Leg 113. In Barker, P.F., Kennett, J.P., et al., *Proc. ODP, Sci. Results*, 113: College Station, TX (Ocean Drilling Program), 865–880.
- , 1991. Abrupt deep-sea warming, paleoceanographic changes and benthic extinctions at the end of the Palaeocene. *Nature*, 353:225–229.
- Koch, P.L., Zachos, J.C., and Dettman, D.L., 1995. Stable isotope stratigraphy and palaeoclimatology of the Palaeogene Bighorn Basin. *Palaeogeogr. Palaeoclimatol. Palaeoecol.*, 115:61–89.
- Koch, P.L., Zachos, J.C., and Gingerich, P.D., 1992. Correlation between isotope records in marine and continental carbon reservoirs near the Palaeocene/Eocene boundary. *Nature*, 358:319–322.
- Mikolajewicz, U., Maier-Reimer, E., Crowley, T.J., and Kim, K.-Y., 1993. Effect of Drake and Panamanian gateways on the circulation of an ocean model. *Paleoceanography*, 8:409–426.
- Miller, K.G., Janecek, T.R., Katz, M.E., and Keil, D.J., 1987. Abyssal circulation and benthic foraminiferal changes near the Paleocene/Eocene boundary. *Paleoceanography*, 2:741–761.
- Miller, K.G., and Katz, M.E., 1987. Oligocene to Miocene benthic foraminiferal and abyssal circulation changes in the North Atlantic. *Micropaleontology*, 33:97–149.
- Miller, K.G., Mountain, G.S., Browning, J.V., Kominz, M., Sugarman, P.J., Christie-Blick, N., Katz, M.E., and Wright, J.D., 1998. Cenozoic global sea level, sequences, and the New Jersey transect: results from coastal plain and continental slope drilling. *Rev. Geophys.*, 36:569–601.
- Miller, K.G., Wright, J.D., and Fairbanks, R.G., 1991. Unlocking the Ice House: Oligocene–Miocene oxygen isotopes, eustasy, and margin erosion. *J. Geophys. Res.*, 96:6829–6848.
- Moore, T.C., Jr., Rabinowitz, P.D., et al., 1984. *Init. Repts. DSDP*, 74: Washington (U.S. Govt. Printing Office).
- Norris, R.D., Kroon, D., and Klaus, A., 2001. Introduction: Cretaceous–Paleogene climatic evolution of the western North Atlantic: results from ODP Leg 171B, Blake Nose. In Kroon, D., Norris, R.D., and Klaus, A. (Eds.), *Proc. ODP, Sci. Results*, 171B: College Station TX (Ocean Drilling Program), 1–11.
- Norris, R.D., and Röhl, U., 1999. Carbon cycling and chronology of climate warming during the Palaeocene/Eocene transition. *Nature*, 401:775–778.

- Oglesby, R.J., 1991. Joining Australia to Antarctica: GCM implications for the Cenozoic record of Antarctic glaciation. *Clim. Dynam.*, 6:13–22.
- Pak, D.K., and Miller, K.G., 1992. Paleocene to Eocene benthic foraminiferal isotopes and assemblages: implications for deepwater circulation. *Paleoceanography*, 7:405–422.
- Paytan, A., Kastner, M., Campbell, D., and Thiemens, M.H., 1998. Sulfur isotopic composition of Cenozoic seawater sulfate. *Science*, 282:1459–1462.
- Pearson, P.N., and Palmer, M.R., 2000. Atmospheric carbon dioxide concentrations over the past 60 million years. *Nature*, 406:695–699.
- Peterson, L.C., and Backman, J., 1990. Late Cenozoic carbonate accumulation and the history of the carbonate compensation depth in the western equatorial Indian Ocean. In Duncan, R.A., Backman, J., Peterson, L.C., et al., *Proc. ODP, Sci. Results*, 115: College Station, TX (Ocean Drilling Program), 467–507.
- Rabinowitz, P.D., and Simpson, E.S.W., 1984. Geophysical site survey results on the Walvis Ridge. In Moore, T.C., Jr., Rabinowitz, P.D., et al., *Init. Repts. DSDP*, 74: Washington (U.S. Govt. Printing Office), 795–825.
- Raymo, M.E., Ruddiman, W.F., Shackleton, N.J., and Oppo, D.W., 1990. Evolution of Atlantic-Pacific $\delta^{13}\text{C}$ gradients over the last 2.5 m.y. *Earth Planet. Sci. Lett.*, 97:353–368.
- Rea, D.K., Zachos, J.C., Owen, R.M., and Gingerich, P.D., 1990. Global change at the Paleocene–Eocene boundary: climatic and evolutionary consequences of tectonic events. *Palaeogeogr., Palaeoclimatol., Palaeoecol.*, 79:117–128.
- Rind, D., and Chandler, M., 1991. Increased ocean heat transport and warmer climate. *J. Geophys. Res.*, 96:7437–7461.
- Robert, C., and Kennett, J.P., 1994. Antarctic subtropical humid episode at the Paleocene–Eocene boundary: clay mineral evidence. *Geology*, 22:211–214.
- , 1997. Antarctic continental weathering changes during Eocene–Oligocene cryosphere expansion: clay mineral and oxygen isotope evidence. *Geology*, 25:587–590.
- Röhl, U., Bralower, T.J., Norris, R.D., and Wefer, G., 2000. New chronology for the late Paleocene Thermal Maximum and its environmental implications. *Geology*, 28:927–930.
- Salamy, K.A., and Zachos, J.C., 1999. Latest Eocene–early Oligocene climate change and Southern Ocean fertility: inferences from sediment accumulation and stable isotope data. *Palaeogeogr., Palaeoclimatol., Palaeoecol.*, 145:61–77.
- Schmitz, B., Charisi, S.D., Thompson, E.I., and Speijer, R.P., 1997. Barium, SiO_2 (excess), and P_2O_5 as proxies of biological productivity in the Middle East during the Palaeocene and the latest Palaeocene benthic extinction event. *Terra Nova*, 9:95–99.
- Shackleton, N., and Boersma, A., 1981. The climate of the Eocene ocean. *J. Geol. Soc. London*, 138:153–157.
- Shackleton, N.J., and Hall, M.A., 1984. Carbon isotope data from Leg 74 sediments, In Moore, T.C., Jr., Rabinowitz, P.D., et al., *Init. Repts. DSDP*, 74: Washington (U.S. Govt. Printing Office), 613–619.

- Sloan, L.C., and Barron, E.J., 1992. A comparison of Eocene climate model results to quantified paleoclimatic interpretations. *Palaeogeogr., Palaeoclimatol., Palaeoecol.*, 93:183–202.
- Sloan, L.C., and Rea, D.K., 1996. Atmospheric carbon dioxide and early Eocene climate—a general circulation modeling sensitivity study. *Palaeogeogr., Palaeoclimatol., Palaeoecol.*, 119:275–292.
- Sloan, L.C., Walker, J.C.G., and Moore, T.C., Jr., 1995. Possible role of oceanic heat transport in early Eocene climate. *Paleoceanography*, 10:347–356.
- Sloan, L.C., Walker, J.C.G., Moore, T.C., Rea, D.K., and Zachos, J.C., 1992. Possible methane-induced polar warming in the early Eocene. *Nature*, 357:320–322.
- Stott, L.D., and Kennett, J.P., 1989. New constraints on early Tertiary palaeoproductivity from carbon isotopes in foraminifera. *Nature*, 342:526–529.
- , 1990. Antarctic Paleogene planktonic foraminifer biostratigraphy: ODP Leg 113, Sites 689 and 690. In Barker, P.F., Kennett, J.P., et al., *Proc. ODP, Sci. Results*, 113: College Station, TX (Ocean Drilling Program), 549–569.
- Thomas, D.J., Bralower, T.J., and Zachos, J.C., 1999. New evidence for subtropical warming during the late Paleocene Thermal Maximum: stable isotopes from Deep Sea Drilling Project Site 527, Walvis Ridge. *Paleoceanography*, 14:561–570.
- Thomas, E., and Gooday, A.J., 1996. Cenozoic deep-sea benthic foraminifers: tracers for changes in oceanic productivity? *Geology*, 24:355–358.
- Thomas, E., and Shackleton, N., 1996. The Palaeocene–Eocene benthic foraminiferal extinction and stable isotope anomalies. In Knox, R.W.O'B., Corfield, R.M., and Dunay, R.E. (Eds.), *Correlation of the Early Paleogene in Northwest Europe*. Spec. Publ.—Geol. Soc. London, 101:401–441.
- Thomas, E., and Ward, P.D.E., 1990. Late Cretaceous–early Eocene mass extinctions in the deep sea. In Sharpton, V.L., and Ward, P.D. (Eds.), *Global Catastrophes in Earth History*. Spec. Publ.—Geol. Soc. Am., 247.
- Thomas, E., Zachos, J.C., Bralower, T.J., 2000. Deep-sea environments on a warm Earth: latest Paleocene–early Eocene. In Huber, B.T., MacLeod, K.G.E., and Wing, S.L.E. (Eds.), *Warm Climates in Earth History*: Cambridge (Cambridge Univ. Press), 132–160.
- Thunell, R.C., and Corliss, B.H., 1986. Late Eocene–early Oligocene carbonate sedimentation in the deep sea. In Pomeroy, C., and Premoli Silva, I. (Eds.), *Terminal Eocene Events*: Amsterdam (Elsevier), Dev. in Palaeontol. and Stratigr., 9:363–380.
- van Andel, T.H., 1975. Mesozoic/Cenozoic calcite compensation depth and the global distribution of calcareous sediments. *Earth Planet. Sci. Lett.*, 26:187–194.
- Wolfe, J.A., 1980. Tertiary climates and floristic relationships at high latitudes in the Northern Hemisphere. *Palaeogeogr., Palaeoclimatol., Palaeoecol.*, 30:313–323.
- Zachos, J.C., and Arthur, M.A., 1986. Paleocyanography of the Cretaceous/Tertiary boundary event: inferences from stable isotopic and other data. *Paleoceanography*, 1:5–26.
- Zachos, J.C., Arthur, M.A., and Dean, W.E., 1989. Geochemical evidence for suppression of pelagic marine productivity at the Cretaceous/Tertiary boundary. *Nature*, 337:61–64.

- Zachos, J.C., Breza, J.R., and Wise, S.W., 1992. Early Oligocene ice-sheet expansion on Antarctica: stable isotope and sedimentological evidence from Kerguelen Plateau, southern Indian Ocean. *Geology*, 20:569–573.
- Zachos, J.C., Lohmann, K.C., Walker, J.C.G., and Wise, S.W., Jr., 1993. Abrupt climate changes and transient climates during the Paleogene: a marine perspective. *J. Geol.*, 101:191–213.
- Zachos, J.C., Pagani, M., Sloan, L., Thomas, E., and Billups, K., 2001. Trends, rhythms, and aberrations in global climate 65 Ma to present. *Science*, 292:686–693.
- Zachos, J.C., Quinn, T.M., and Salamy, K., 1996. Earliest Oligocene climate transition: constraints from high resolution (10^4 yr) deep-sea foraminiferal $\delta^{18}\text{O}$ and $\delta^{13}\text{C}$ time-series. *Paleoceanography*, 21:251–266.
- Zachos, J.C., Stott, L.D., and Lohmann, K.C., 1994. Evolution of early Cenozoic marine temperatures. *Paleoceanography*, 9:353–387.

TABLE CAPTIONS

Table 1. Leg 208 proposed sites.

Table 2. Leg 208 operations plan and time estimates.

FIGURE CAPTIONS

Figure 1. Overview map of Walvis Ridge. The boxes indicate locations of more detailed maps to follow.

Figure 2. Area of Leg 208 operations on Walvis Ridge. *Meteor* track lines cross existing DSDP Leg 74 and proposed ODP Leg 208 sites.

Figure 3. Area of Leg 208 operations on central Walvis Ridge. Open circles = proposed primary and alternate sites.

Figure 4. The location of Leg 74 sites along *Meteor* line GeoB01-030.

Figure 5. Lithostratigraphy of DSDP Leg 74 Sites 528 and 529 (Moore, Rabinowitz, et al., 1984). White gaps = unrecovered intervals.

Figure 6. Low-resolution bulk sediment carbon isotope stratigraphies for the Leg 74 sites (Shackleton and Hall, 1984).

Figure 7. Cenozoic deep-sea stable isotope record based on a compilation of benthic foraminifer data from several dozen pelagic cores (modified from Zachos et al., 2001). The oxygen isotope record primarily reflects on changes in deepwater temperature and ice volume.

Figure 8. Benthic foraminifer isotope records of the Paleocene–Eocene Thermal Maximum (PETM) (Zachos et al., 2001).

Figure 9. Box model simulated response of the ocean C-isotopes and lysocline to gradual (10 k.y.) input of 1200 gigatons of methane-derived carbon into the ocean (Dickens, 2000).

Figure 10. DSDP Site 527 planktic foraminiferal stable isotope records plotted against depth for the three size fractions of *Acarinina soldadoensis* (90–150, 150–250, and 300–355 μm). The gray band indicates the position of the claystone interval within Core 24. The CaCO_3 record reveals a low carbonate layer coincident with the PETM (Thomas et al., 1999).

Figure 11. A composite of the *Cibicidoides* spp. stable carbon and oxygen isotope records for Sites 522, 744, and 689 plotted as a function of age for the period 31–35 Ma (Zachos et al., 1996; Diester-Haas and Zahn, 1996). The EOGM spans the interval 33.0–33.4 Ma. Age model is based on the geomagnetic polarity timescale of Cande and Kent (1992). Lower scale shows bottom-water temperature for an ice-free world (pre-EOGM) assuming calcite formation in oxygen isotope equilibrium (Zachos et al., 1996).

Figure 12. DSDP Site 525 on multichannel seismic line GeoB01-031 and DSDP Site 528 stratigraphic column (from Moore, Rabinowitz, et al., 1984).

Figure 13. DSDP Site 525 and proposed Sites WALV-8A, WALV-8B and WALV-8C on multichannel seismic line GeoB01-031.

Figure 14. Common depth point–annotated track chart around proposed Sites WALV-8, WALV-9, and WALV-10 (shown as open circles). Solid circles = existing DSDP sites. Bold lines = profiles included into the data package.

Figure 15. Common depth point–annotated track chart around proposed sites WALV-11A, WALV-11B, WALV-11C, and WALV-11D (shown as open circles). Solid circles = existing DSDP sites. Bold lines = profiles included into the data package.

Figure 16. Common depth point–annotated track chart around proposed sites WALV-12A, WALV-12B, and WALV-12C (shown as open circles). Bold lines = profiles included into the data package.

Table T1. Leg 208 proposed sites.

Proposed site	Priority	Order of drilling	Latitude	Longitude	Water depth (m)	Total sediment thickness TWT (ms)	Approximate total sediment thickness (m)	Target depth (mbsf)	Approved penetration depth (mbsf)	Seismic lines	Digital parasound	Reference site
WALV-8A	2		28°31.96'S	2°50.73'E	2530	690	621	500	600	GeoB01-031, CDP 7884; GeoB01-046, CDP 1047	Geob01-031, 20.01.01, 17:42h, Geob01-046, 23.01.01, 23:25h	DSDP 525
WALV-8B	1	2	28°37.85'S	2°52.29'E	2557	590	531	450	530	GeoB01-031, CDP 6766; GeoB01-048, CDP 647	Geob01-031, 20.01.01, 16:46h, Geob01-048, 24.01.01, 01:01h	DSDP 525
WALV-8C	2		28°47.74'S	2°54.83'E	2531	460	414	400	400	GeoB01-031, CDP 4892; GeoB01-052, CDP 4175	Geob01-031, 20.01.01, 15:13h, Geob01-052, 24.01.01, 15:16h	DSDP 525
WALV-9A	1	3	28°51.19'S	2°37.14'E	2979	650	585	360	360	GeoB01-048, CDP 4138; GeoB01-055, CDP 4600	Geob01-048, 24.01.01, 03:57h, Geob01-055, 25.01.01, 01:05h	DSDP 529
WALV-9B	2		28°50.10'S	2°38.36'E	3083	570	513	400	500	GeoB01-048, CDP 3854; GeoB01-030, distance to site 1630 m, azimuth to site 225°; GeoB01-055, dist. to site 2840 m, azimuth to site 45°	Geob01-048, 24.01.01, 03:57h, Geob01-055, 25.01.01, 01:05h	DSDP 529
WALV-10A	2		28°31.49'S	2°19.44'E	3820	460	450.8	450	475	GeoB01-030, CDP 12623; GeoB01-044, CDP 2757	Geob01-030, 19.01.01, 22:47h, Geob01-044, 23.01.01, 17:51h	DSDP 528
WALV-10B	2		28°32.62'S	2°22.47'E	3719	490	480.2	450	450	GeoB01-059, CDP 2560; GeoB01-066, CDP 711, distance to site 1610 m, azimuth to site 143°	Geob01-059, 25.01.01, 11:08h	DSDP 528
WALV-10C	1	4	28°28.54'S	2°19.37'E	3842	480	470.4	450	450	GeoB01-059, CDP 1649; GeoB01-044, CDP 3024, dist. to site 4270 m, azimuth to site 330°; GeoB01-064, CDP 1215, dist. to site 5610 m, azimuth to site 150°	Geob01-059, 25.01.01, 10:22h	DSDP 528
WALV-10D	2		28°24.55'S	2°16.79'E	3961	450	441	450	450	GeoB01-059, CDP 800; GeoB01-064, CDP 1215, dist. to site 2860 m, azimuth to site 330°; GeoB01-062, CDP 1405, dist. to site 3160 m, azimuth to site 151°	Geob01-059, 25.01.01, 10:22h	DSDP 528
WALV-11A	2		28°2.49'S	1°45.80'E	4434	360	324	300	350	GeoB01-030, CDP 4932; GeoB01-039, CDP 4377	Geob01-030, 19.01.01, 16:24h, Geob01-039, 22.01.01, 22:23h	DSDP 527
WALV-11B	1	5	28°5.88'S	1°42.66'E	4375	360	324	300	330	GeoB01-039, CDP 3566; GeoB01-030, CDP 4932, dist. to site 8100 m, azimuth to site 219°	Geob01-039, 22.01.01, 21:42h	DSDP 527
WALV-11C	2		27°54.72'S	1°52.66'E	4313	340	306	280	350	GeoB01-039, CDP 6200; GeoB01-030, CDP 4932, dist. to site 18,220 m, azimuth to site 038°	Geob01-039, 22.01.01, 23:54h	DSDP 527
WALV-11D	2		28°5.52'S	1°10.15'E	4526	300	270	300	300	GeoB01-038b, CDP 2380	Geob01-038, 22.01.01, 15:15h	DSDP 527
WALV-12A	1	1	27°11.16'S	1°34.62'E	4762	280	252	230	340	GeoB01-035, CDP 2832	Geob01-035, 21.01.01, 12:26h	DSDP 527
WALV-12B	2		27°4.06'S	0°58.01'E	4726	240	216	200	360	GeoB01-036, CDP 3349 (moved per PPSP request)	Geob01-036, 21.01.01, 19:18h	DSDP 527
WALV-12C	2		26°49.61'S	0°48.63'E	4768	300	270	200	340	GeoB01-036, CDP 6438	Geob01-036, 21.01.01, 21:45h	DSDP 527
WALV-13B	2		24°37.70'S	4°40.69'E	3768	480	432	430	430	GeoB01-029b, CDP 2890	Geob01-029, 18.01.01, 00:08h	

Table T2. Leg 208 operations plan and time estimates.

Site	Location (lat/long)	Water depth (mbrf)	Operations	Transit (days)	Drilling (days)	Logging (days)
Rio de Janeiro Transit to WALV-12B: 2472 nmi @ 10.5 kt				9.0		
WALV-12A	27°11.16iS 01°34.62iE	4762	Hole A: APC to ~200 mbsf, Or, HF Hole B: APC to ~200 mbsf, Or Hole C: APC to ~200 mbsf, Or		1.5 1.4 1.8	
Transit from WALV-12B to WALV-8B: 100 nmi @ 10.5 kt				0.4		
WALV-8B	28°37.85iS 02°52.29iE	2557	Hole A: APC to ~250 mbsf, Or, HF, XCB to 450 mbsf Hole B: APC to ~250 mbsf, Or, XCB to 450 mbsf Hole C: APC to ~250 mbsf, Or Log: Triple combo, FMS-sonic, WST, and hole prep		3.5 3.0 1.5	1.7
Transit from WALV-8B to WALV-9A: 19 nmi @ 10.5 kt				0.1		
WALV-9A	28°51.19iS 02°37.14iE	2979	Hole A: APC to ~250 mbsf, Or, HF, XCB to 360 mbsf Hole B: APC to ~250 mbsf, Or, XCB to 360 mbsf Hole C: APC to ~250 mbsf, Or Log: Triple combo, FMS-sonic, and hole prep		2.4 2.0 1.6	1.1
Transit from WALV-9A to WALV-10C: 32 nmi @ 10.5 kt				0.1		
WALV-10C	28°28.54iS 02°19.37iE	3842	Hole A: APC to ~250 mbsf, Or, HF, XCB to 450 mbsf Hole B: APC to ~250 mbsf, Or, XCB to 450 mbsf Log: Triple combo, FMS-sonic, and hole prep		3.6 3.5	1.3
Transit from WALV-10C to WALV-11B: 36 nmi @ 10.5 kt				0.1		
WALV-11B	28°05.88iS 01°42.66iE	4375	Hole A: APC to ~250 mbsf, Or, HF, XCB to 300 mbsf Hole B: APC to ~250 mbsf, Or, XCB to 300 mbsf Hole C: APC to ~250 mbsf, Or Log: Triple combo, FMS-sonic, WST, and hole prep		2.7 2.2 2.0	1.8
Rio de Janeiro Transit to Port: 2202 nmi @ 10.5 kt				8.7		
SUBTOTAL:				18.4	32.7	5.9
TOTAL OPERATING DAYS:				57.0		
ALTERNATE SITES:						
WALV-8A	28°31.96iS 02°50.73iE	2530	Hole A: APC to ~250 mbsf, Or, HF, XCB to 600 mbsf Hole B: APC to ~250 mbsf, Or, XCB to 600 mbsf Log: Triple combo, FMS-sonic, WST, and hole prep		4.7 4.6	1.9
WALV-8C	28°47.74iS 02°54.83iE	2531	Hole A: APC to ~250 mbsf, Or, HF, XCB to 400 mbsf Hole B: APC to ~250 mbsf, Or, XCB to 400 mbsf Log: Triple combo, FMS-sonic, WST, and hole prep		2.5 2.5	1.6
WALV-9B	28°50.10iS 02°38.36iE	3083	Hole A: APC to ~250 mbsf, Or, HF, XCB to 360 mbsf Hole B: APC to ~250 mbsf, Or, XCB to 360 mbsf Hole C: APC to ~200 mbsf, Or Log: Triple Combo, FMS-Sonic, and Hole Prep		2.4 2.0 1.6	1.1
WALV-10A	28°31.49iS 02°19.44iE	3820	Hole A: APC to ~250 mbsf, Or, HF, XCB to 450 mbsf Hole B: APC to ~250 mbsf, Or, XCB to 450 mbsf Hole C: APC to ~250 mbsf, Or Log: Triple combo, FMS-sonic, WST, and hole prep		3.4 3.0 1.9	1.9
WALV-10B	28°32.62iS 02°22.47iE	3719	Hole A: APC to ~250 mbsf, Or, HF, XCB to 450 mbsf Hole B: APC to ~250 mbsf, Or, XCB to 450 mbsf Hole C: APC to ~250 mbsf, Or Log: Triple combo, FMS-sonic, WST, and hole prep		3.4 3.0 1.9	1.8

Table T2 (continued).

Site	Location (lat/long)	Water depth (mbrf)	Operations	Transit (days)	Drilling (days)	Logging (days)
WALV-10D	28°24.55iS	3961	Hole A: APC to ~250 mbsf, Or, HF, XCB to 450 mbsf		3.7	
	02°16.79iE		Hole B: APC to ~250 mbsf, Or, XCB to 450 mbsf		3.5	
			Log: Triple combo, FMS-sonic, WST, and hole prep			1.9
WALV-11A	28°02.49iS	4434	Hole A: APC to ~250 mbsf, Or, HF, XCB to 300 mbsf		2.6	
	01°45.80iE		Hole B: APC to ~250 mbsf, Or, XCB to 300 mbsf		2.1	
			Hole C: APC to ~250 mbsf, Or		2.1	
			Log: Triple combo, FMS-sonic, and hole prep			1.4
WALV-11C	27°54.72iS	4313	Hole A: APC to ~250 mbsf, Or, HF, XCB to 350 mbsf		2.9	
	01°52.66iE		Hole B: APC to ~250 mbsf, Or, XCB to 350 mbsf		2.4	
			Hole C: APC to ~250 mbsf, Or		2.0	
			Log: Triple combo, FMS-sonic, and hole prep			1.8
WALV-11D	28°05.52iS	4526	Hole A: APC to ~250 mbsf, Or, HF, XCB to 300 mbsf		2.6	
	01°10.15iE		Hole B: APC to ~250 mbsf, Or, XCB to 300 mbsf		2.1	
			Hole C: APC to ~250 mbsf, Or		2.1	
			Log: Triple combo, FMS-sonic, and hole prep			1.8
WALV-12B	27°04.06iS	4726	Hole A: APC to ~200 mbsf, Or, HF		1.8	
	00°58.01iE		Hole B: APC to ~200 mbsf, Or		1.4	
			Hole C: APC to ~200 mbsf, Or		1.9	
WALV-12C	26°49.61iS	4768	Hole A: APC to ~200 mbsf, Or, HF		1.5	
	00°48.63iE		Hole B: APC to ~200 mbsf, Or		1.4	
			Hole C: APC to ~200 mbsf, Or		1.8	
WALV-13B	24°37.70iS	3768	Hole A: APC to ~250 mbsf, Or, HF, XCB to 430 mbsf		3.3	
	04°40.69iE		Hole B: APC to ~250 mbsf, Or, XCB to 430 mbsf		3.1	
			Hole C: APC to ~250 mbsf, Or		1.9	
			Log: Triple combo, FMS-sonic, WST, and hole prep			1.8

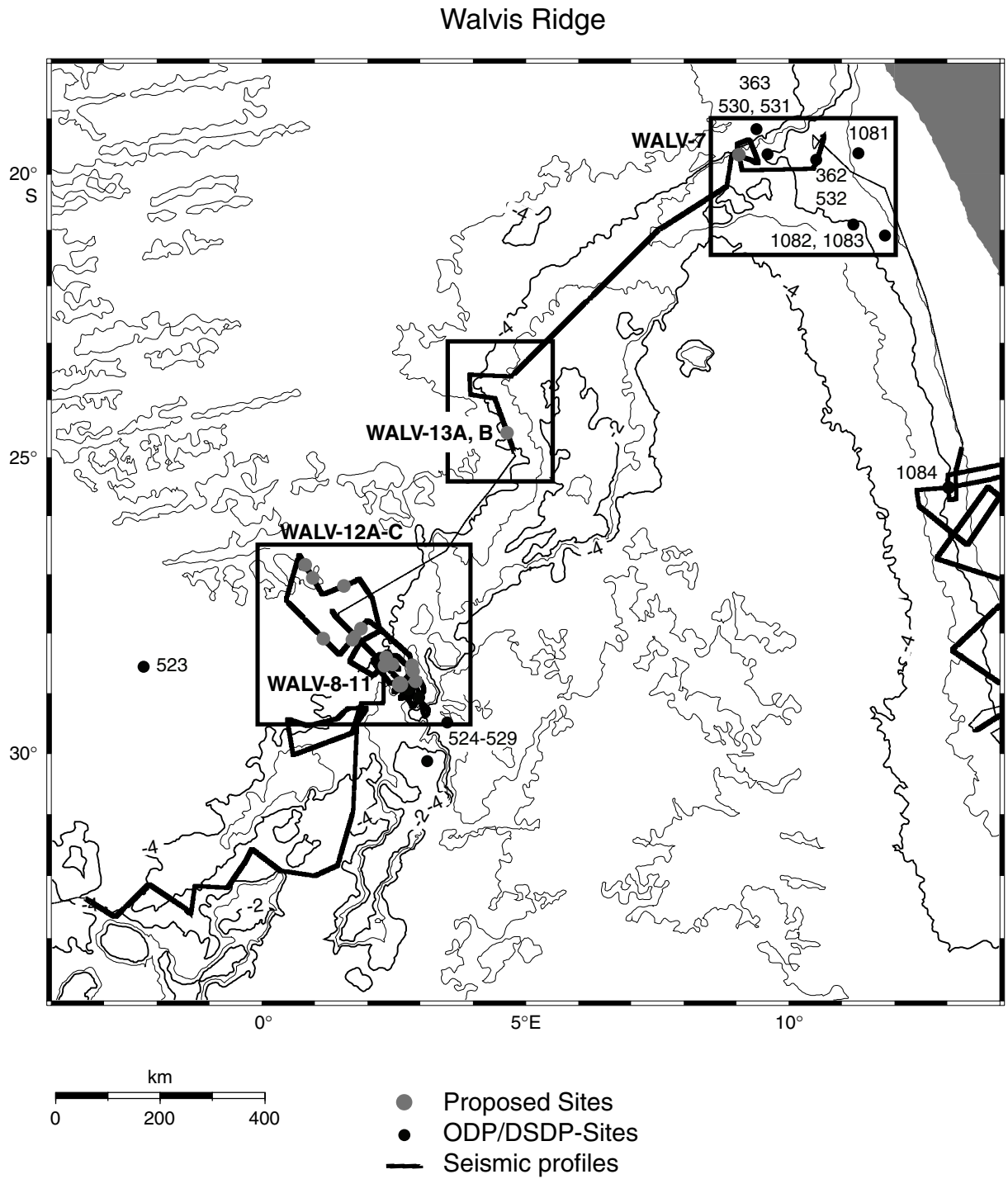


Figure F1

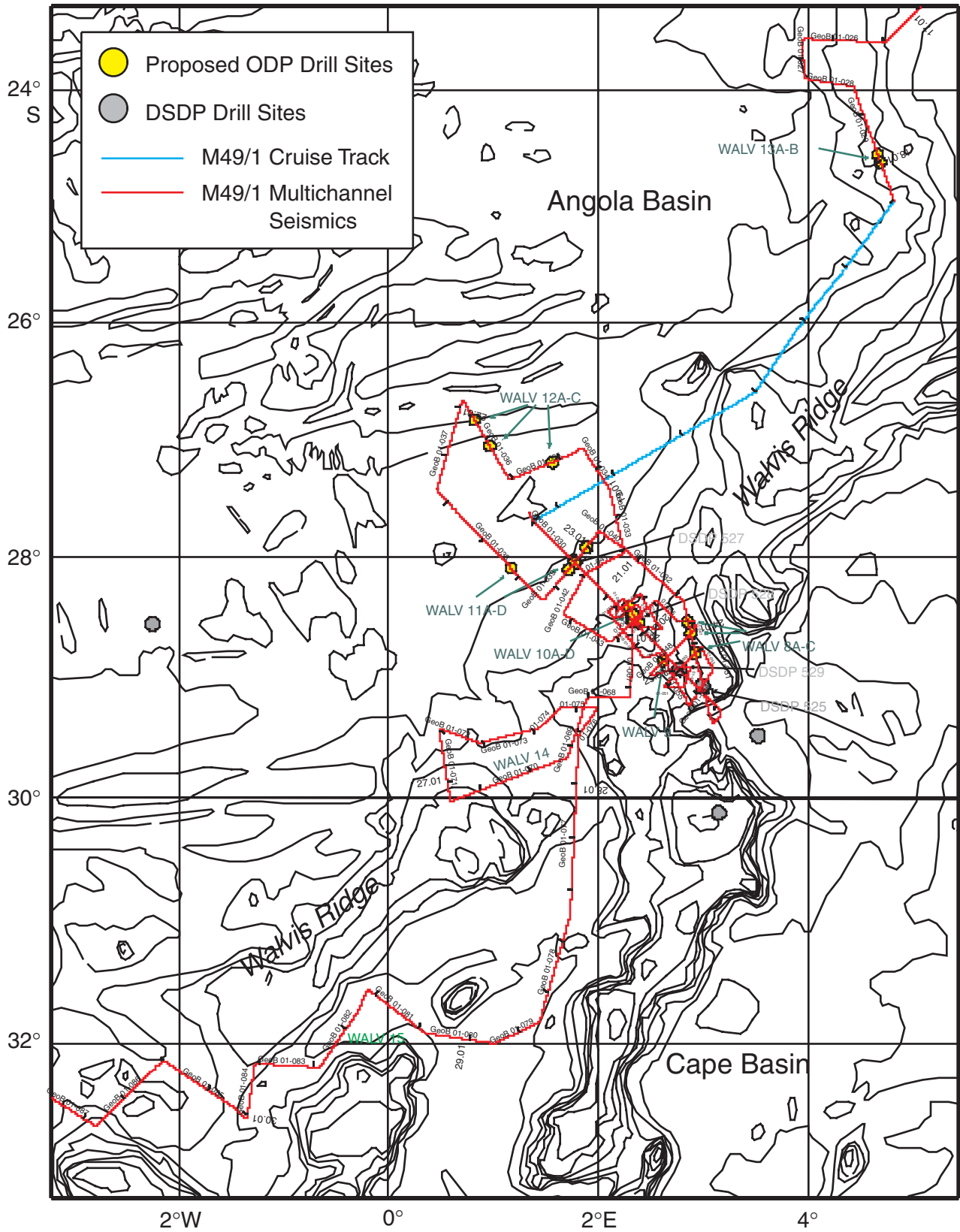


Figure F2

Multichannel Seismic Line GeoB 01-030: GI Gun 0.4 L (25 in³)

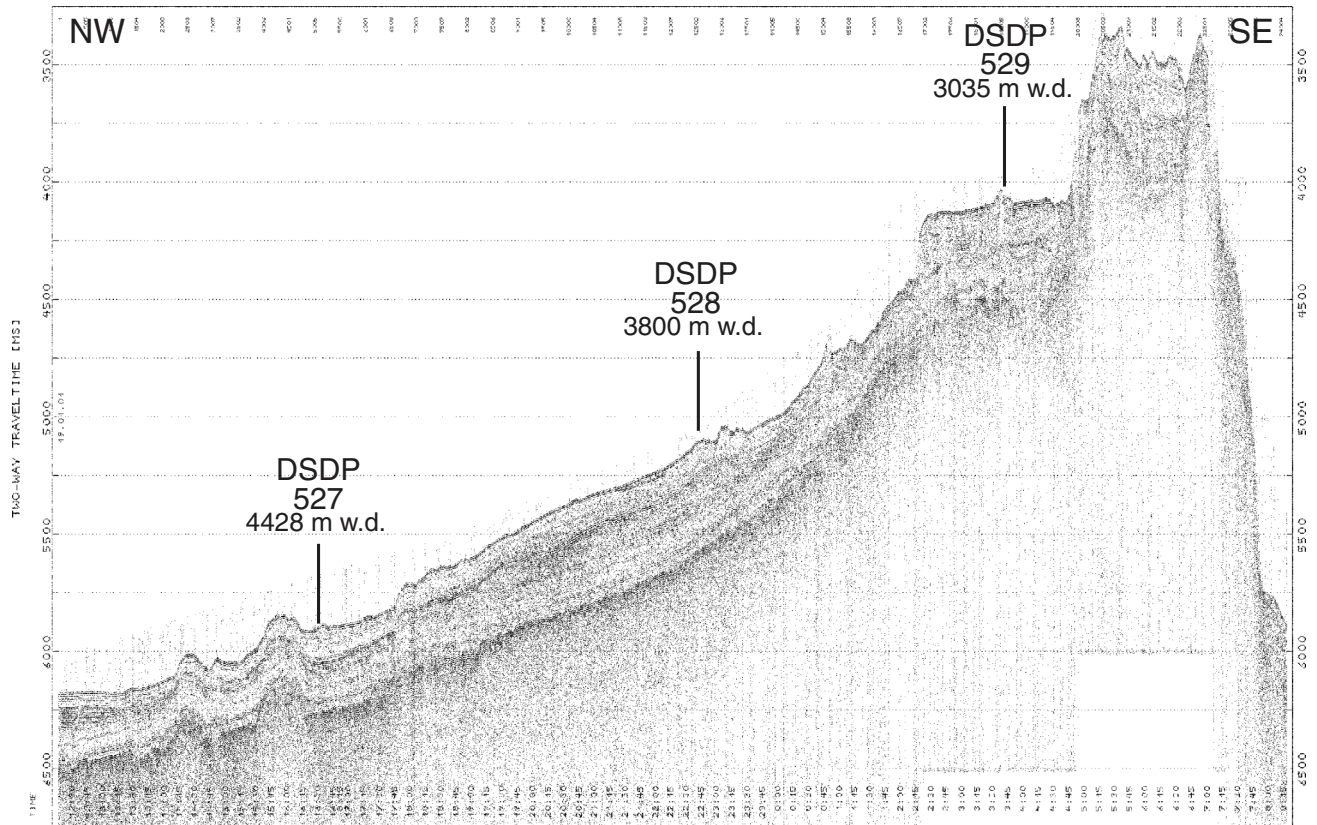


Figure F4

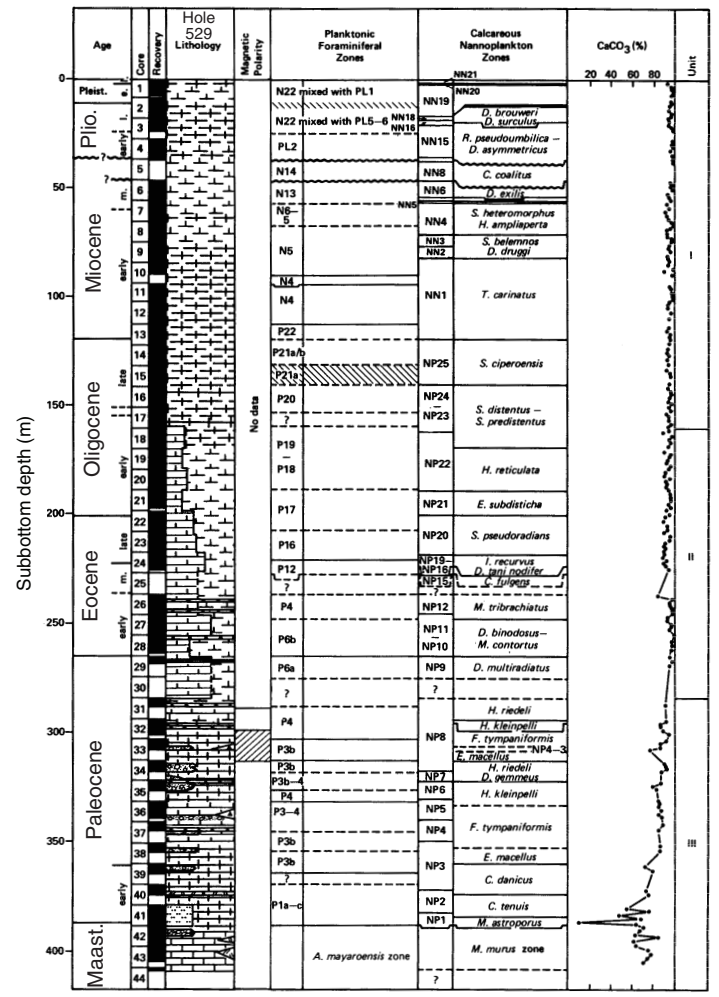
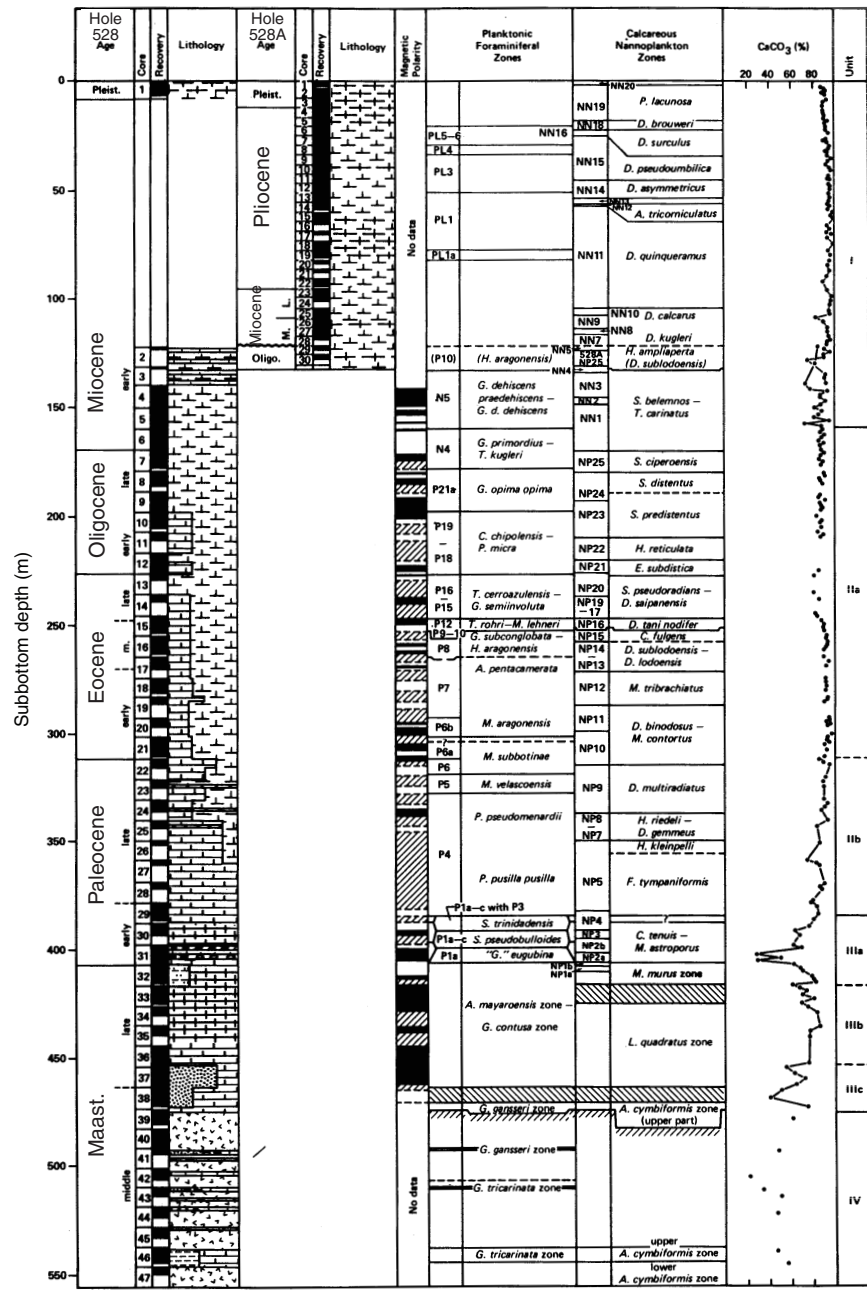


Figure F5

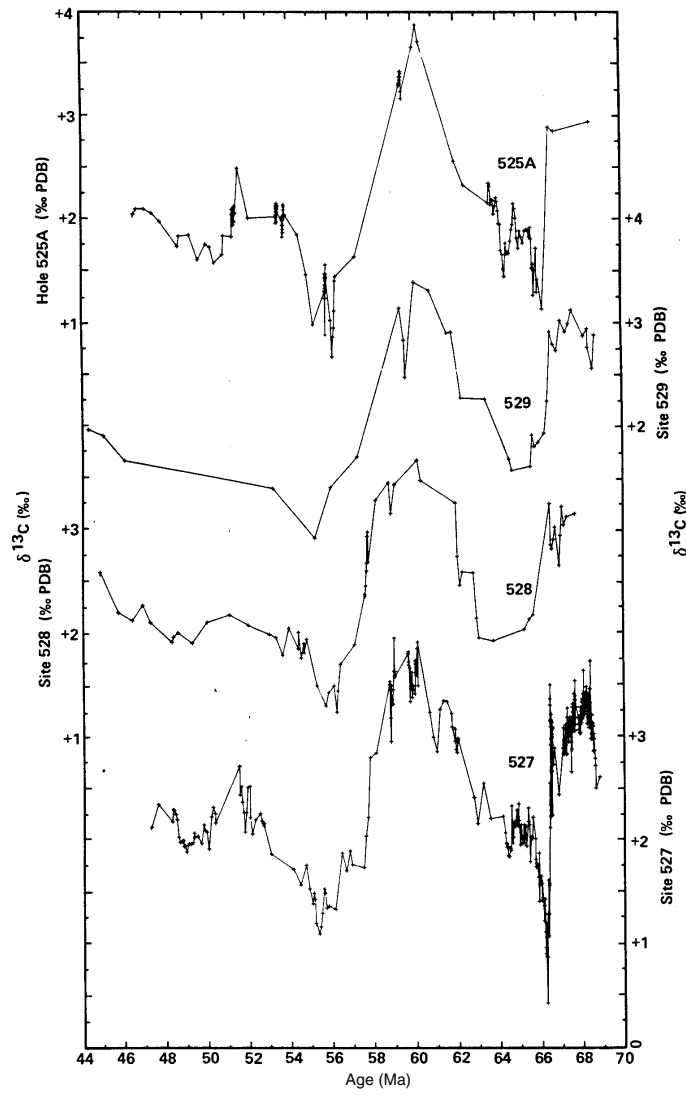


Figure F6

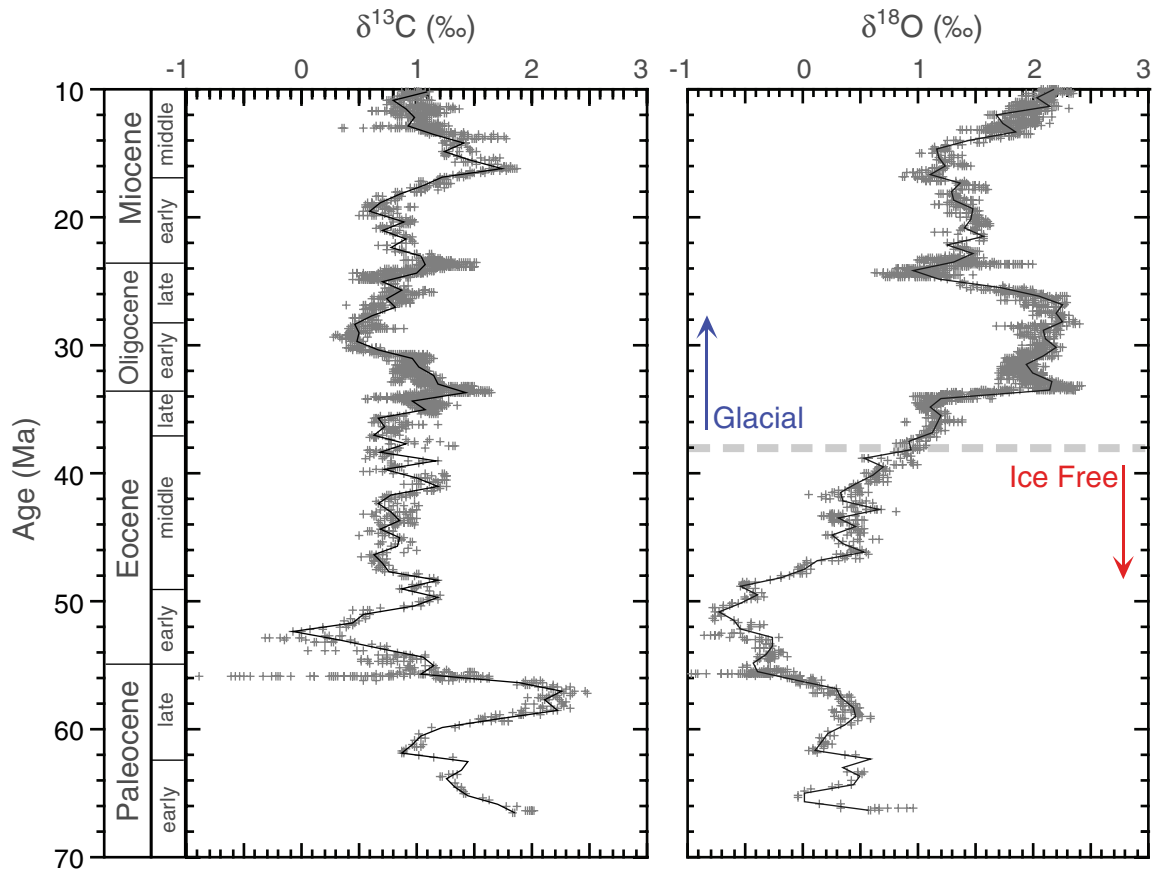


Figure F7

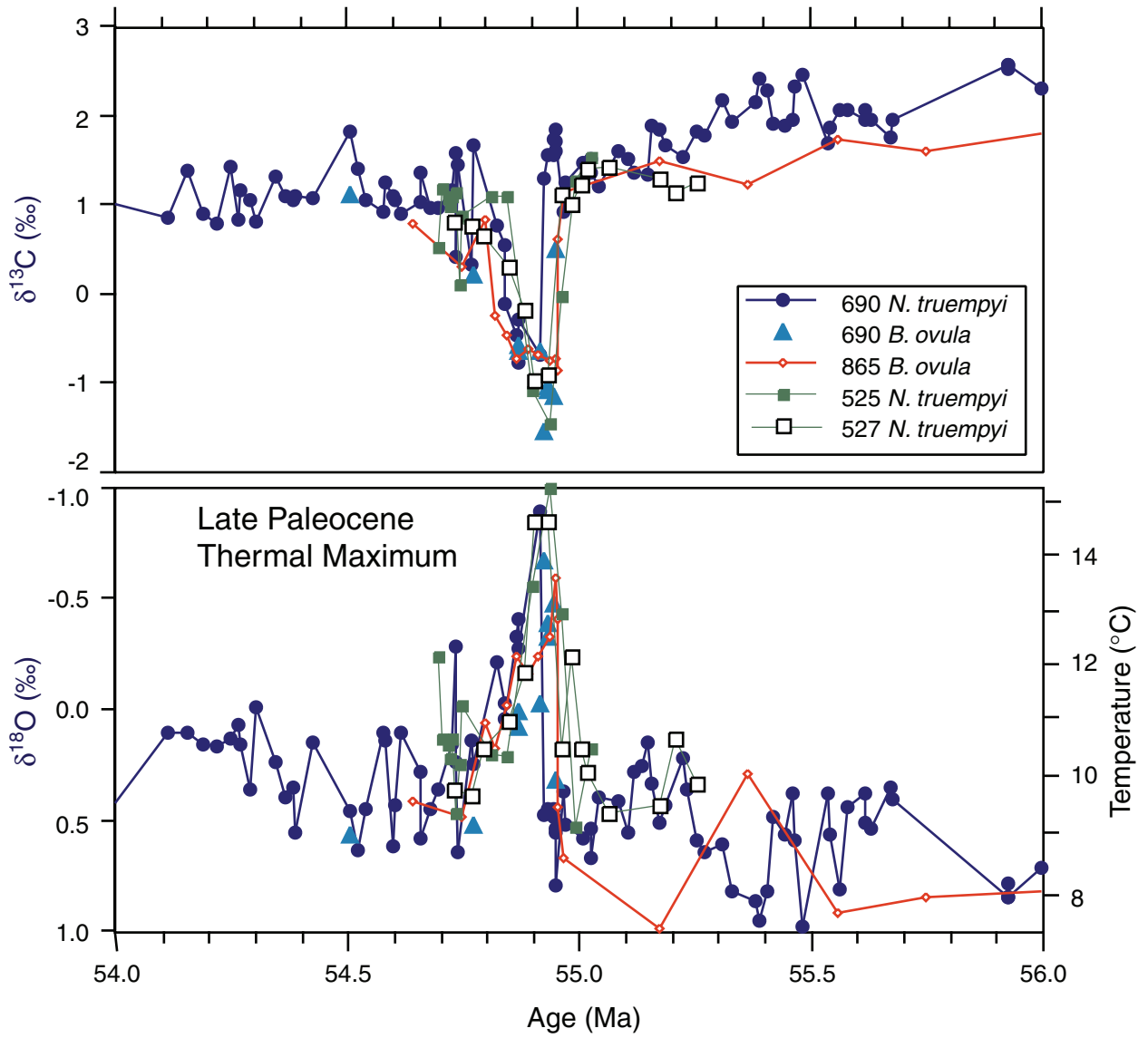


Figure F8

Model Simulation of Lysocline Response to Rapid Release of Carbon

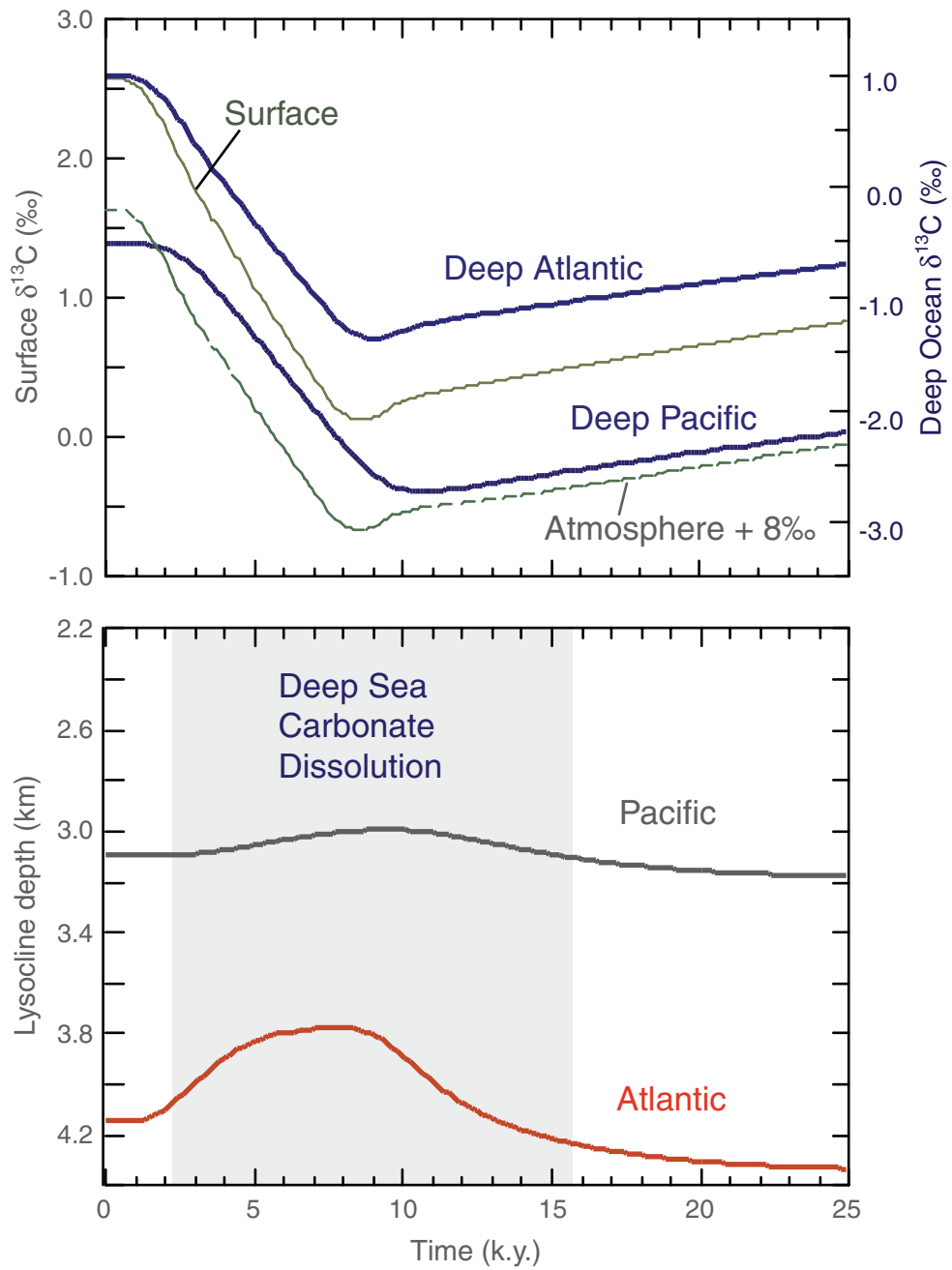


Figure F9

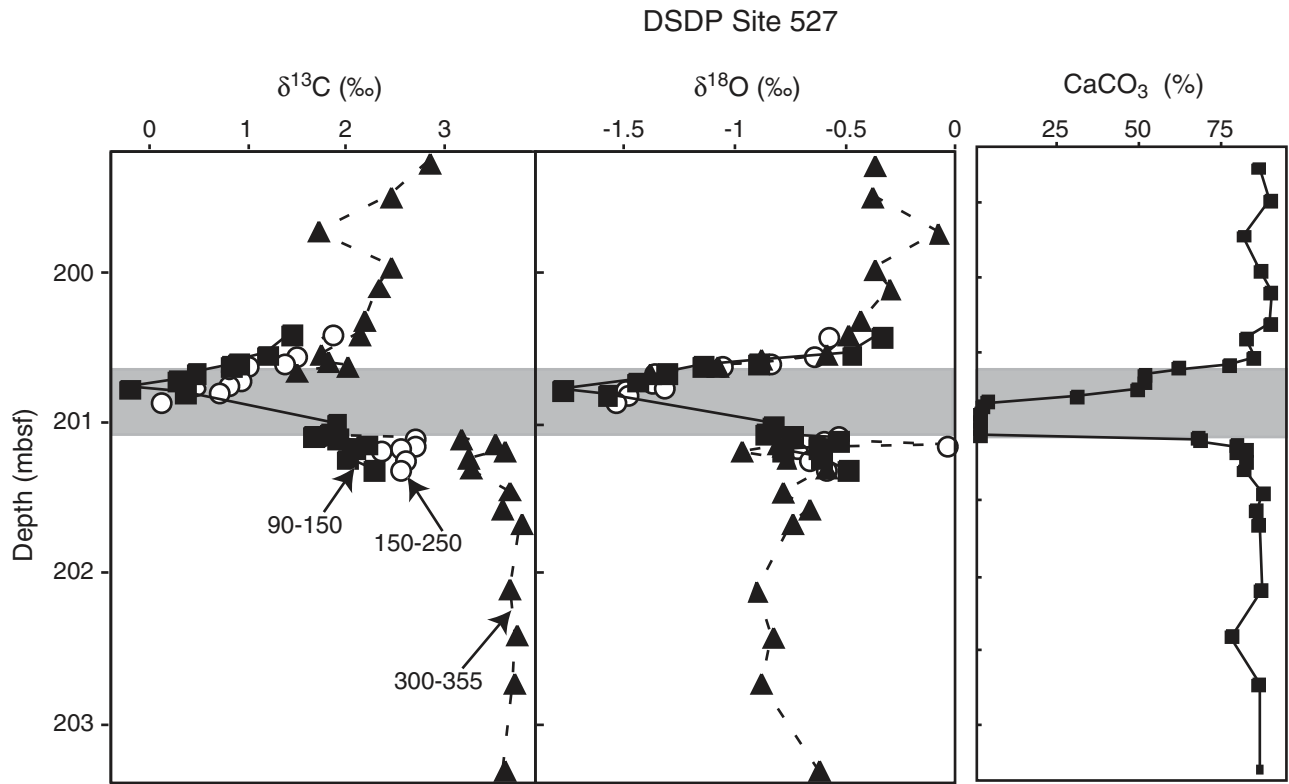


Figure F10

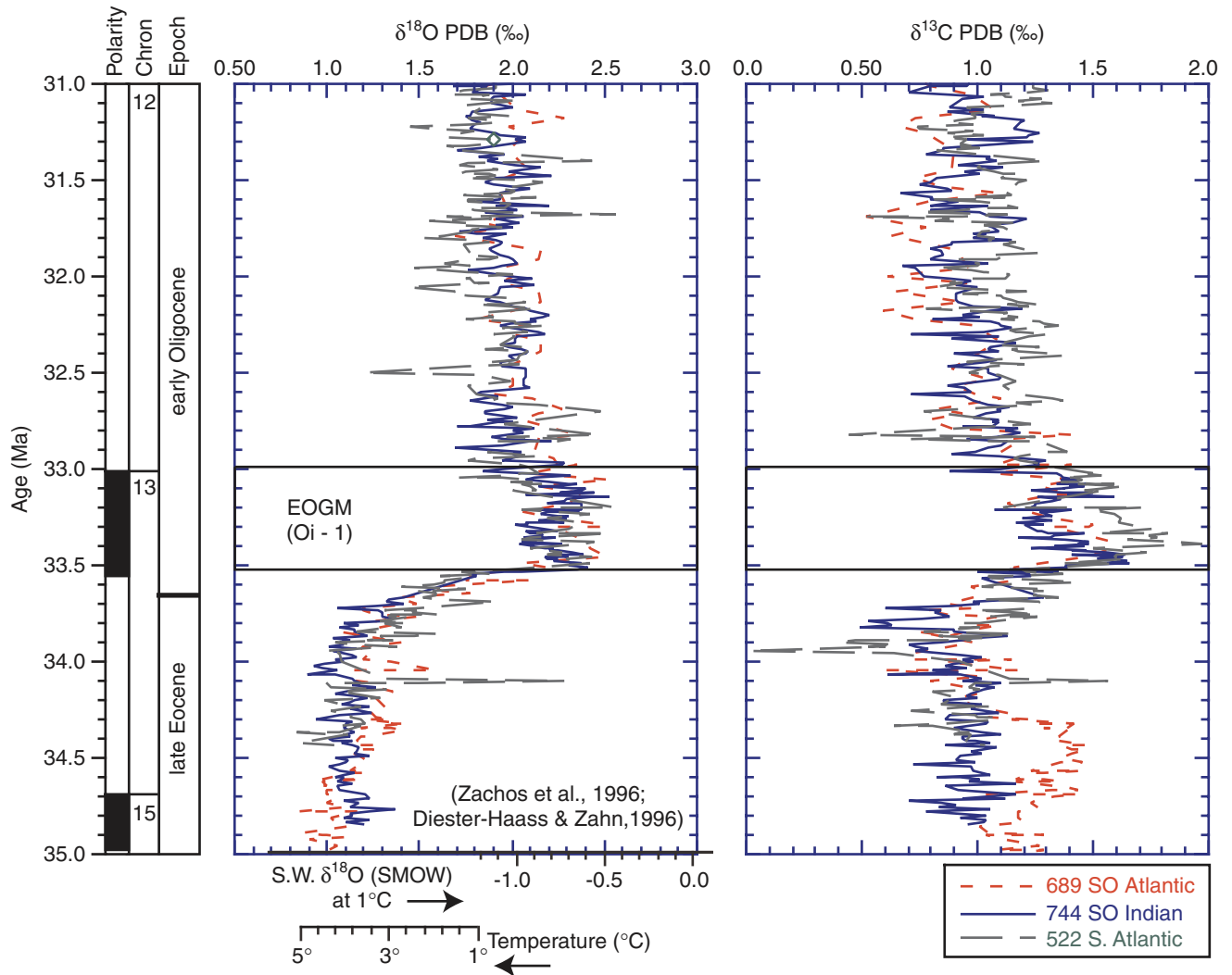


Figure F11

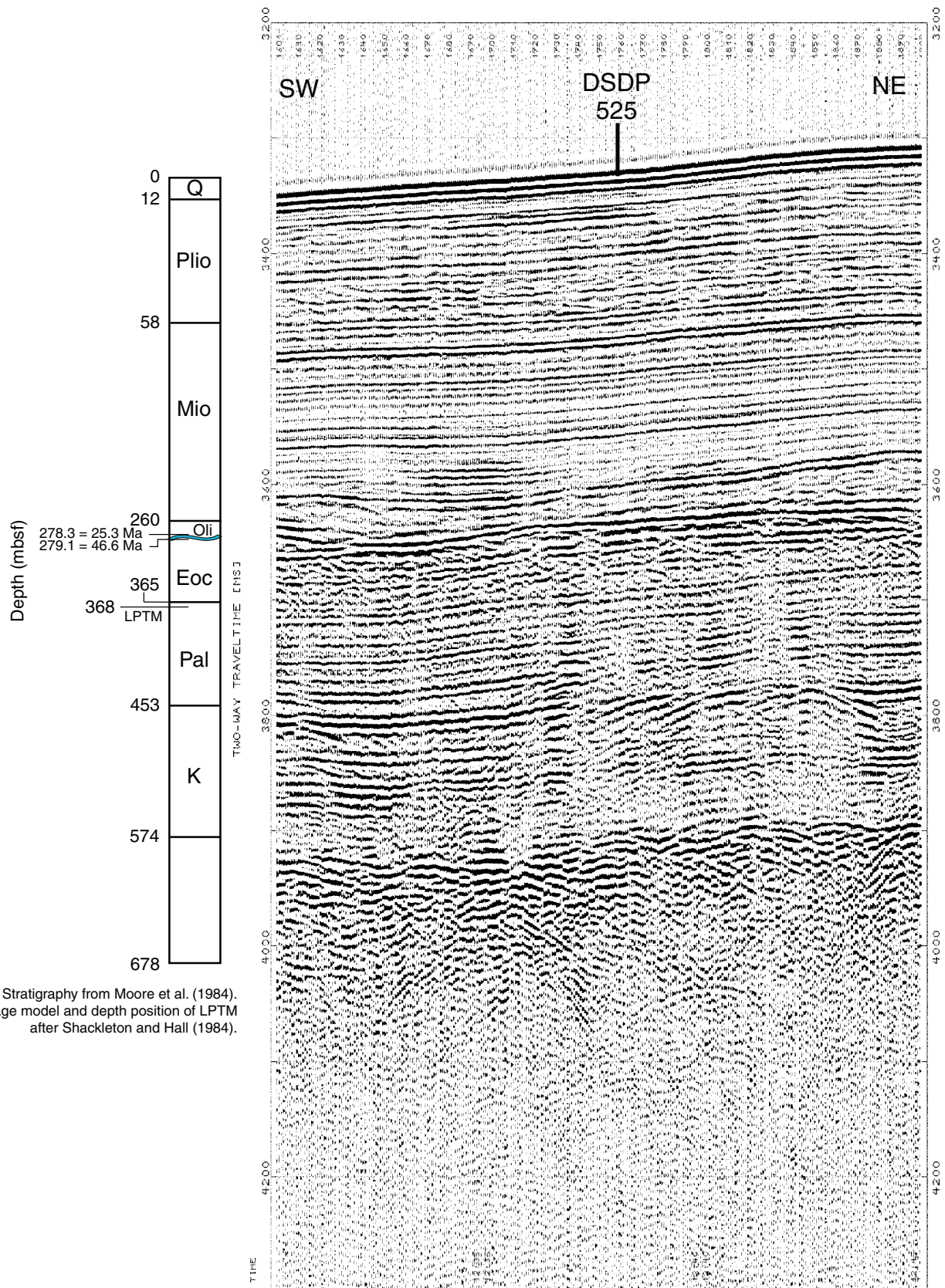


Figure F12

Multichannel Seismic Line GeoB 01-031 GI Gun 0.4 L (25 in³)

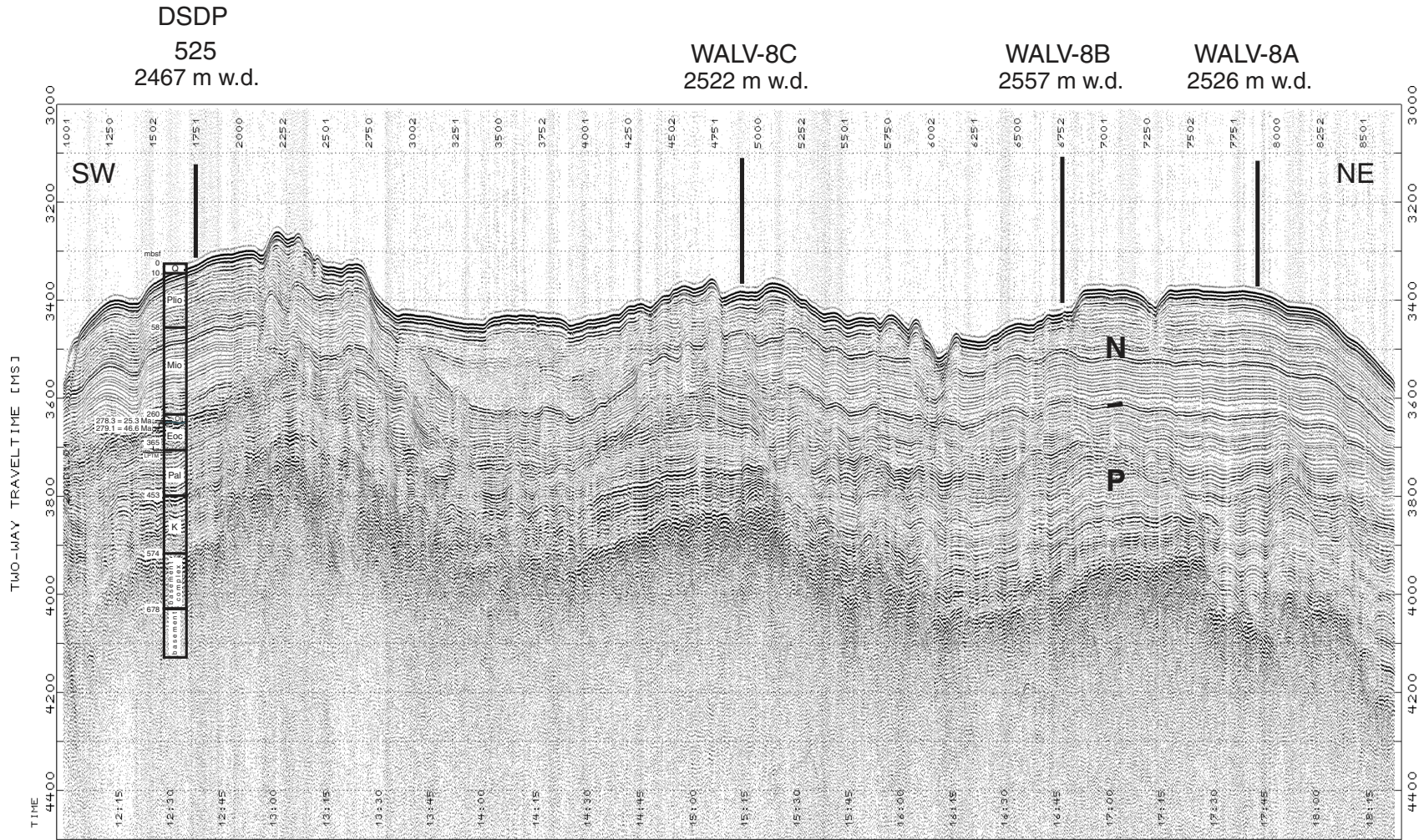


Figure F13

WALV-8, WALV-9, WALV-10

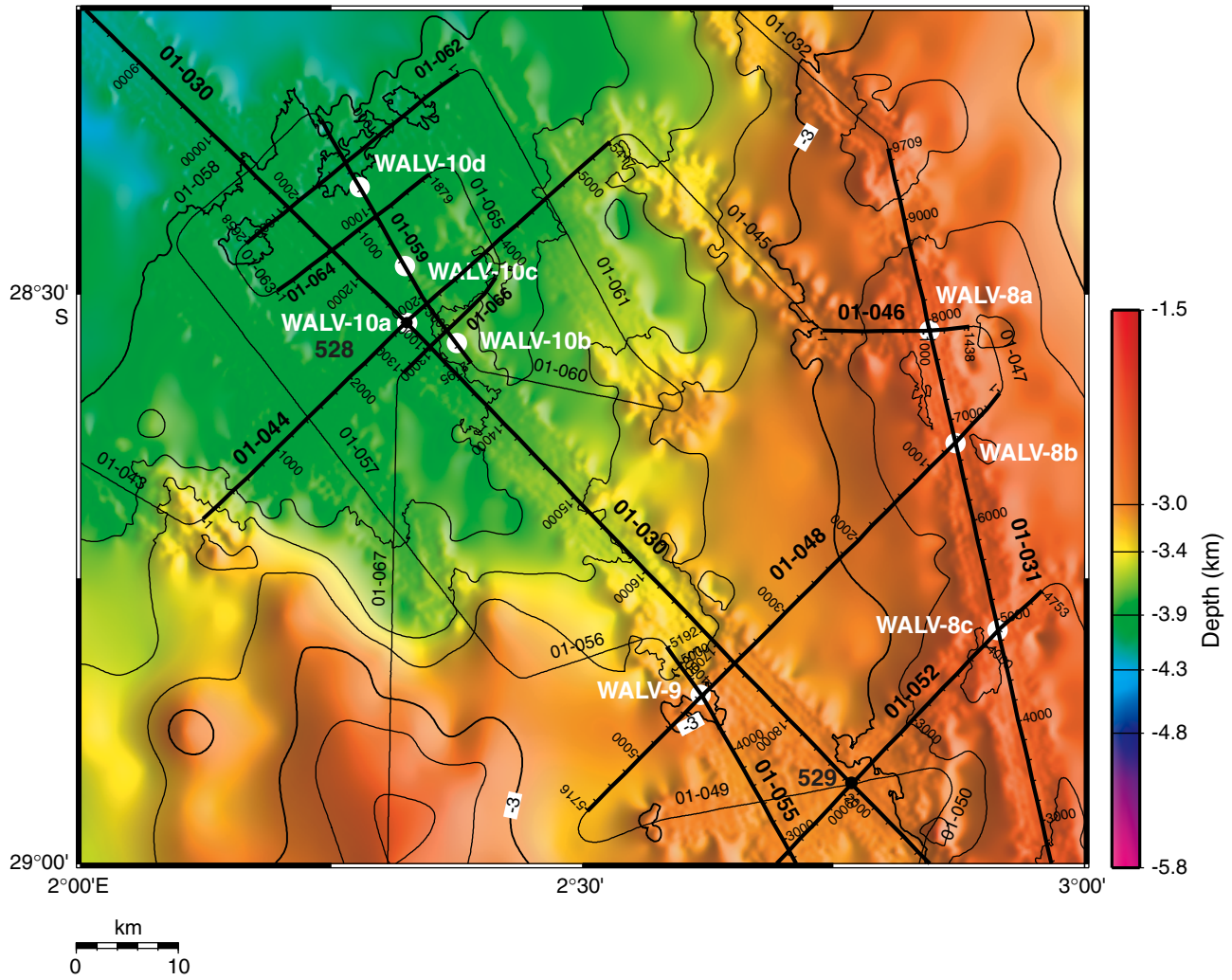


Figure F14

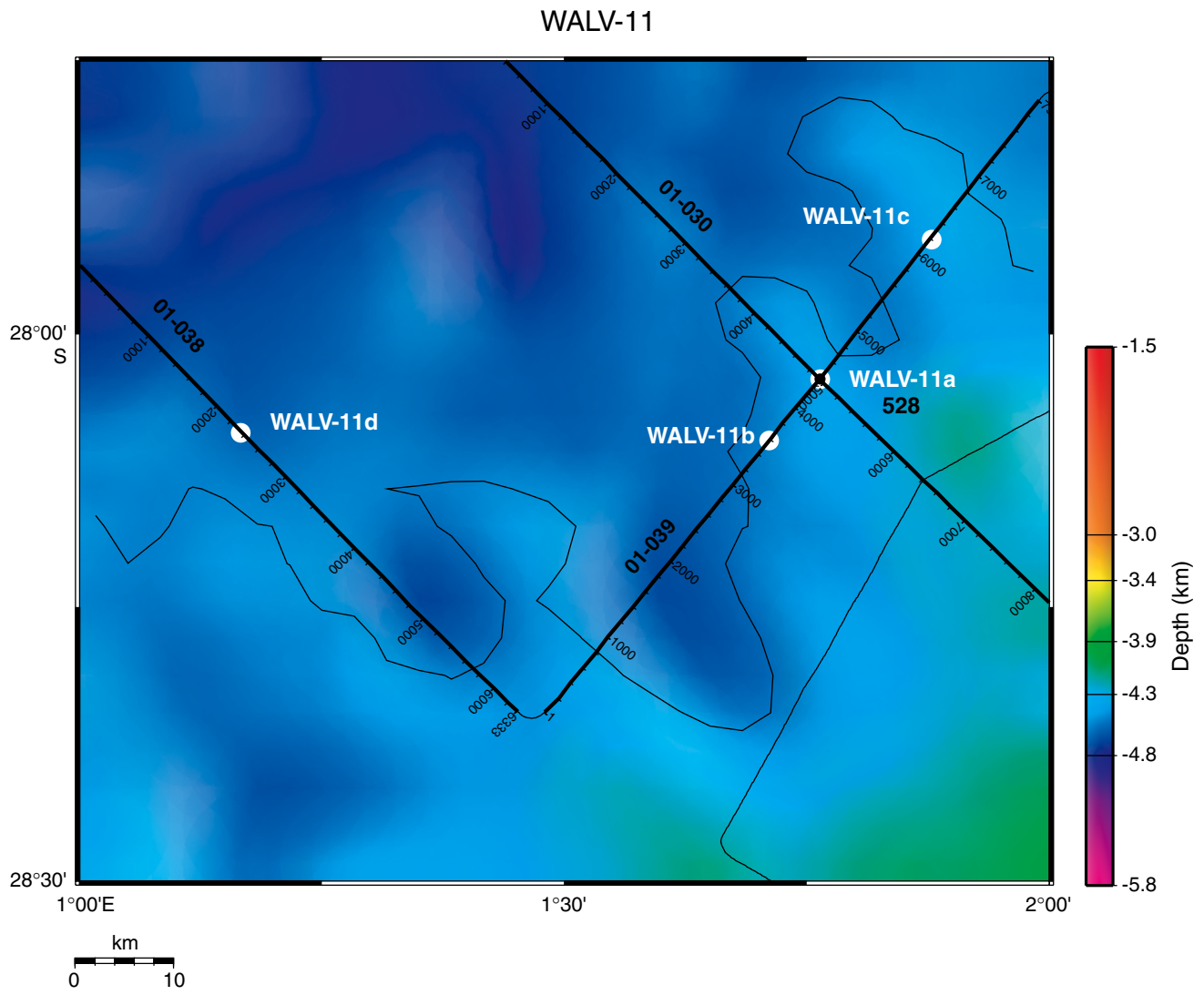


Figure F15

WALV-12

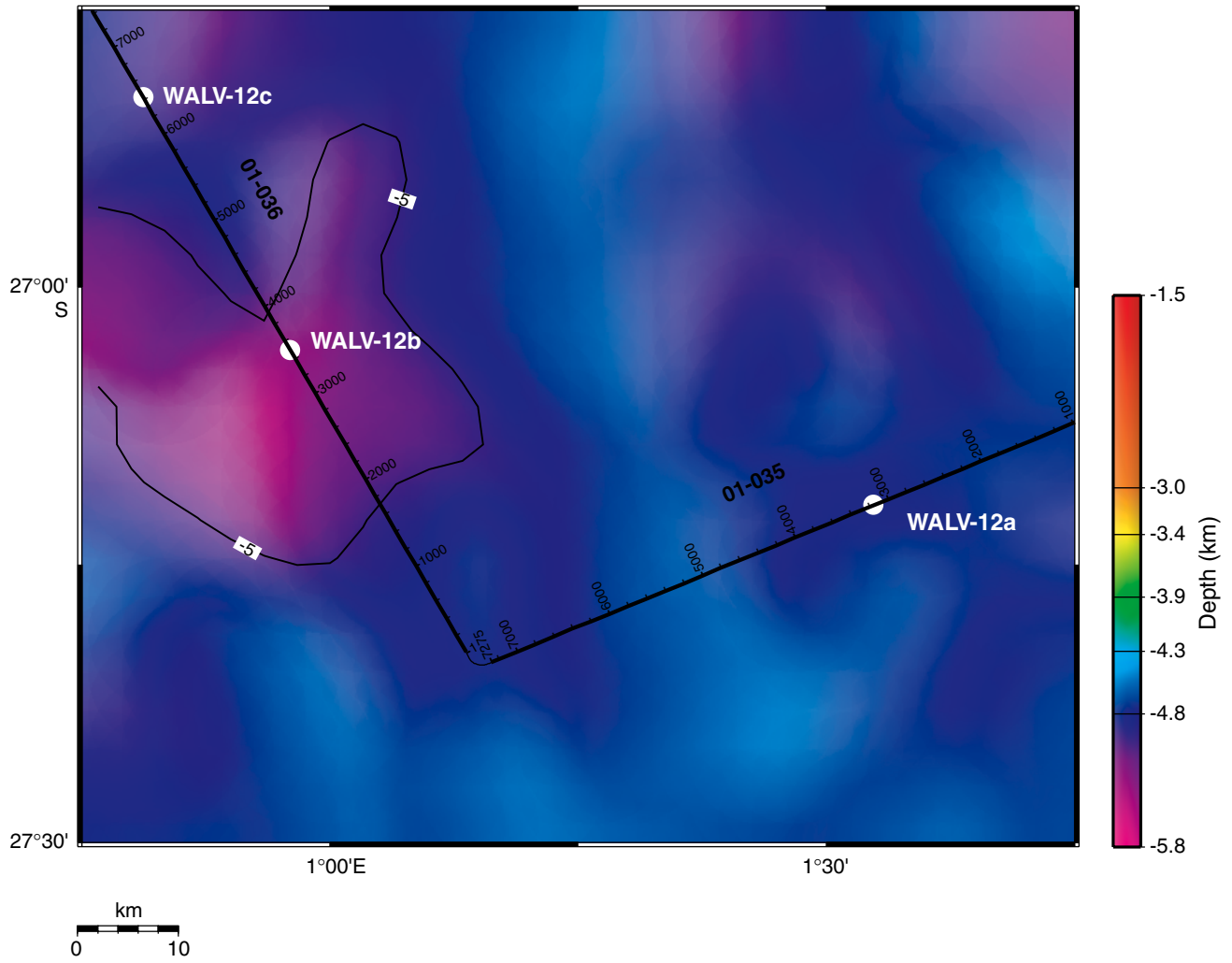


Figure F16

SITE SUMMARIES

Proposed Site: WALV-8A

Priority: 2

Position: 28°31.96'S, 2°50.73'E

Water Depth: 2530 m

Sediment Thickness: 621 m

Target Depth: 500 mbsf

Approved Maximum Penetration: 600 mbsf

Seismic Coverage: MCS line Geob01-031, CDP 7884; line Geob01-046, CDP 1047.

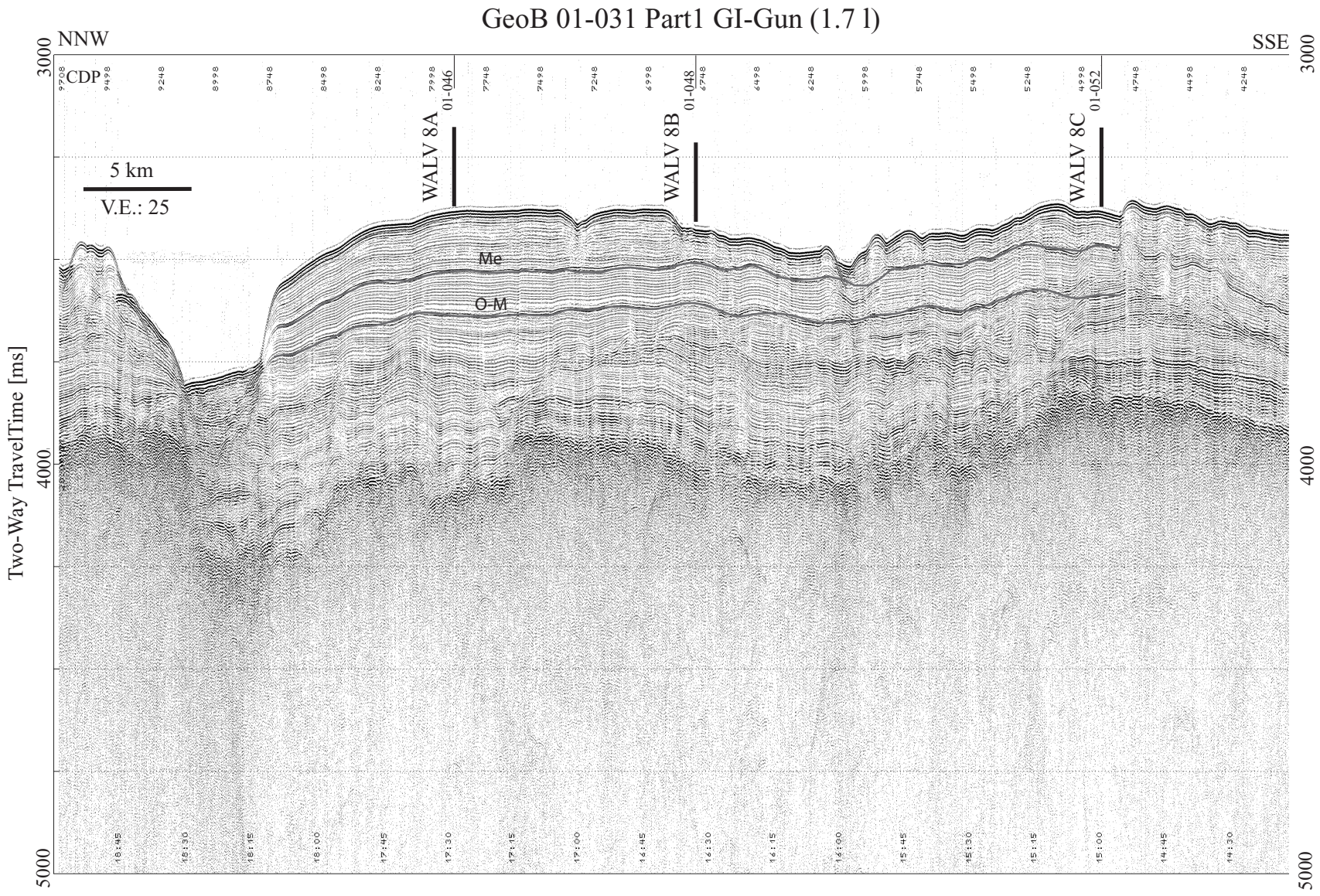
Parasound Coverage: Geob01-031, 20.01.01, 17:42h; Geob01-046, 23.01.01, 23:25h.

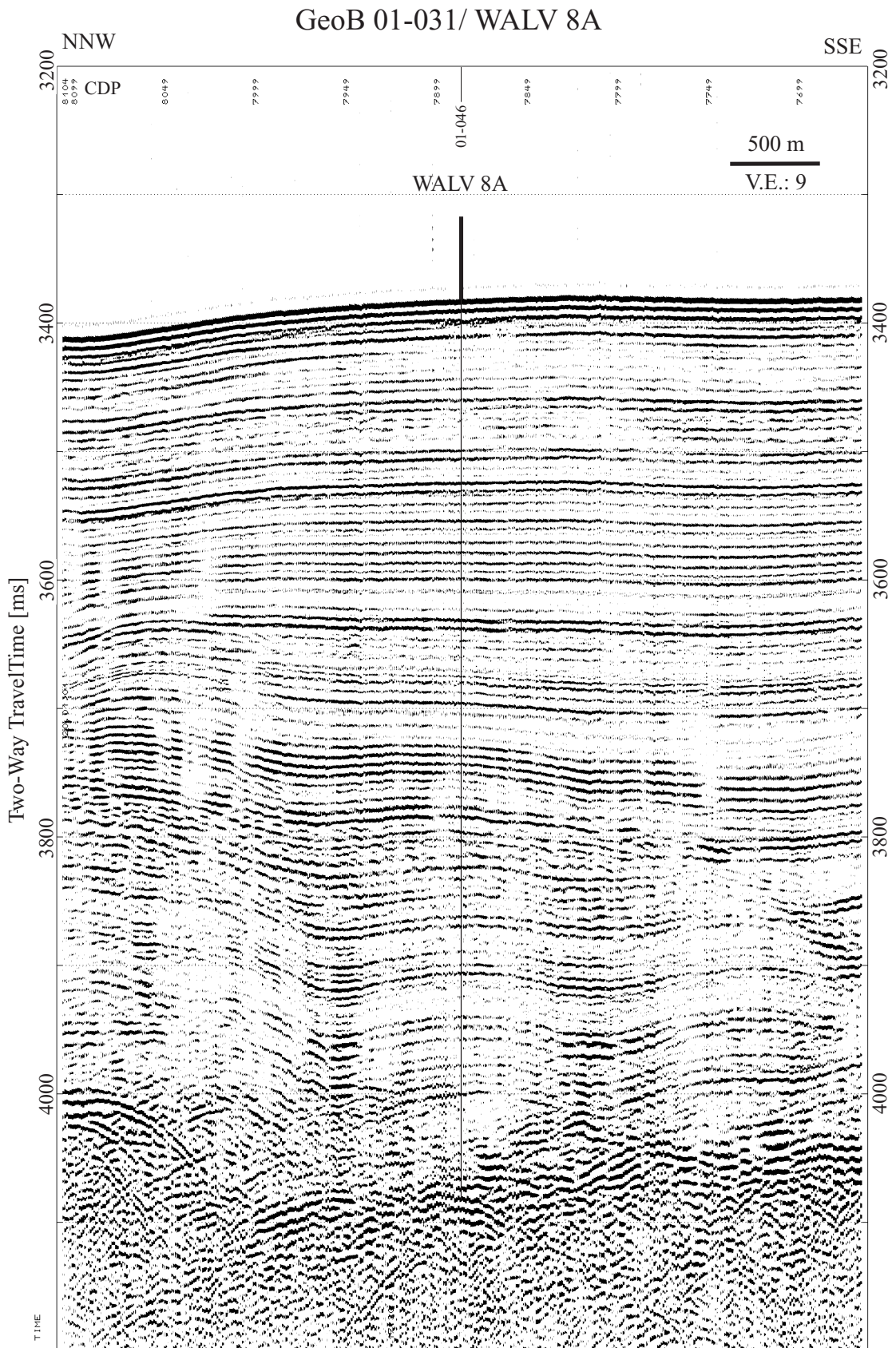
Objectives: See "Scientific Objectives."

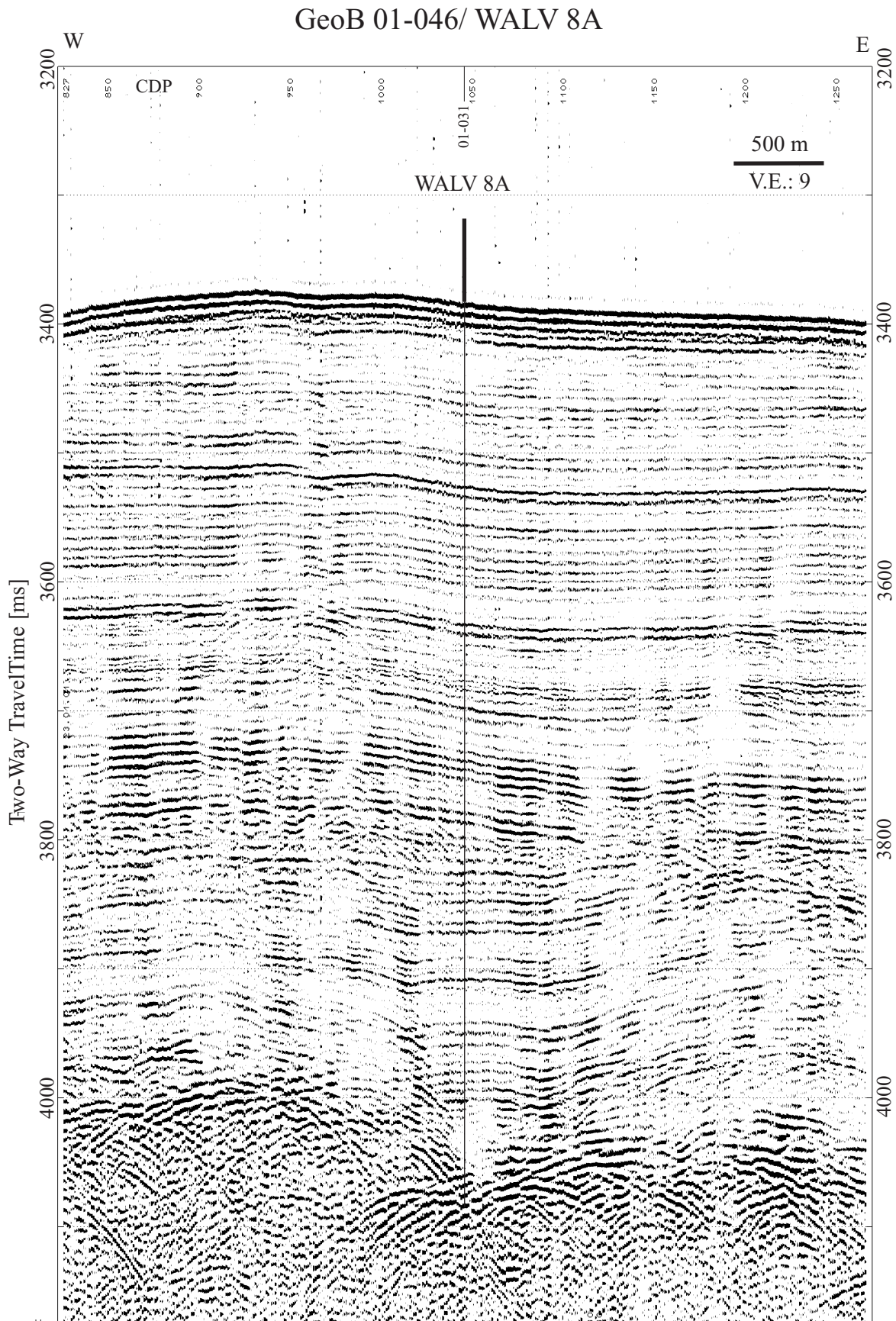
Drilling Program: Double or triple APC to refusal; single or double XCB to target depth.

Downhole Logging Program: Triple-combo, FMS-sonic, WST.

Nature of Rock Anticipated: Calcareous ooze in the upper section, chalk in the lower section.







Proposed Site: WALV-8B

Priority: 1

Position: 28°37.85'S, 2°52.29'E

Water Depth: 2557 m

Sediment Thickness: 531 m

Target Depth: 450 mbsf

Approved Maximum Penetration: 530 mbsf

Seismic Coverage: MCS line Geob01-031, CDP 6766; line Geob01-048, CDP 647

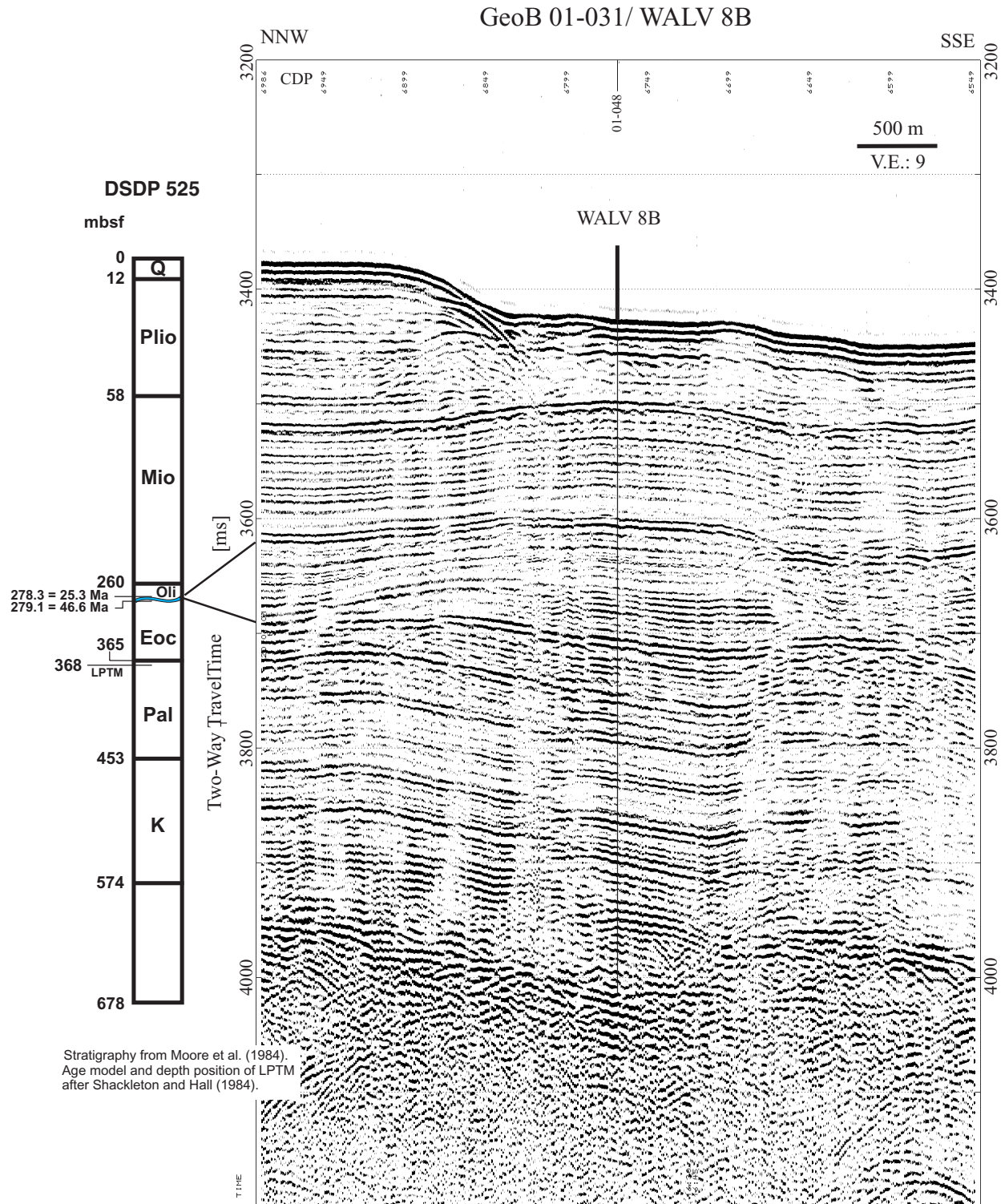
Parasound Coverage: Geob01-031, 20.01.01, 16:46h, Geob01-048, 24.01.01, 01:01h

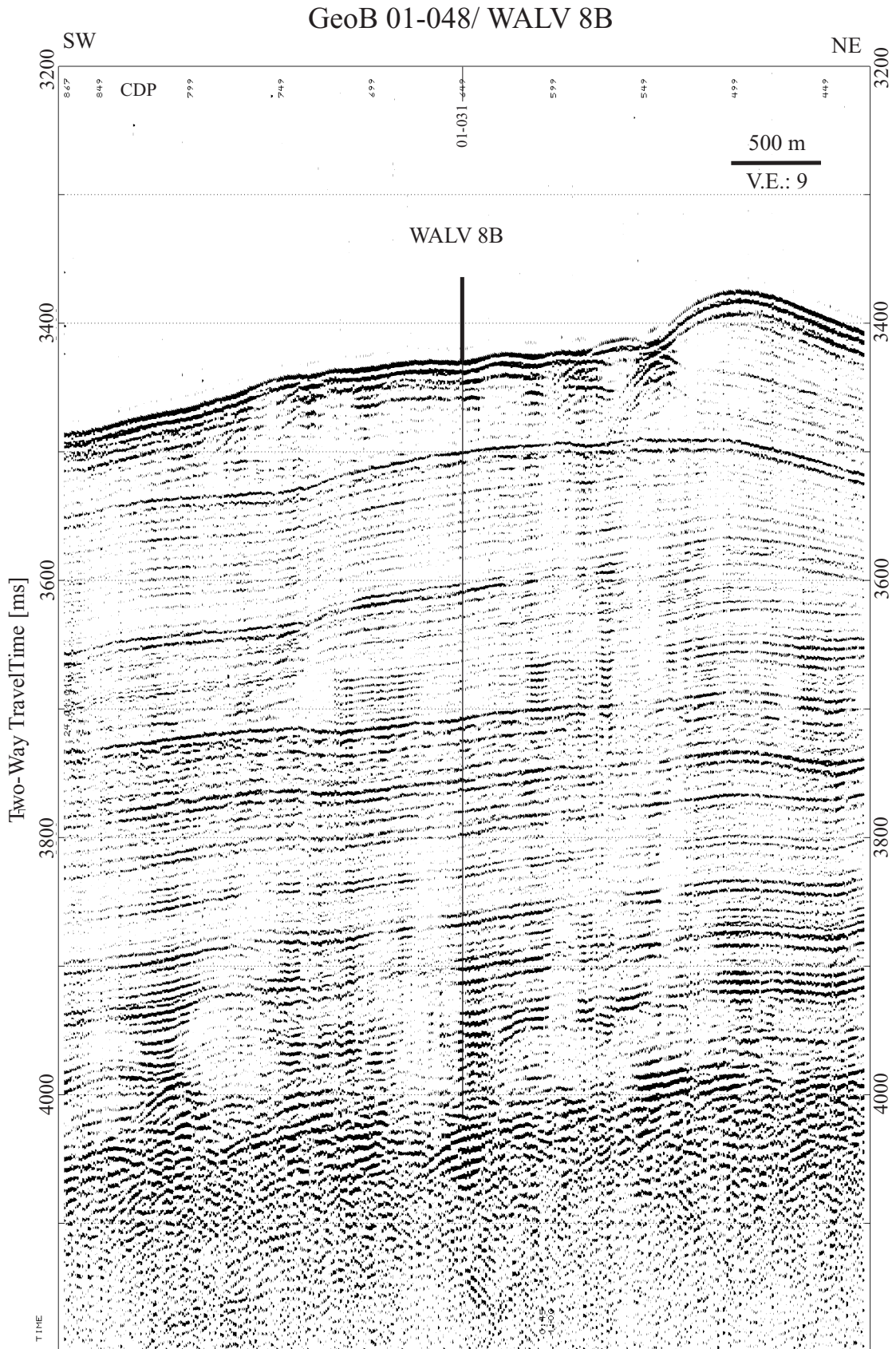
Objectives: See "Scientific Objectives."

Drilling Program: Double or triple APC to refusal; single or double XCB to target depth.

Downhole Logging Program: Triple-combo, FMS-sonic, WST.

Nature of Rock Anticipated: Calcareous ooze in the upper section, chalk in the lower section.





Proposed Site: WALV-8C

Priority: 2

Position: 28°47.74'S, 2°54.83'E

Water Depth: 2531 m

Sediment Thickness: 414 m

Target Depth: 400 mbsf

Approved Maximum Penetration: 400 mbsf

Seismic Coverage: MCS line Geob01-031, CDP 4892; line Geob01-052, CDP 4175.

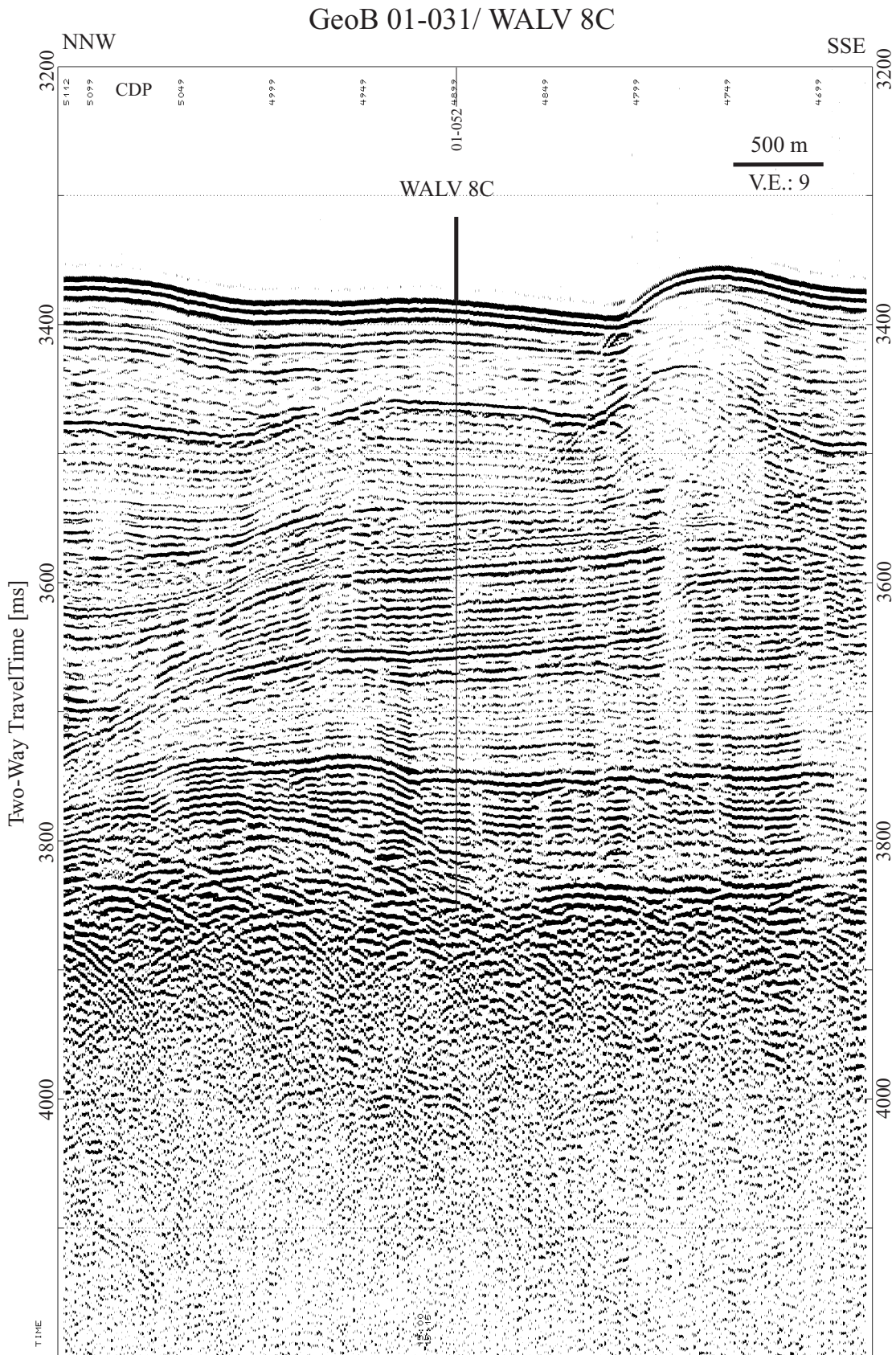
Parasound Coverage: Geob01-031, 20.01.01, 15:13h, Geob01-052, 24.01.01, 15:16h.

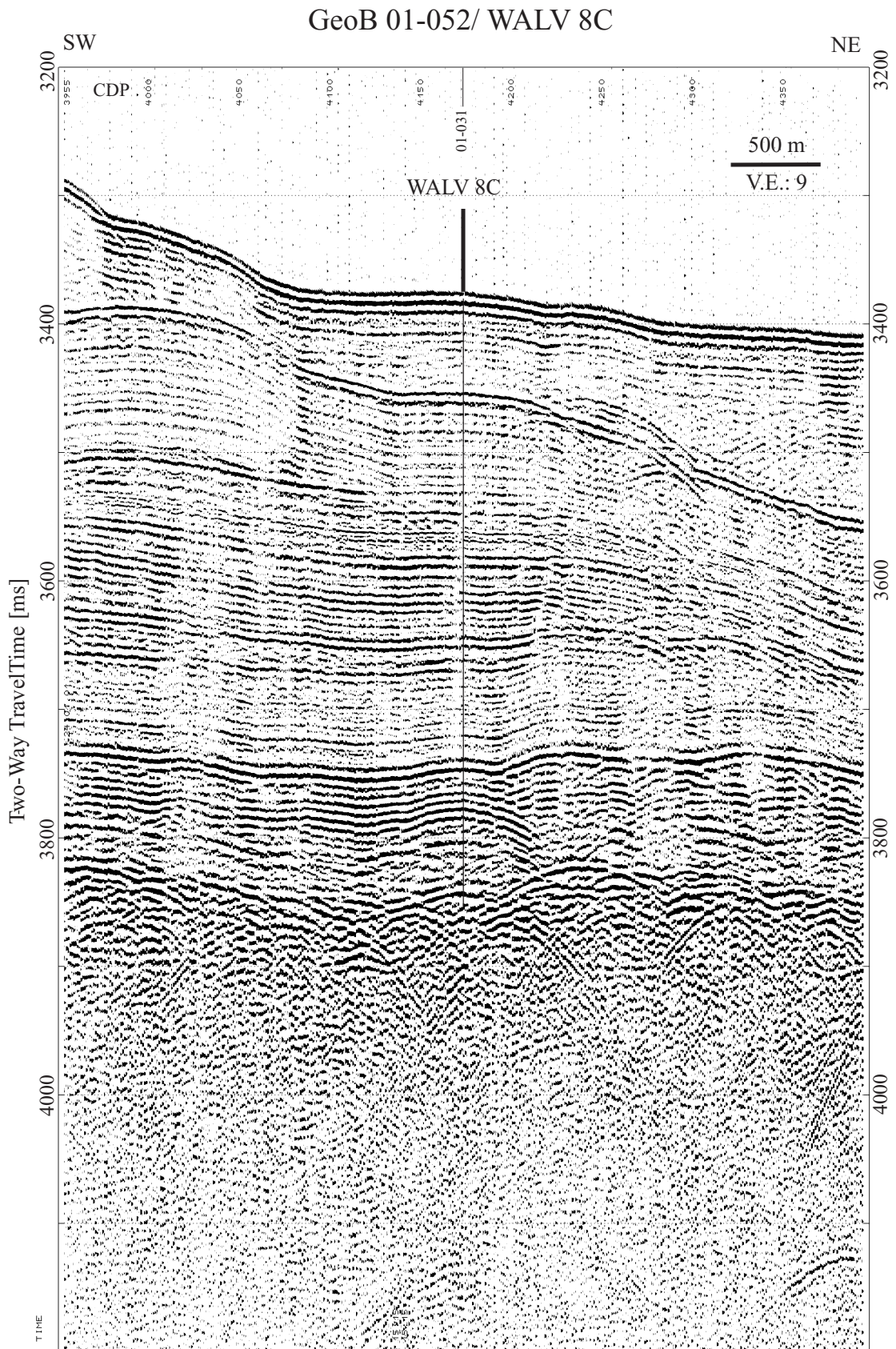
Objectives: See "Scientific Objectives."

Drilling Program: Double or triple APC to refusal; single or double XCB to target depth.

Downhole Logging Program: Triple-combo, FMS-sonic, WST.

Nature of Rock Anticipated: Calcareous ooze in the upper section, chalk in the lower section.





Proposed Site: WALV-9A

Priority: 1

Position: 28°51.19'S, 2°37.14'E

Water Depth: 2979 m

Sediment Thickness: 585 m

Target Depth: 360 mbsf

Approved Maximum Penetration: 360 mbsf

Seismic Coverage: MCS line Geob01-048, CDP 4138; line Geob01-055, CDP 4600.

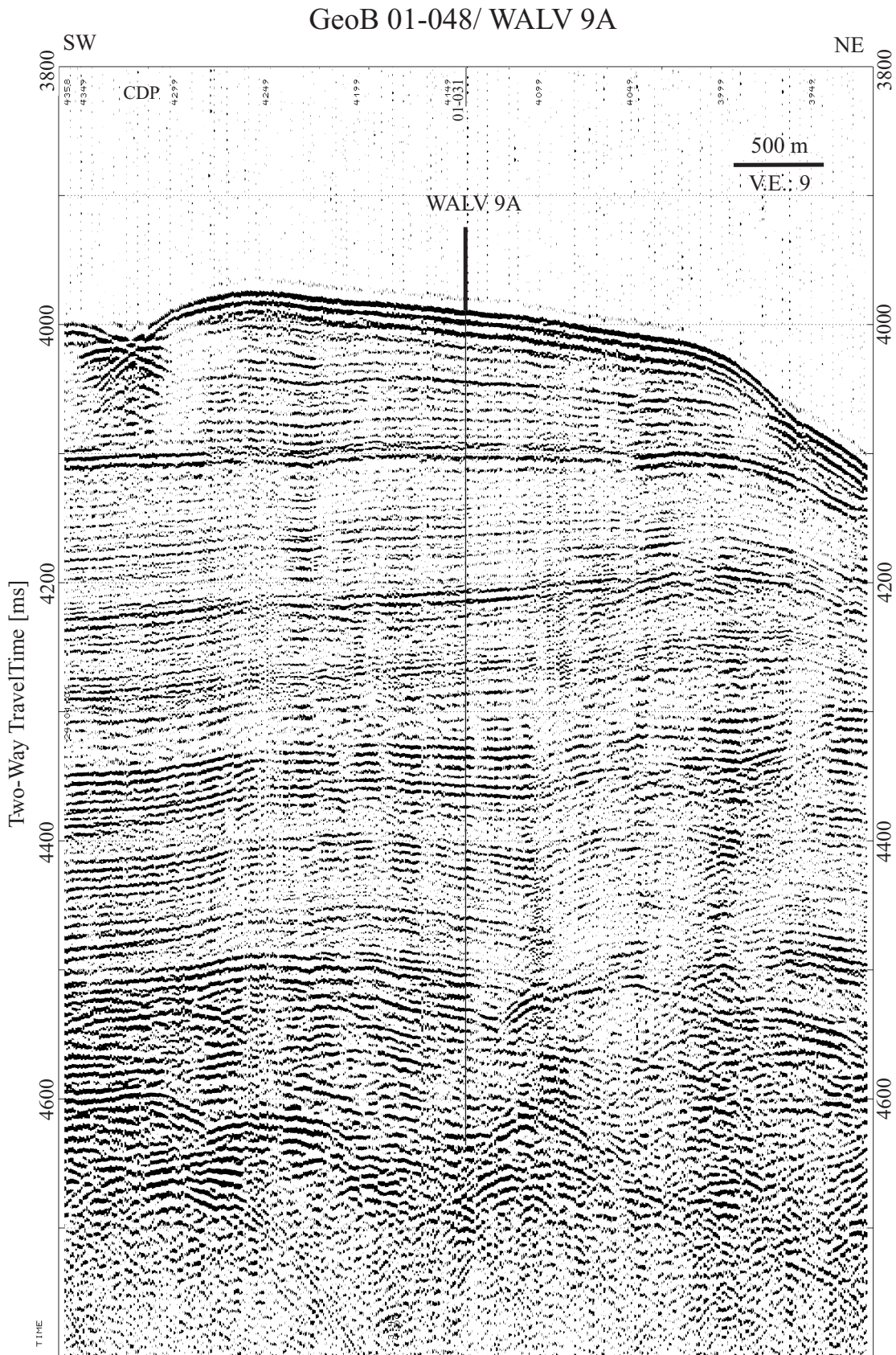
Parasound Coverage: Geob01-048, 24.01.01, 03:57h; Geob01-055, 25.01.01, 01:05h.

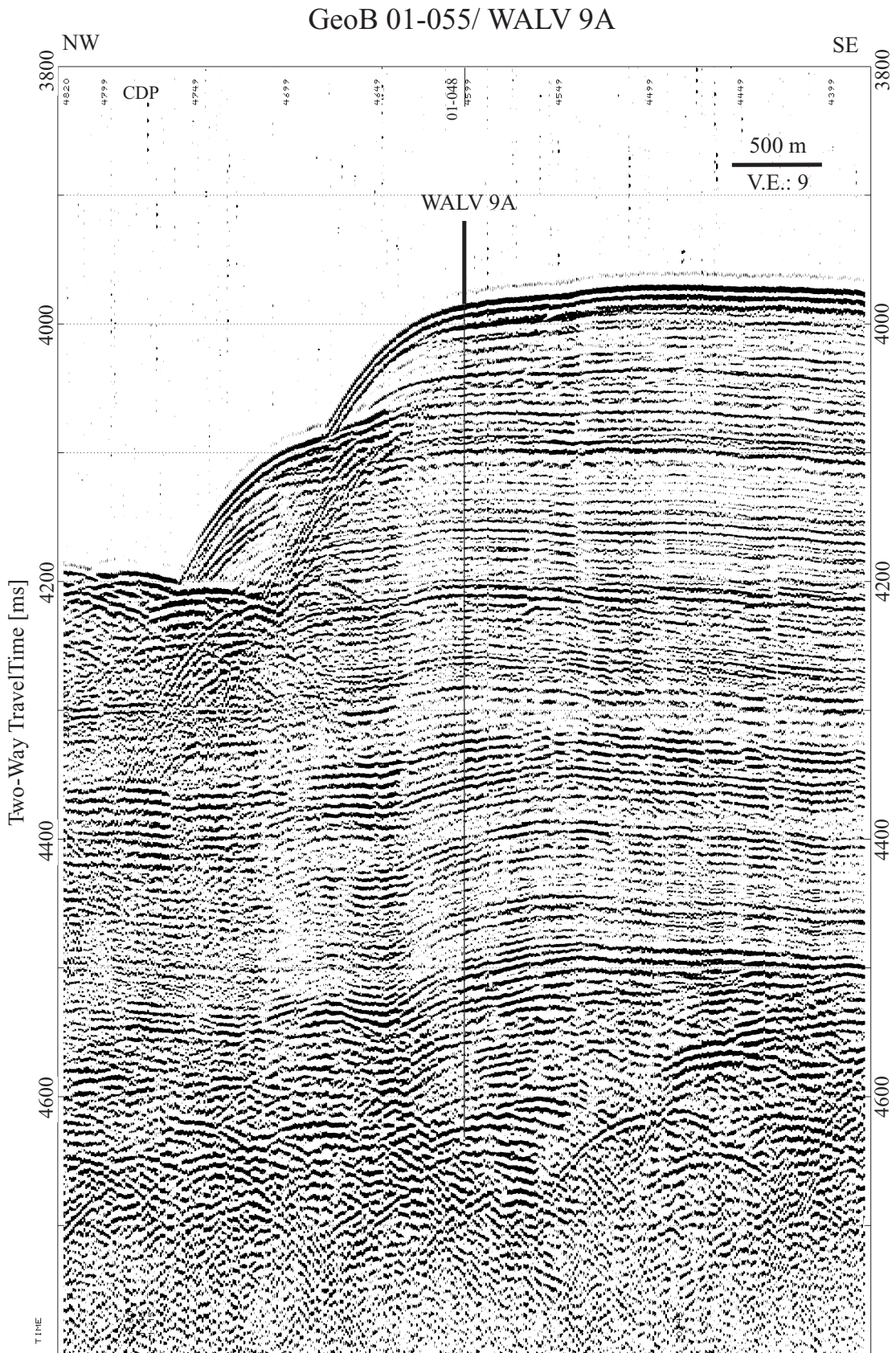
Objectives: See "Scientific Objectives."

Drilling Program: Double or triple APC to refusal; single or double XCB to target depth.

Downhole Logging Program: Triple-combo, FMS-sonic, WST.

Nature of Rock Anticipated: Calcareous ooze in the upper section, chalk in the lower section.





Proposed Site: WALV-9B

Priority: 2

Position: 28°50.10'S, 2°38.36'E

Water Depth: 3083 m

Sediment Thickness: 513 m

Target Depth: 400 mbsf

Approved Maximum Penetration: (500 mbsf requested)

Seismic Coverage: MCS line Geob01-048, CDP 3854; line Geob01-030, distance to site = 1630 m, azimuth to site = 225°; line Geob01-055, distance to site = 2840 m, azimuth to site = 45°.

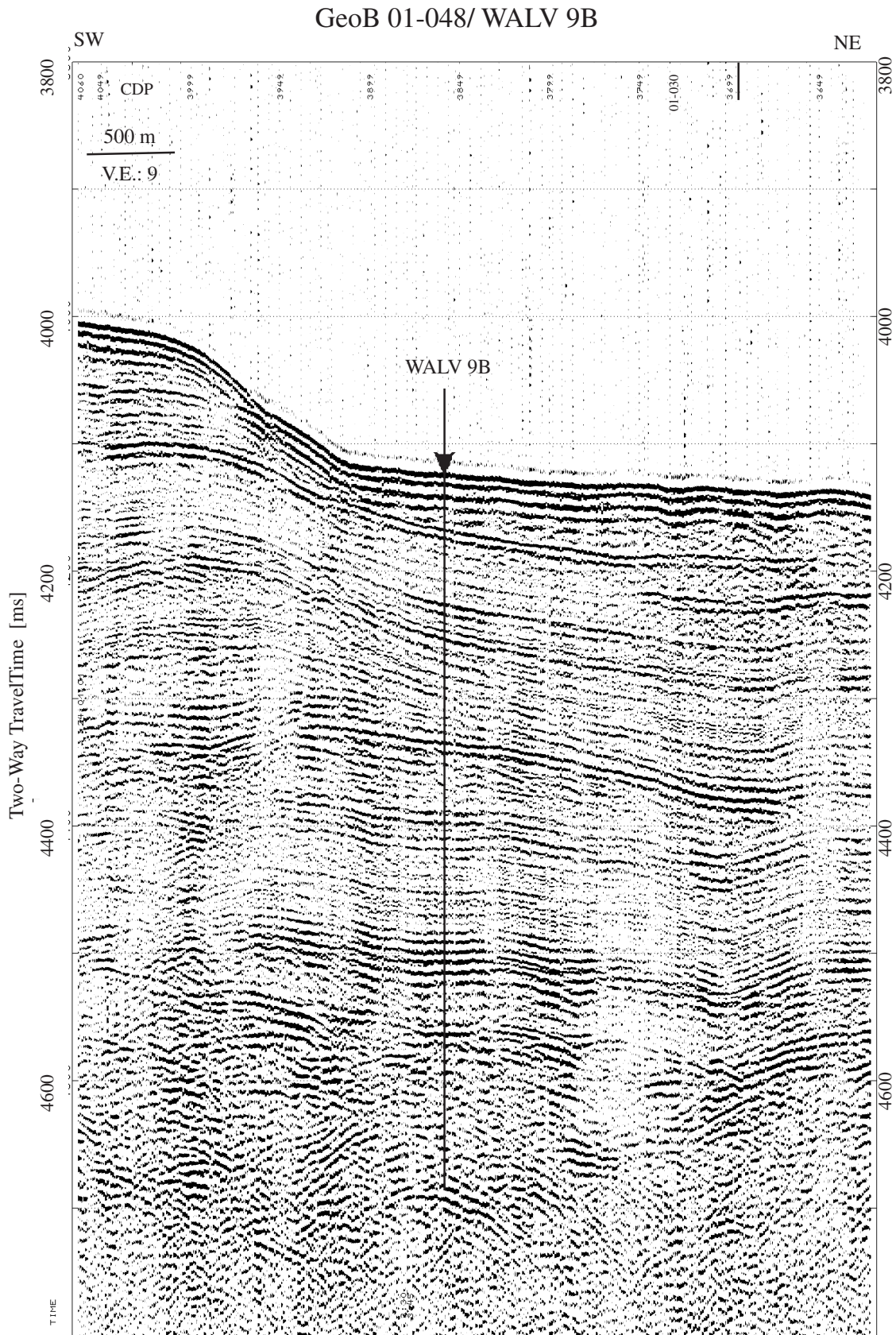
Parasound Coverage: Geob01-048, 24.01.01, 03:57h; Geob01-055, 25.01.01, 01:05h.

Objectives: See "Scientific Objectives."

Drilling Program: Double or triple APC to refusal; single or double XCB to target depth.

Downhole Logging Program: Triple-combo, FMS-sonic, WST.

Nature of Rock Anticipated: Calcareous ooze in the upper section, chalk in the lower section.



Proposed Site: WALV-10A

Priority: 2

Position: 28°31.49'S, 2°19.44'E

Water Depth: 3820 m

Sediment Thickness: 451 m

Target Depth: 450 mbsf

Approved Maximum Penetration: 475 mbsf

Seismic Coverage: MCS line Geob01-030, CDP 12623; line Geob01-044, CDP 2757.

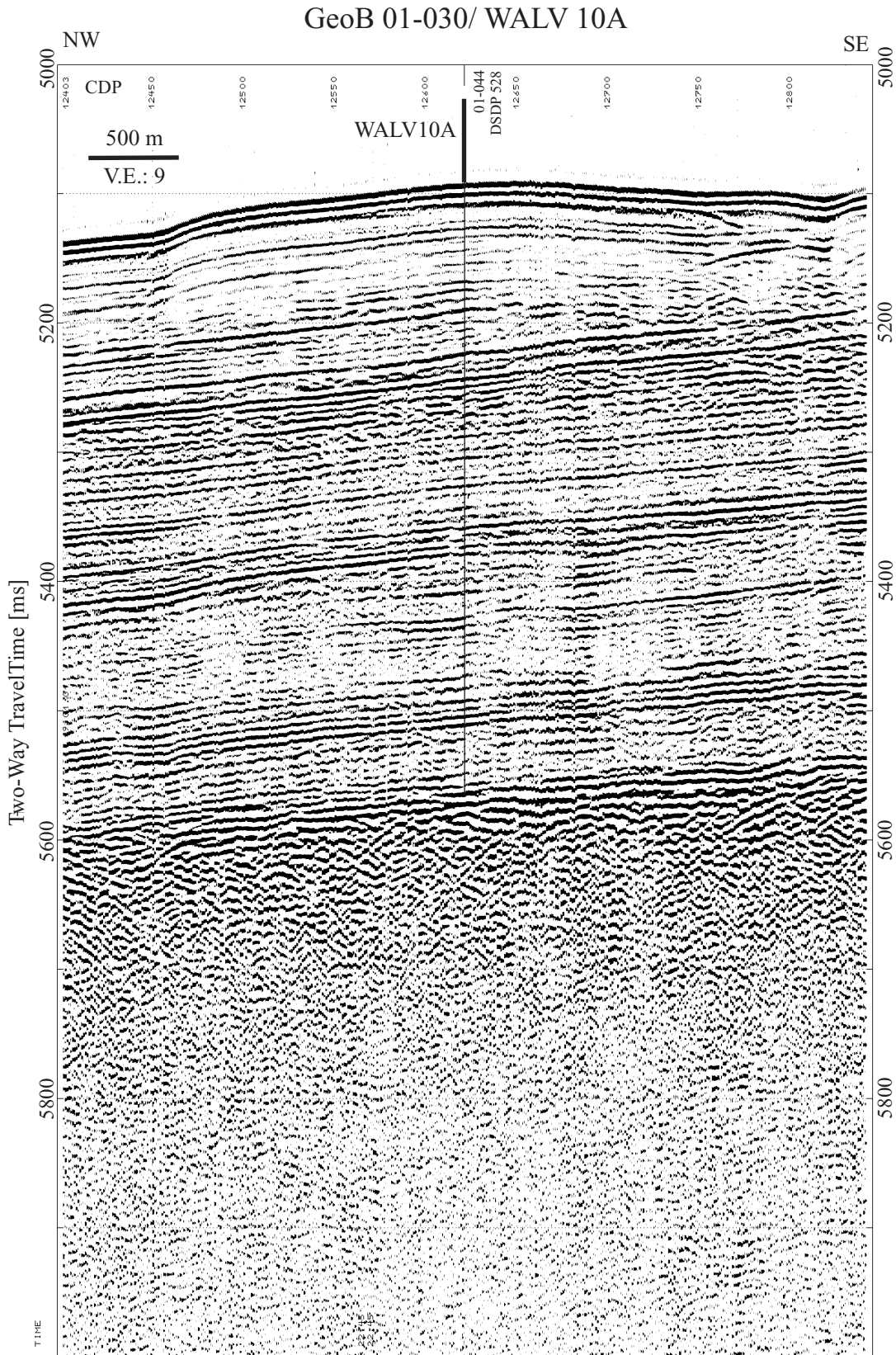
Parasound Coverage: Geob01-030, 19.01.01, 22:47h; Geob01-044, 23.01.01, 17:51h.

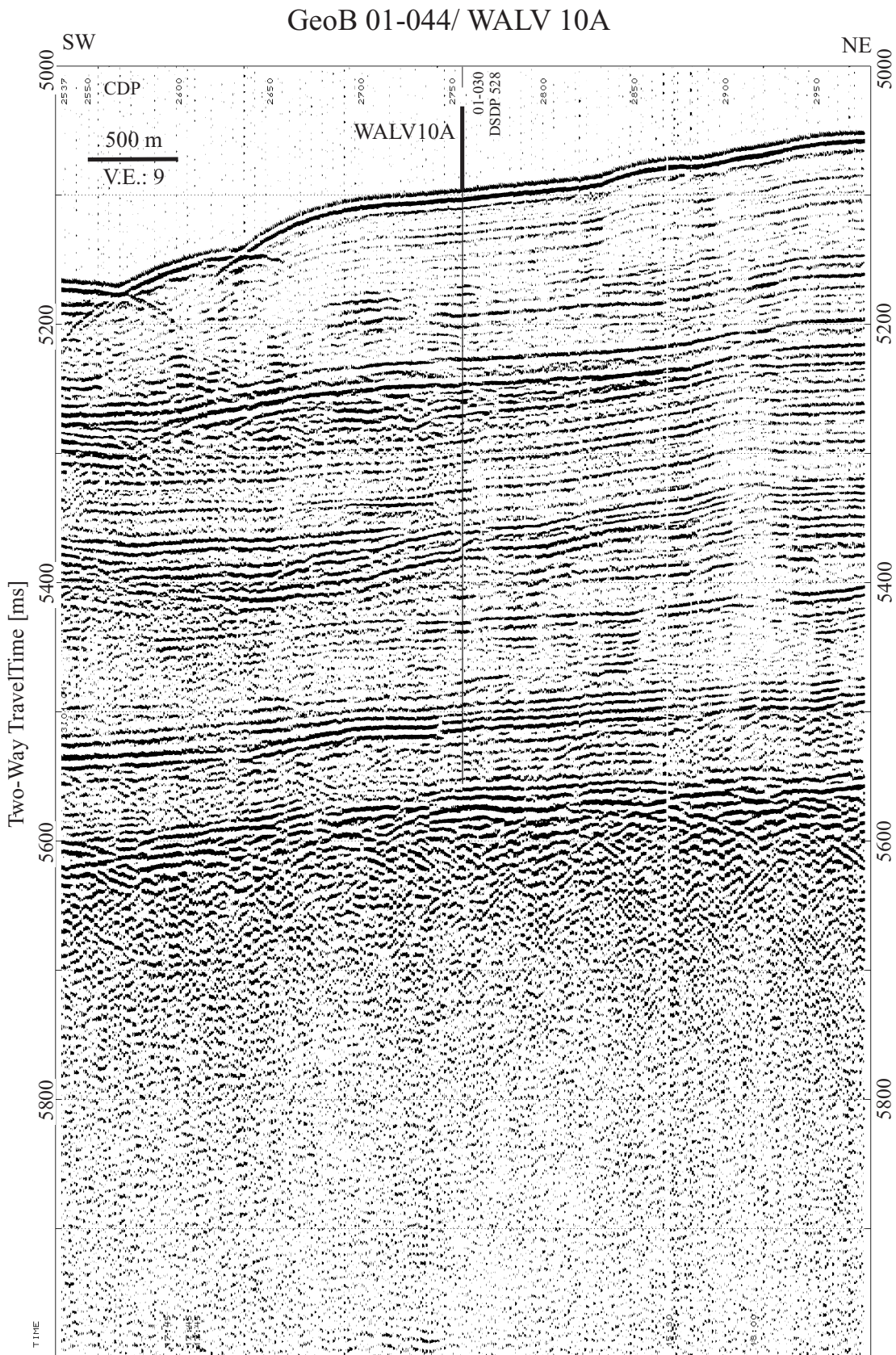
Objectives: See "Scientific Objectives."

Drilling Program: Double or triple APC to refusal; single or double XCB to target depth.

Downhole Logging Program: Triple-combo, FMS-sonic, WST.

Nature of Rock Anticipated: Calcareous ooze in the upper section, chalk in the lower section.





Proposed Site: WALV-10B

Priority: 2

Position: 28°32.62'S, 2°22.47'E

Water Depth: 3719 m

Sediment Thickness: 480 m

Target Depth: 450 mbsf

Approved Maximum Penetration: 450 mbsf

Seismic Coverage: MCS line GeoB01-059, CDP 2560; line GeoB01-066, CDP 711, distance to site = 1610 m, azimuth to site = 143°.

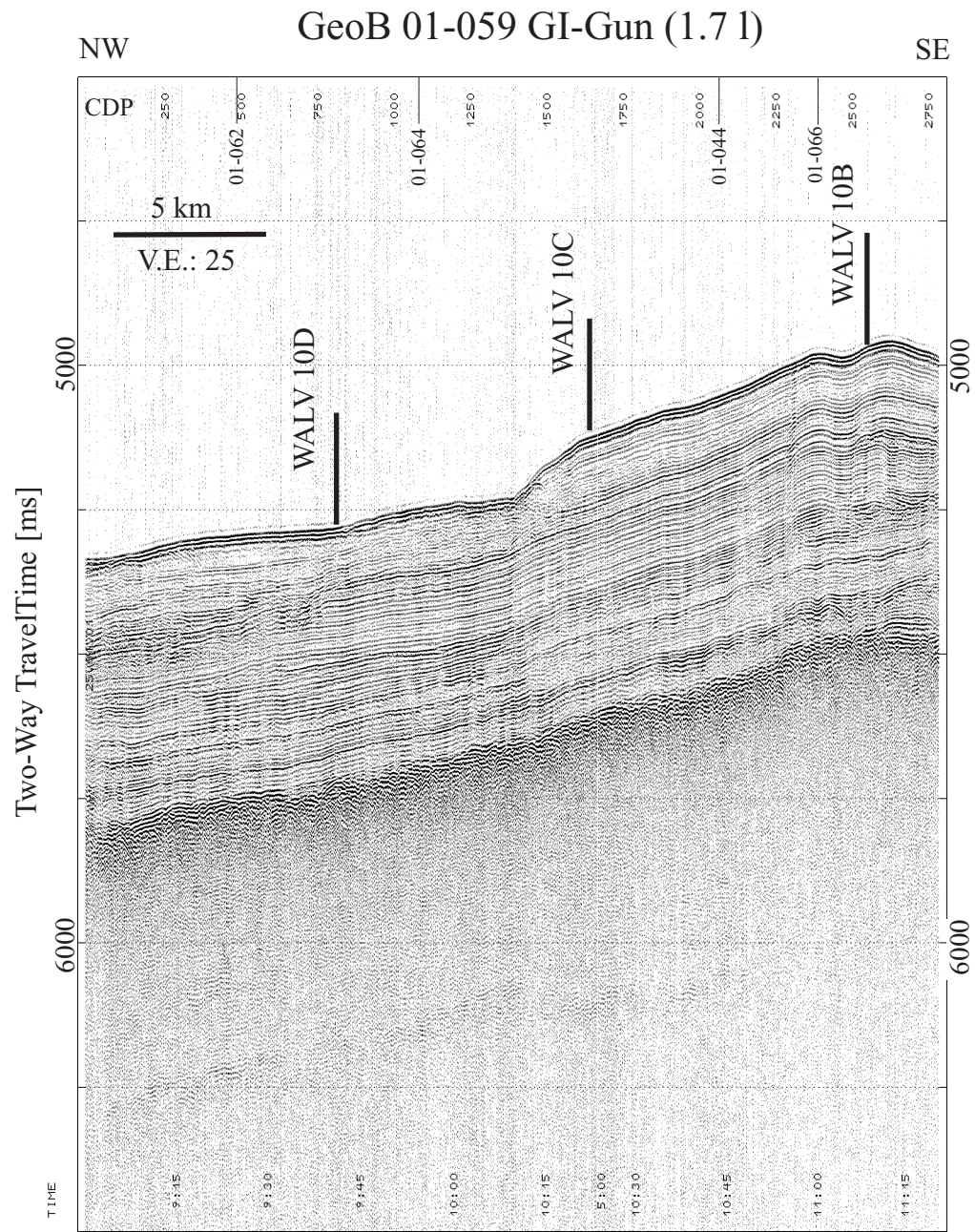
Parasound Coverage: Geob01-059, 25.01.01, 11:08h.

Objectives: See "Scientific Objectives."

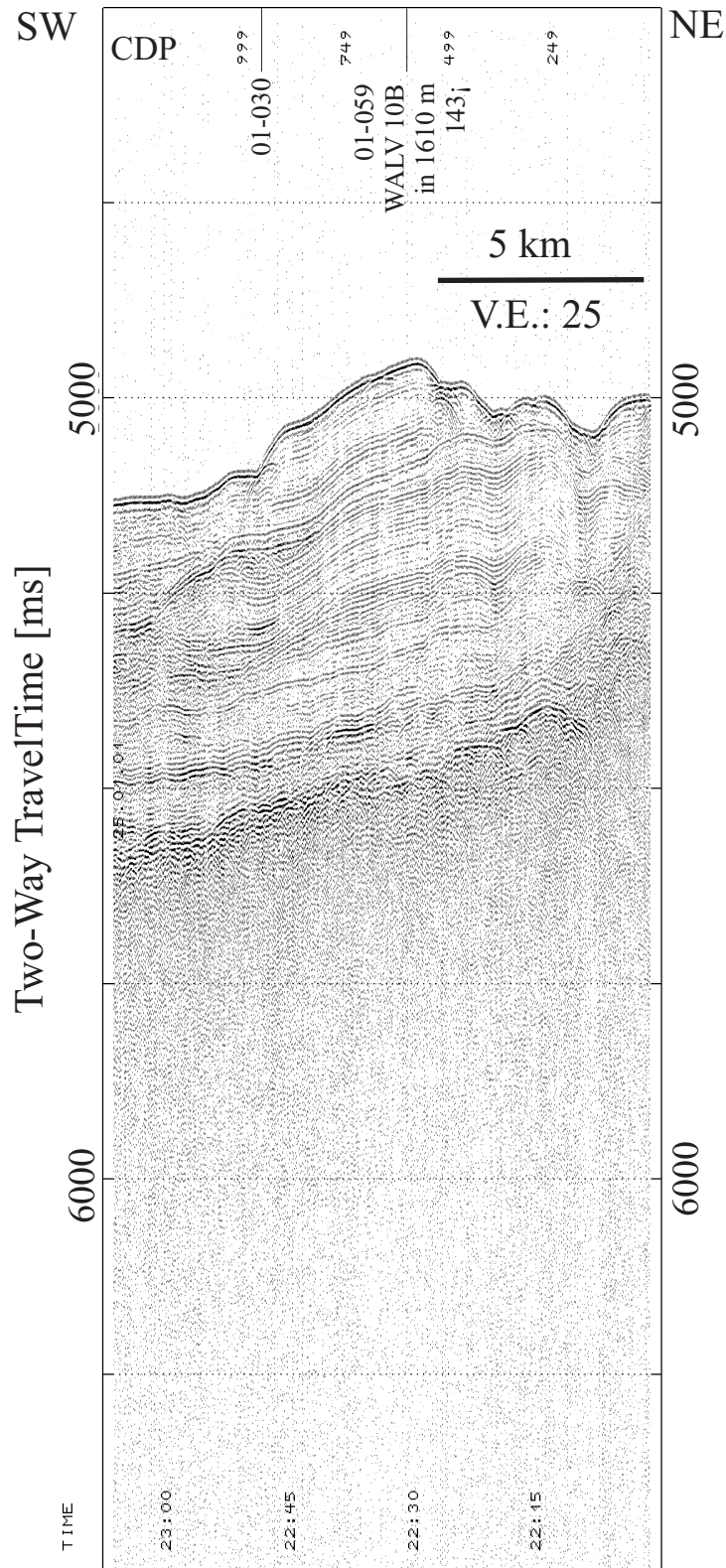
Drilling Program: Double or triple APC to refusal; single or double XCB to target depth.

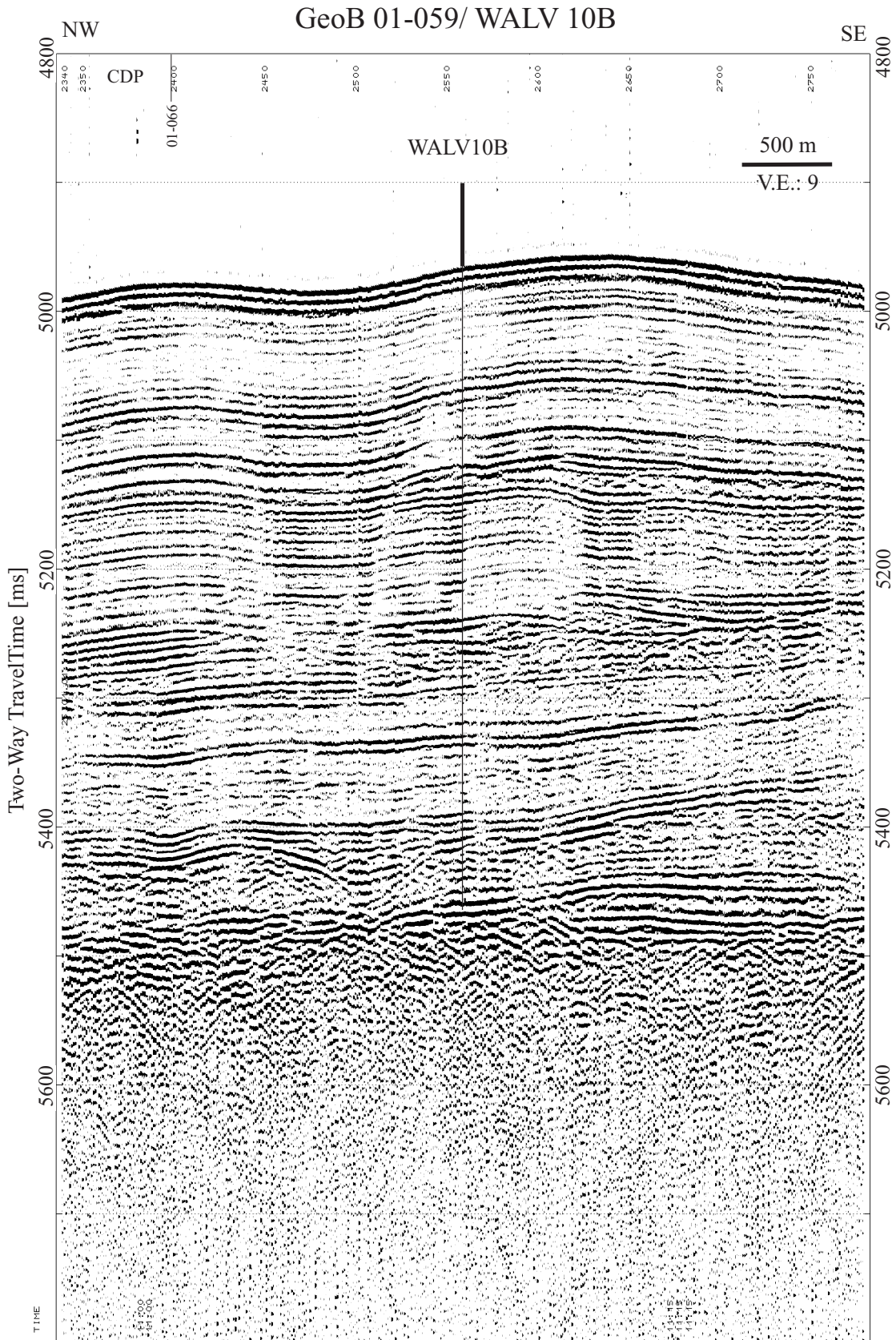
Downhole Logging Program: Triple-combo, FMS-sonic, WST.

Nature of Rock Anticipated: Calcareous ooze in the upper section, chalk in the lower section.



GeoB 01-066 GI-Gun (1.7 l)





Proposed Site: WALV-10C

Priority: 1

Position: 28°28.54'S, 2°19.37'E

Water Depth: 3842 m

Sediment Thickness: 470 m

Target Depth: 450 mbsf

Approved Maximum Penetration: 450 mbsf

Seismic Coverage: MCS line GeoB01-059, CDP 1649; line GeoB01-044, CDP 3024, distance to site = 4270 m, azimuth to site = 330°; line GeoB01-064, CDP 1215, distance to site = 5610 m, azimuth to site = 150°.

Parasound Coverage: Geob01-059, 25.01.01, 10:22h.

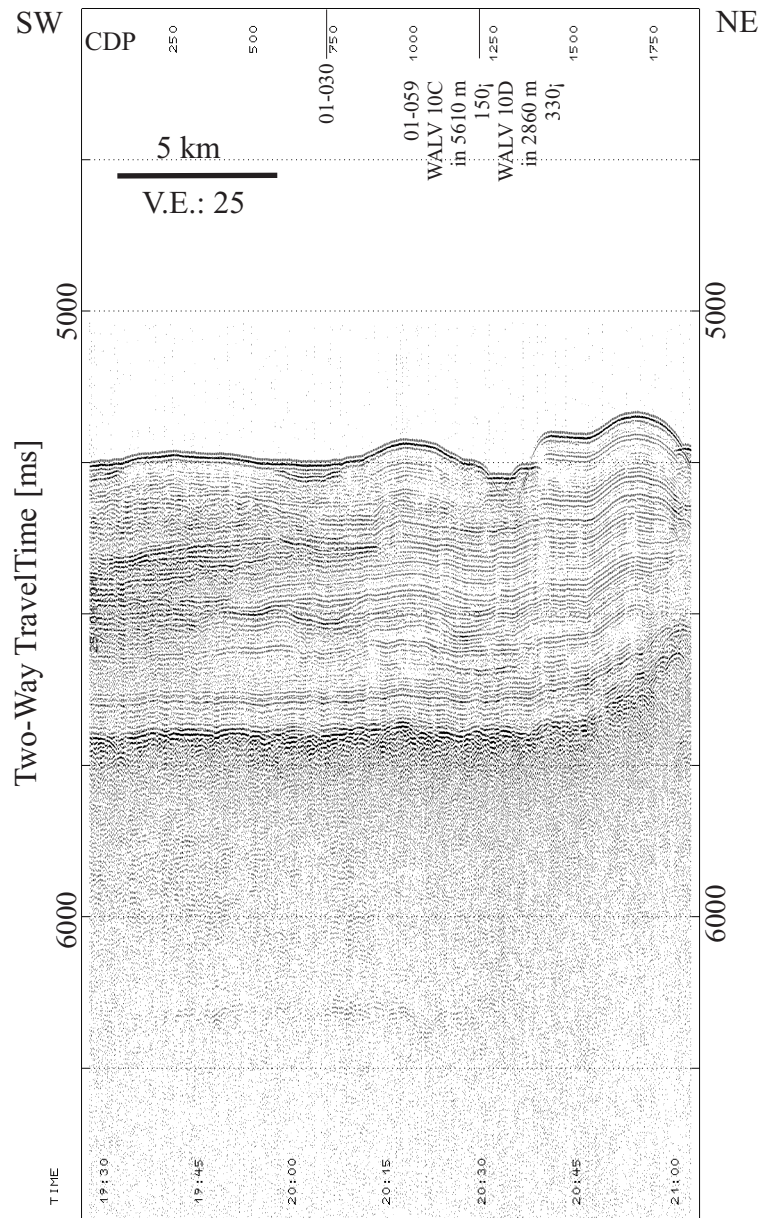
Objectives: See "Scientific Objectives."

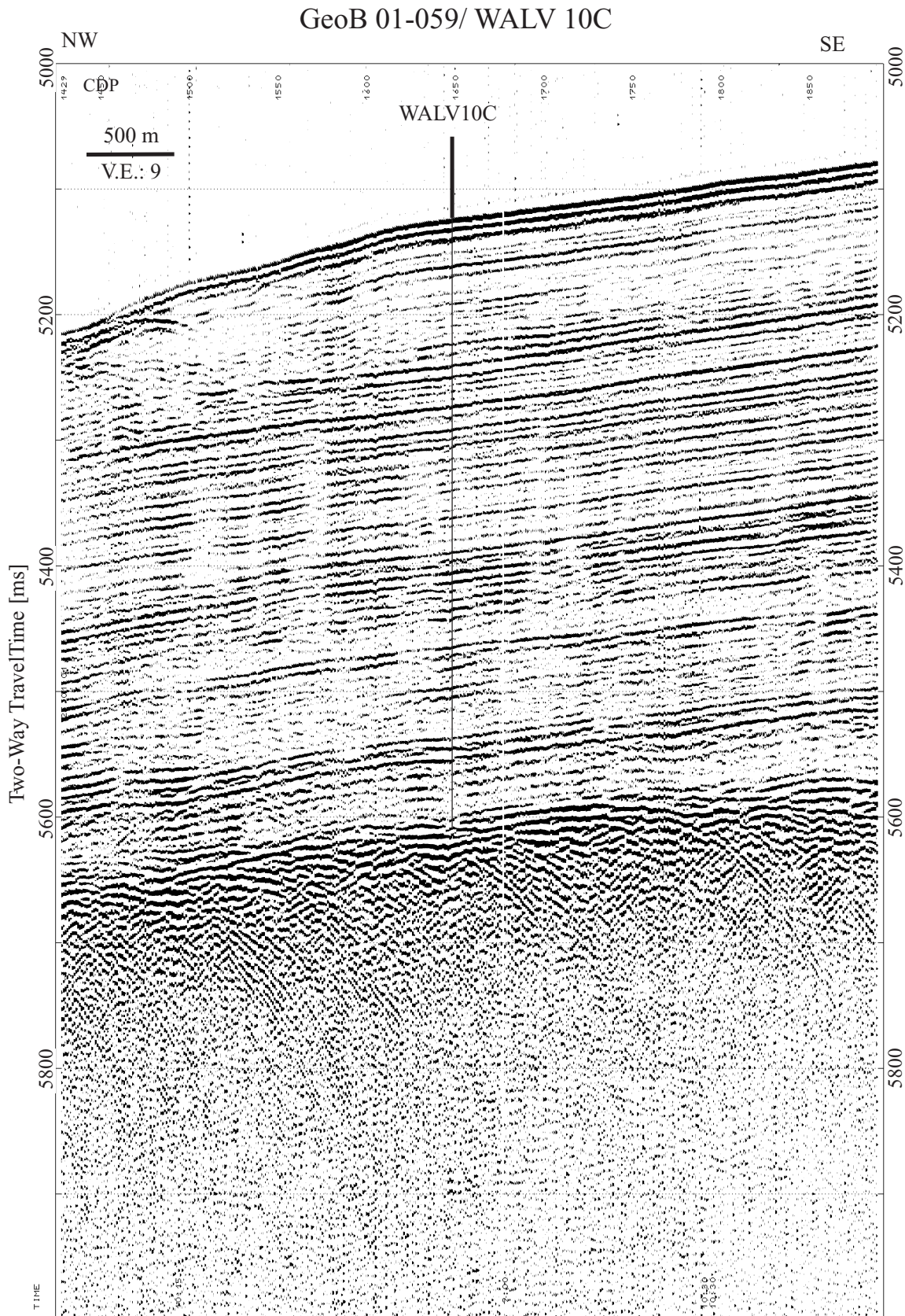
Drilling Program: Double or triple APC to refusal; single or double XCB to target depth.

Downhole Logging Program: Triple-combo, FMS-sonic, WST.

Nature of Rock Anticipated: Calcareous ooze in the upper section, chalk in the lower section.

GeoB 01-064 GI-Gun (1.7 l)





Proposed Site: WALV-10D

Priority: 2

Position: 28°24.55'S, 2°16.79'E

Water Depth: 3961 m

Sediment Thickness: 441 m

Target Depth: 440 mbsf

Approved Maximum Penetration: 450 mbsf

Seismic Coverage: MCS line GeoB01-059, CDP 800; line GeoB01-064, CDP 1215, distance to site = 2860 m, azimuth to site = 330°; line GeoB01-062, CDP 1405, distance to site = 3160 m, azimuth to site = 151°.

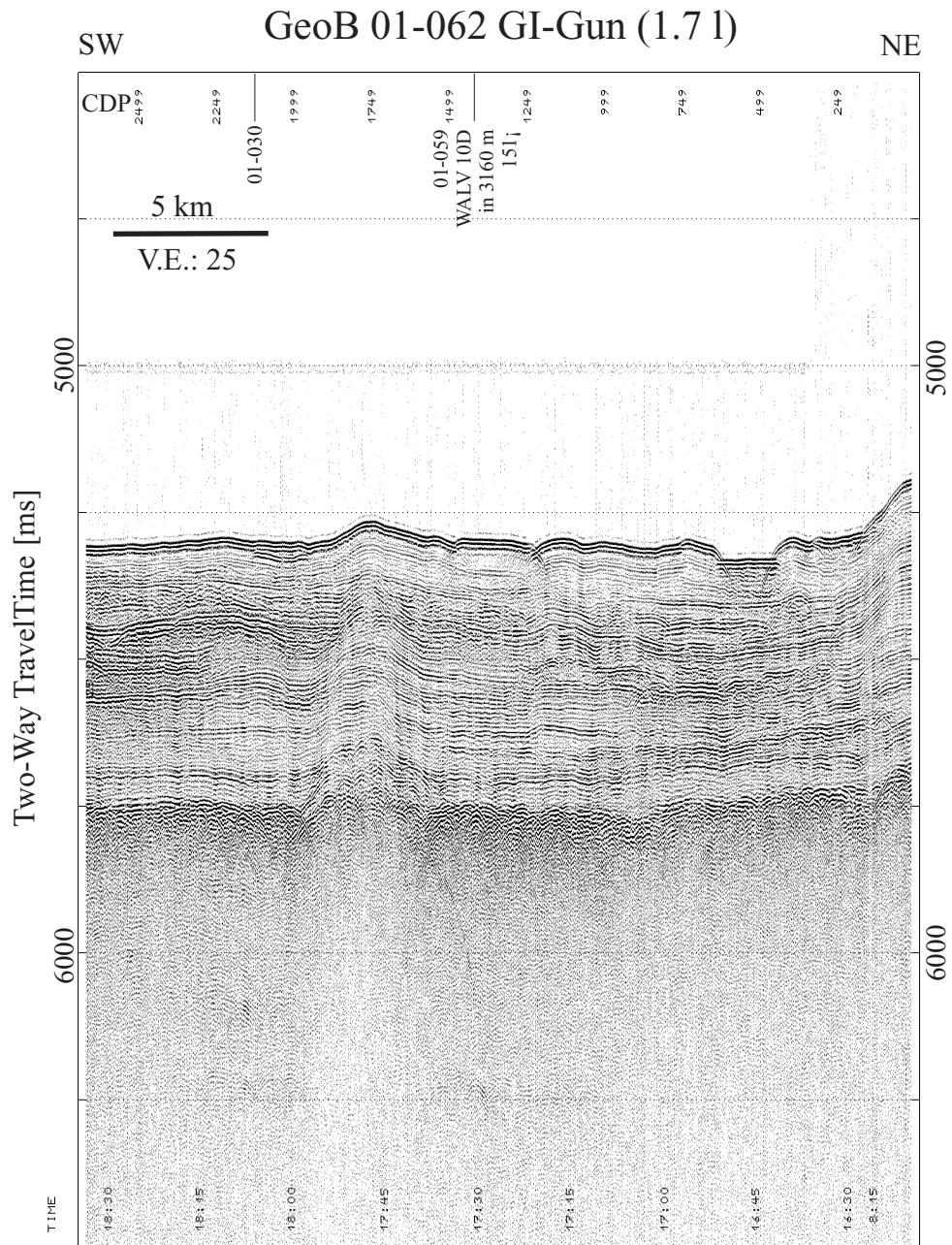
Parasound Coverage: Geob01-059, 25.01.01, 10:22h.

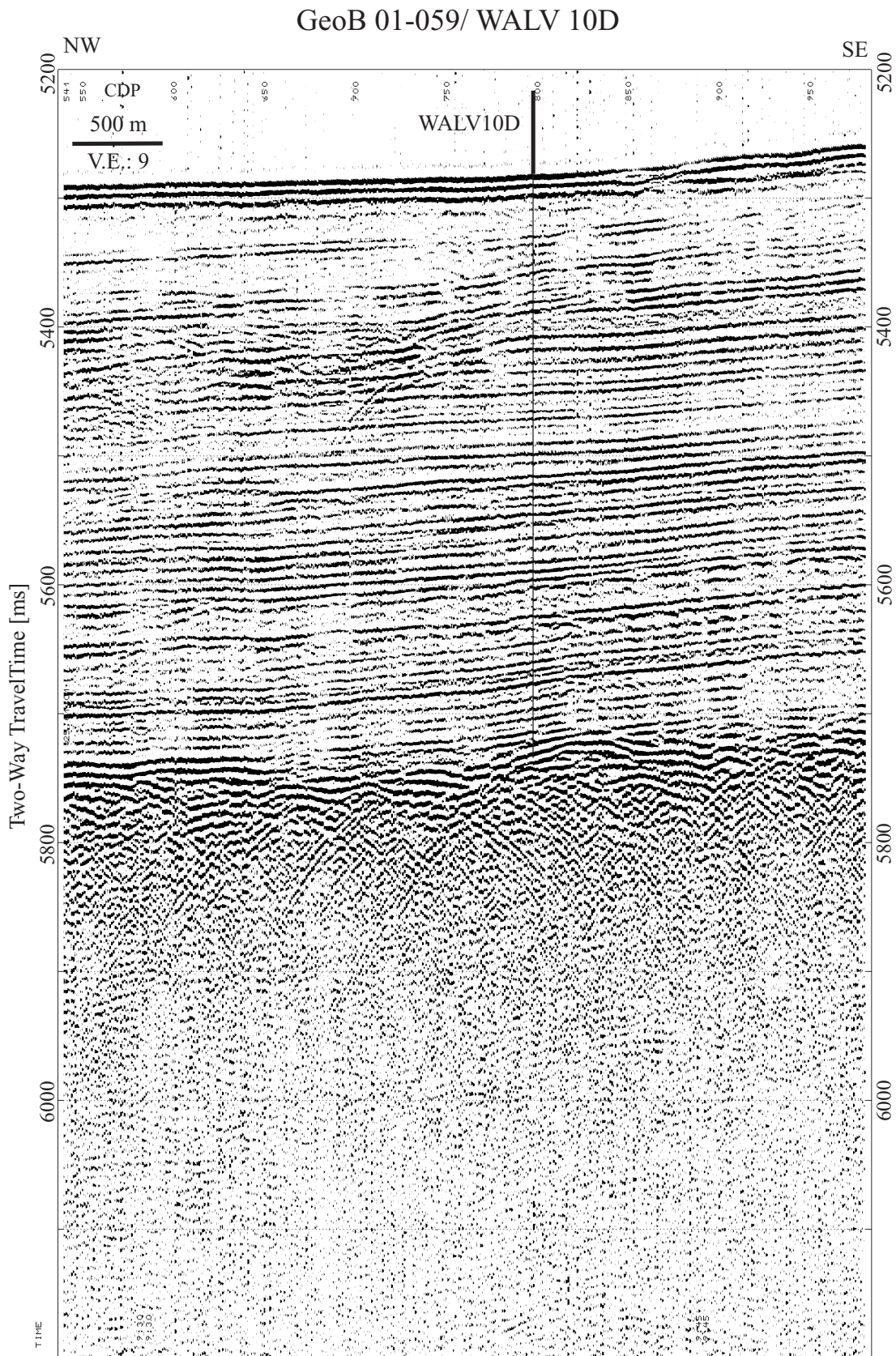
Objectives: See "Scientific Objectives."

Drilling Program: Double or triple APC to refusal; single or double XCB to target depth.

Downhole Logging Program: Triple-combo, FMS-sonic, WST.

Nature of Rock Anticipated: Calcareous ooze in the upper section, chalk in the lower section.





Proposed Site: WALV-11A

Priority: 2

Position: 28°2.49'S, 1°45.80'E

Water Depth: 4434 m

Sediment Thickness: 324 m

Target Depth: 300 mbsf

Approved Maximum Penetration: 350 mbsf

Seismic Coverage: MCS line GeoB01-030, CDP 4932; line GeoB01-039, CDP 4377.

Parasound Coverage: Geob01-030, 19.01.01, 16:24h; GeoB01-039, 22.01.01, 22:23h.

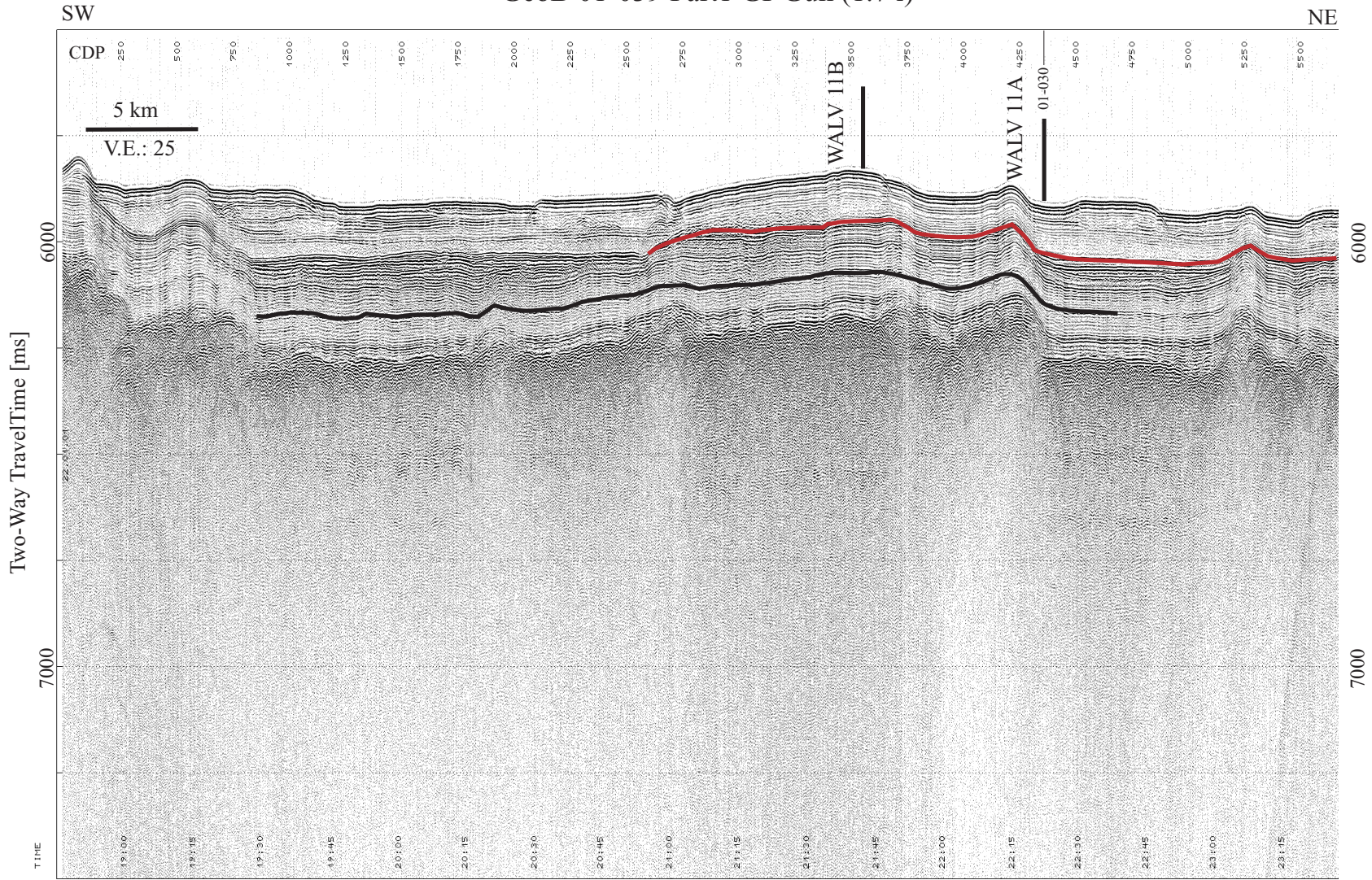
Objectives: See "Scientific Objectives."

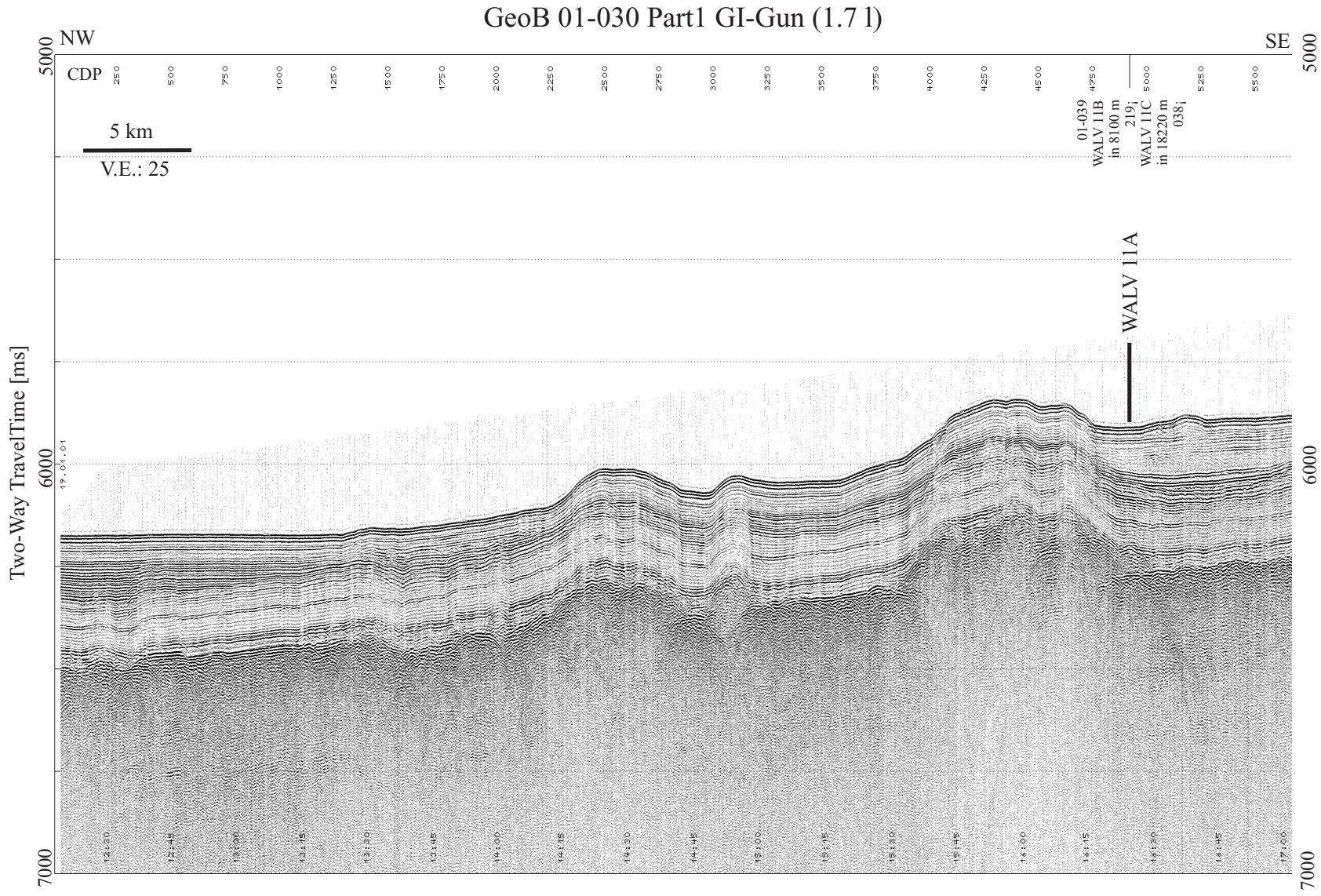
Drilling Program: Double or triple APC to refusal; single or double XCB to target depth.

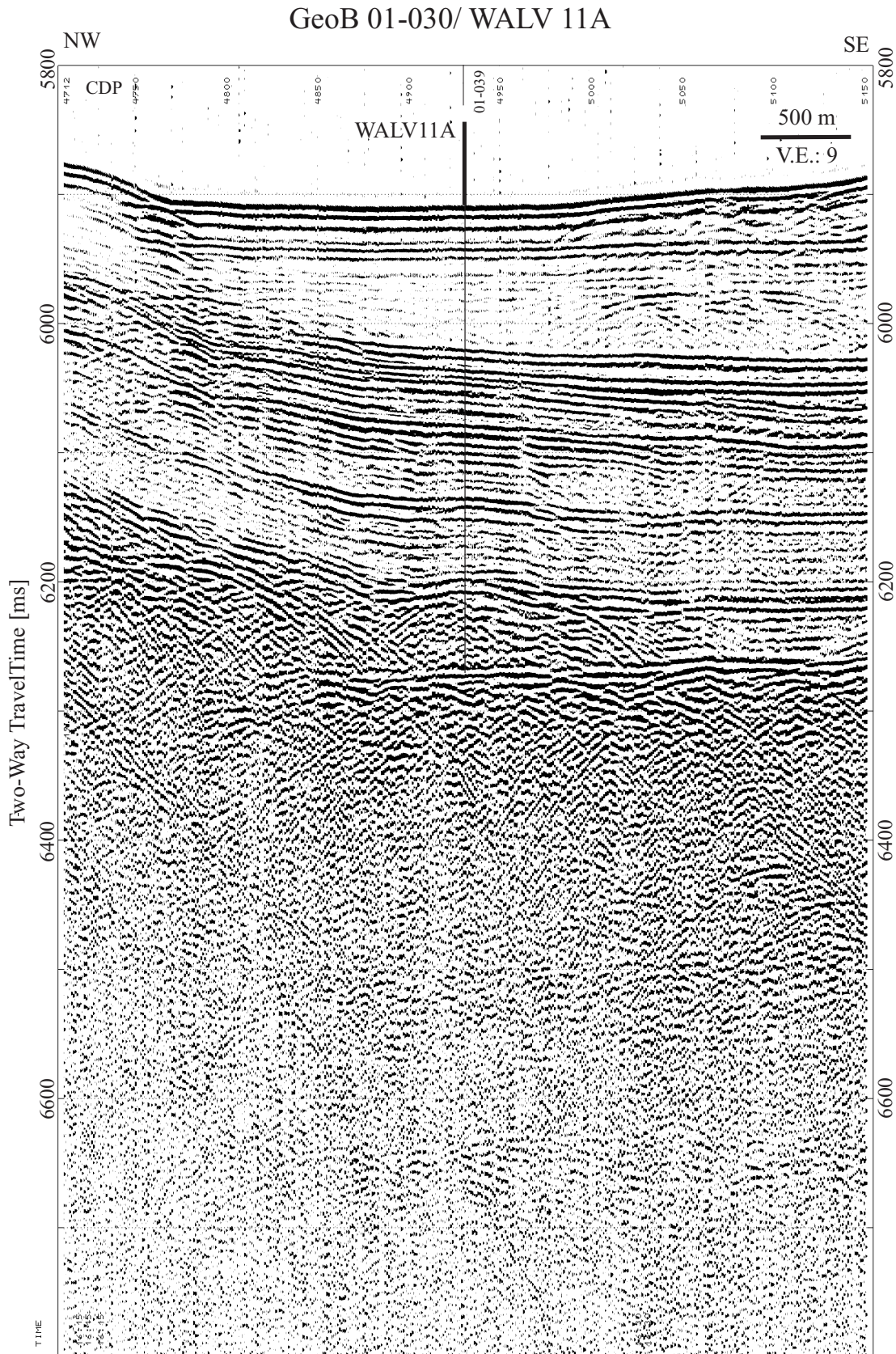
Downhole Logging Program: Triple-combo, FMS-sonic, WST.

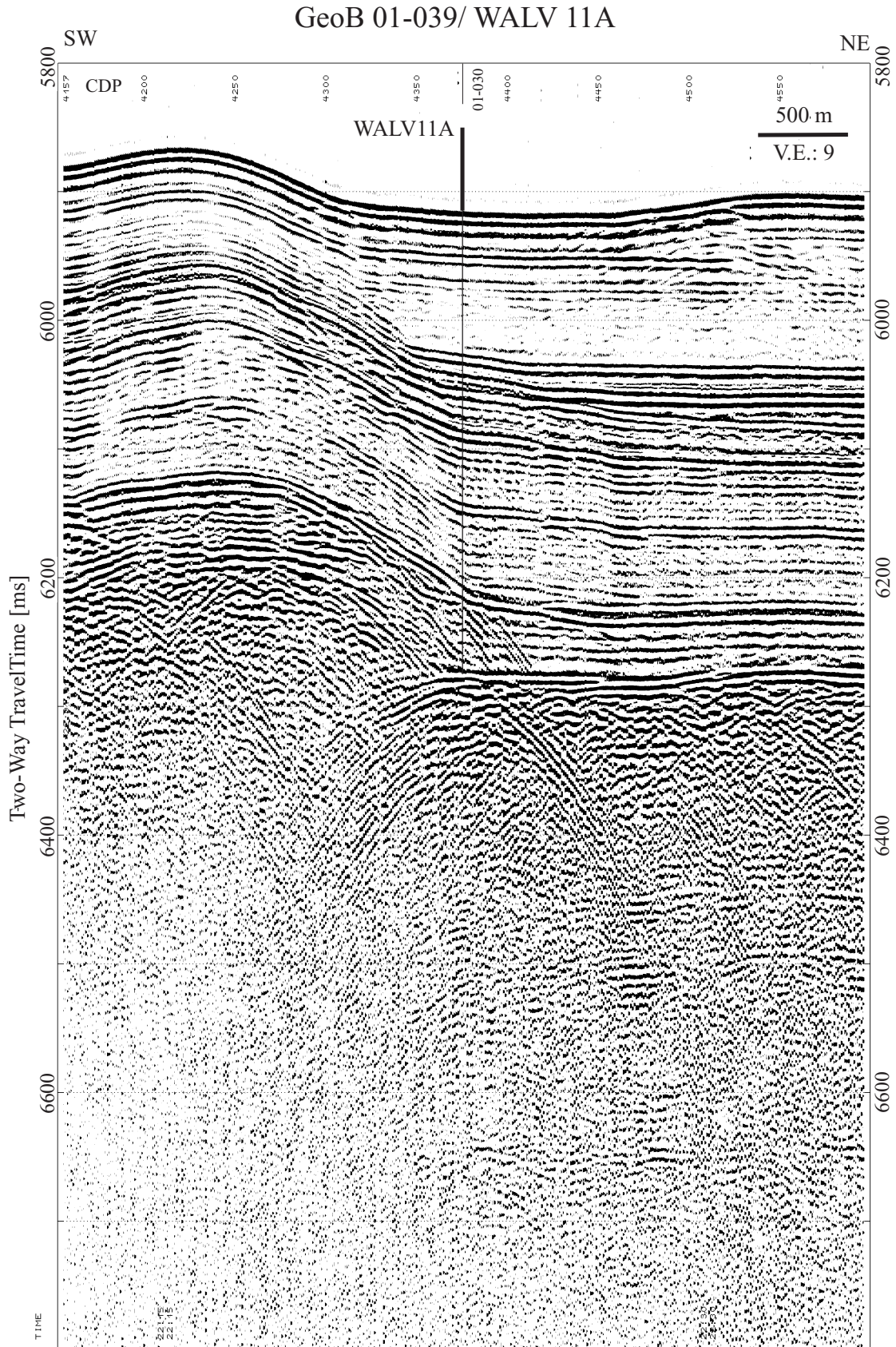
Nature of Rock Anticipated: Calcareous ooze in the upper section, chalk in the lower section.

GeoB 01-039 Part1 GI-Gun (1.71)









Proposed Site: WALV-11B

Priority: 1

Position: 28°5.88'S, 1°42.66'E

Water Depth: 4375 m

Sediment Thickness: 324 m

Target Depth: 300 mbsf

Approved Maximum Penetration: 330 mbsf

Seismic Coverage: MCS line Geob01-039, CDP 3566; line Geob01-030, CDP 4932, distance to site = 8100 m, azimuth to site = 219°.

Parasound Coverage: Geob01-039, 22.01.01, 21:42h.

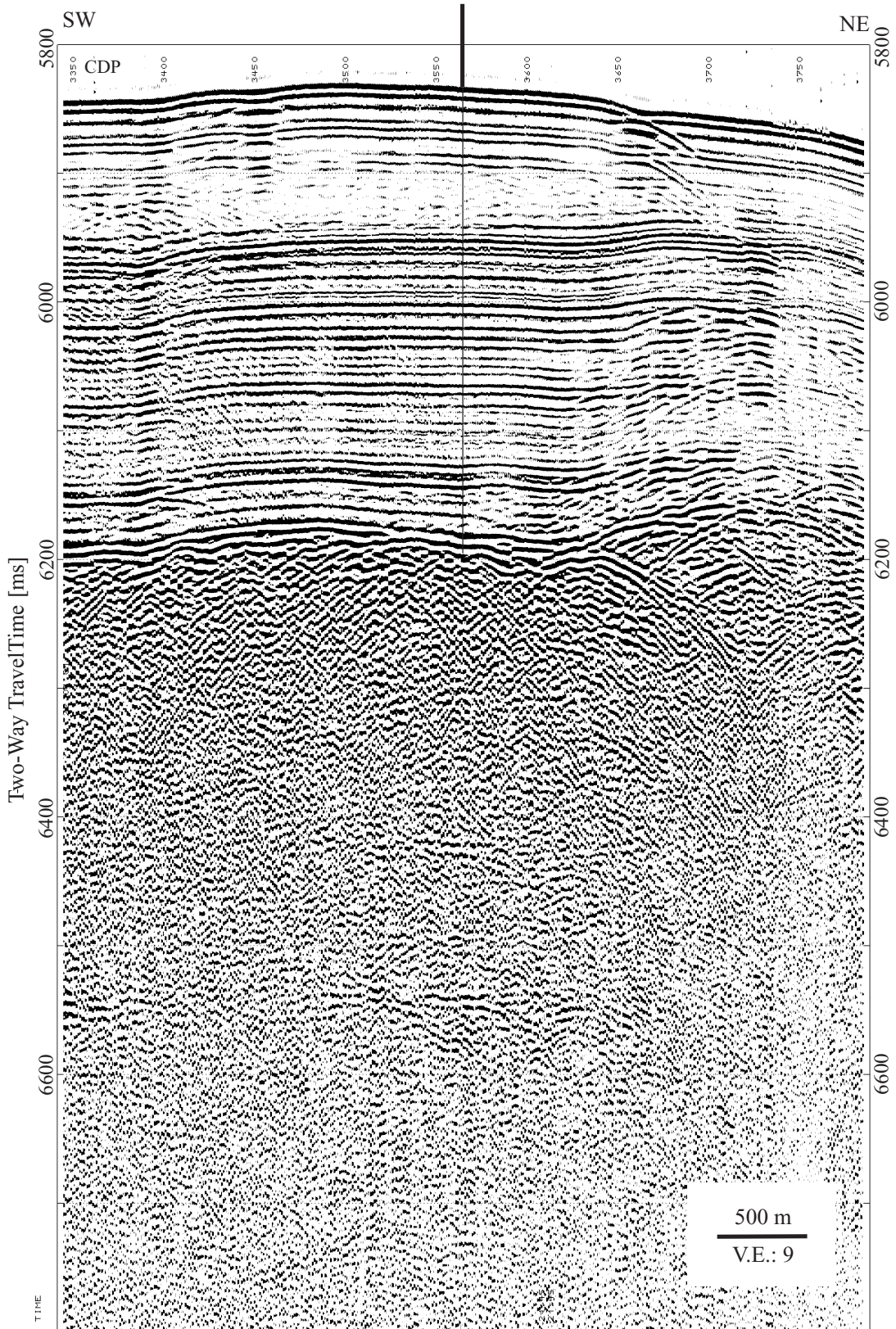
Objectives: See "Scientific Objectives."

Drilling Program: Double or triple APC to refusal; single or double XCB to target depth.

Downhole Logging Program: Triple-combo, FMS-sonic, WST.

Nature of Rock Anticipated: Calcareous ooze in the upper section, chalk in the lower section.

GeoB 01-039/ WALV 11B



Proposed Site: WALV-11C

Priority: 2

Position: 27°54.72'S, 1°52.66'E

Water Depth: 4313 m

Sediment Thickness: 306 m

Target Depth: 280 mbsf

Approved Maximum Penetration: 350 mbsf

Seismic Coverage: MCS line Geob01-039, CDP 6200; line Geob01-030, CDP 4932, distance to site = 18,220 m, azimuth to site = 038°.

Parasound Coverage: Geob01-039, 22.01.01, 23:54h.

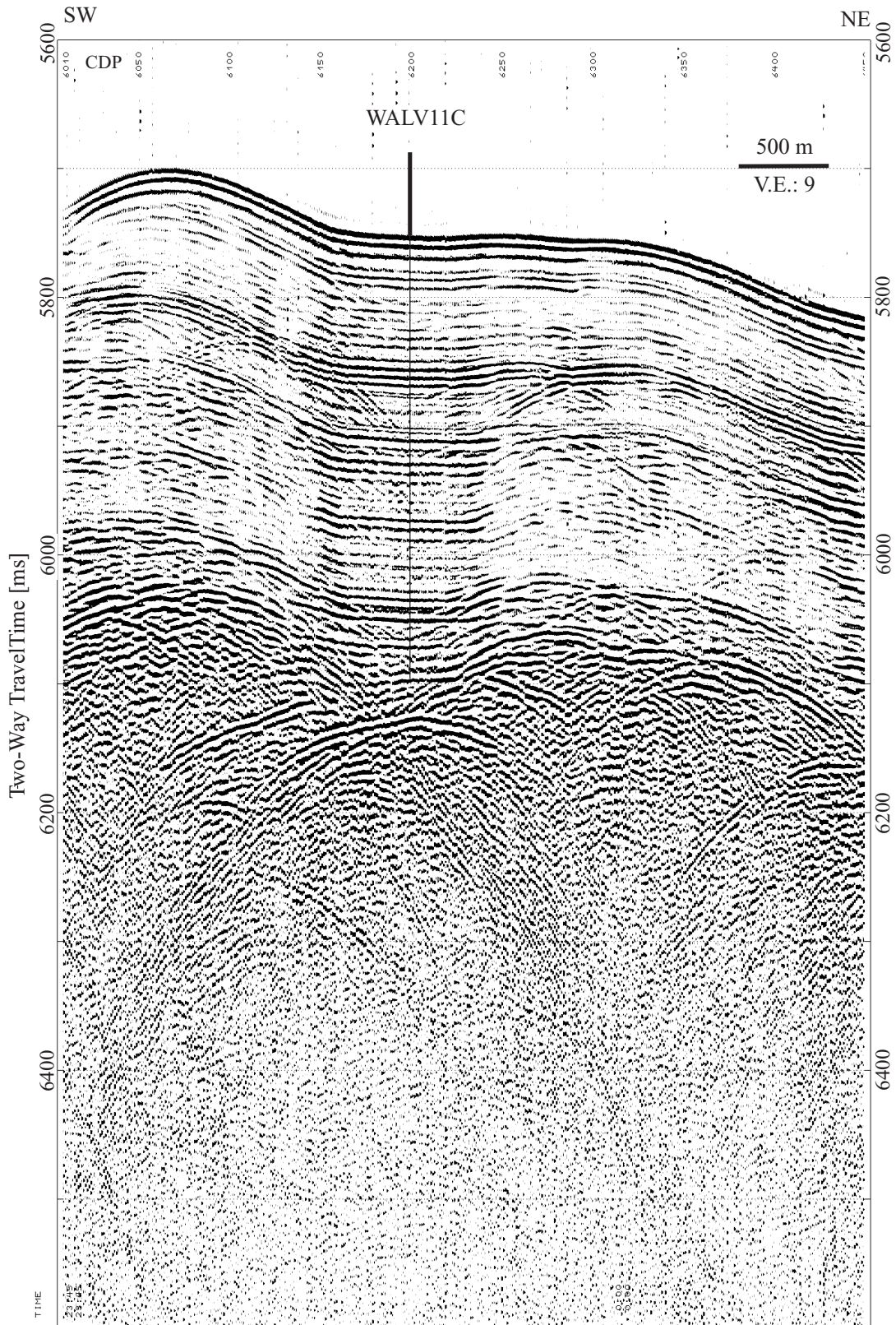
Objectives: See "Scientific Objectives."

Drilling Program: Double or triple APC to refusal; single or double XCB to target depth.

Downhole Logging Program: Triple-combo, FMS-sonic, WST.

Nature of Rock Anticipated: Calcareous ooze in the upper section, chalk in the lower section.

GeoB 01-039/ WALV 11C



Proposed Site: WALV-11D

Priority: 2

Position: 28°5.52'S, 1°10.15'E

Water Depth: 4526 m

Sediment Thickness: 270 m

Target Depth: 270 mbsf

Approved Maximum Penetration: 300 mbsf

Seismic Coverage: MCS line Geob01-038b, CDP 2380.

Parasound Coverage: Geob01-038, 22.01.01, 15:15h.

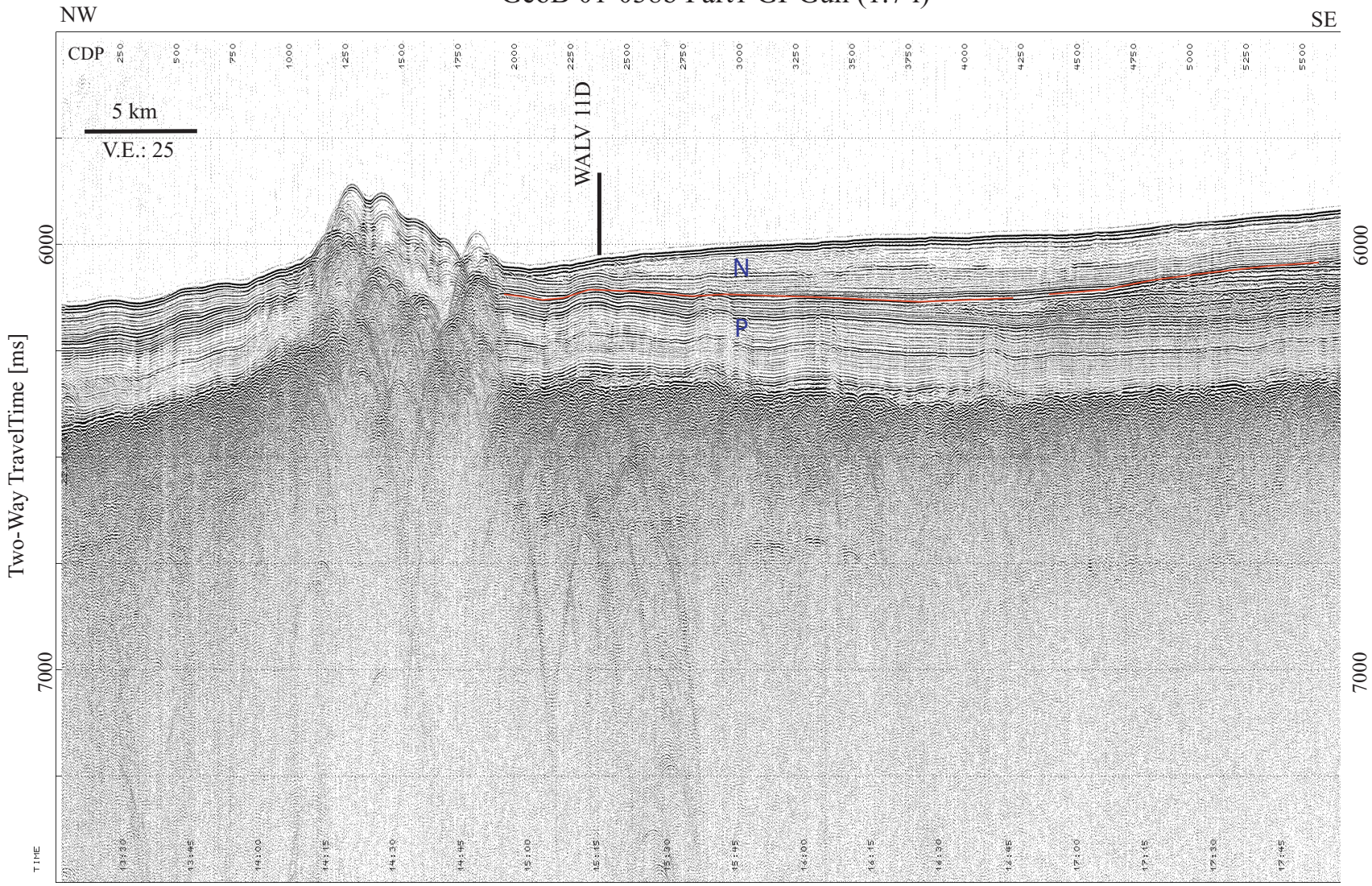
Objectives: See "Scientific Objectives."

Drilling Program: Double or triple APC to refusal; single or double XCB to target depth.

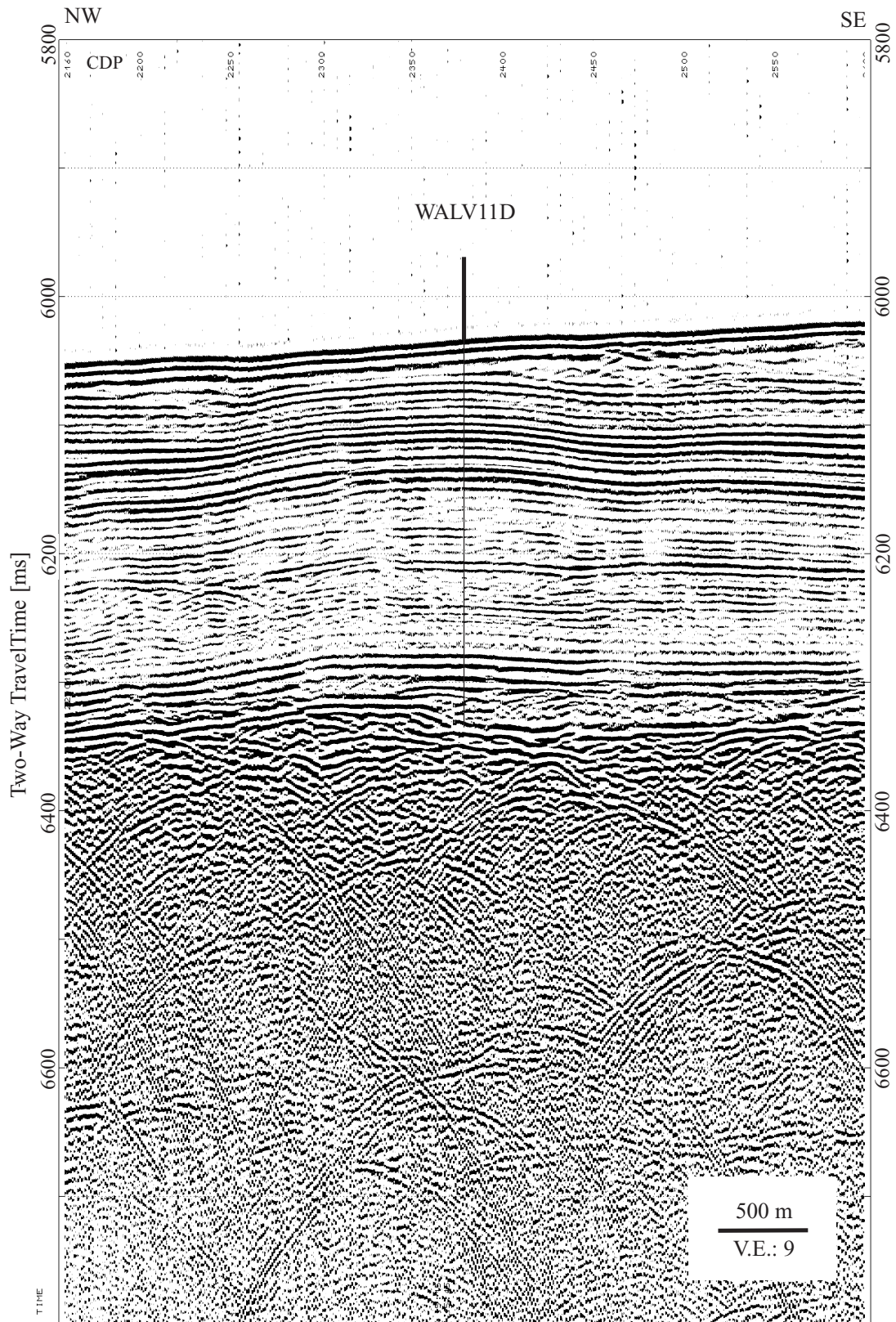
Downhole Logging Program: Triple-combo, FMS-sonic, WST.

Nature of Rock Anticipated: Calcareous ooze in the upper section, chalk in the lower section.

GeoB 01-038b Part1 GI-Gun (1.7 l)



GeoB 01-038/ WALV 11D



Proposed Site: WALV-12A

Priority: 2

Position: 27°11.16'S, 1°34.62'E

Water Depth: 4762 m

Sediment Thickness: 252 m

Target Depth: 230 mbsf

Approved Maximum Penetration: 340 mbsf

Seismic Coverage: MCS line Geob01-035, CDP 2832.

Parasound Coverage: Geob01-035, 21.01.01, 12:26h.

Objectives: See "Scientific Objectives."

Drilling Program: Double or triple APC to refusal; single or double XCB to target depth.

Downhole Logging Program: none.

Nature of Rock Anticipated: Calcareous ooze in the upper section, chalk in the lower section.

Proposed Site: WALV-12B

Priority: 1

Position: 27°4.06'S, 0°58.01'E

Water Depth: 4726 m

Sediment Thickness: 216 m

Target Depth: 200 mbsf

Approved Maximum Penetration: 360 mbsf

Seismic Coverage: MCS line Geob01-036, CDP 3349 (moved per Pollution Prevention and Safety Panel request).

Parasound Coverage: Geob01-036, 21.01.01, 19:18h.

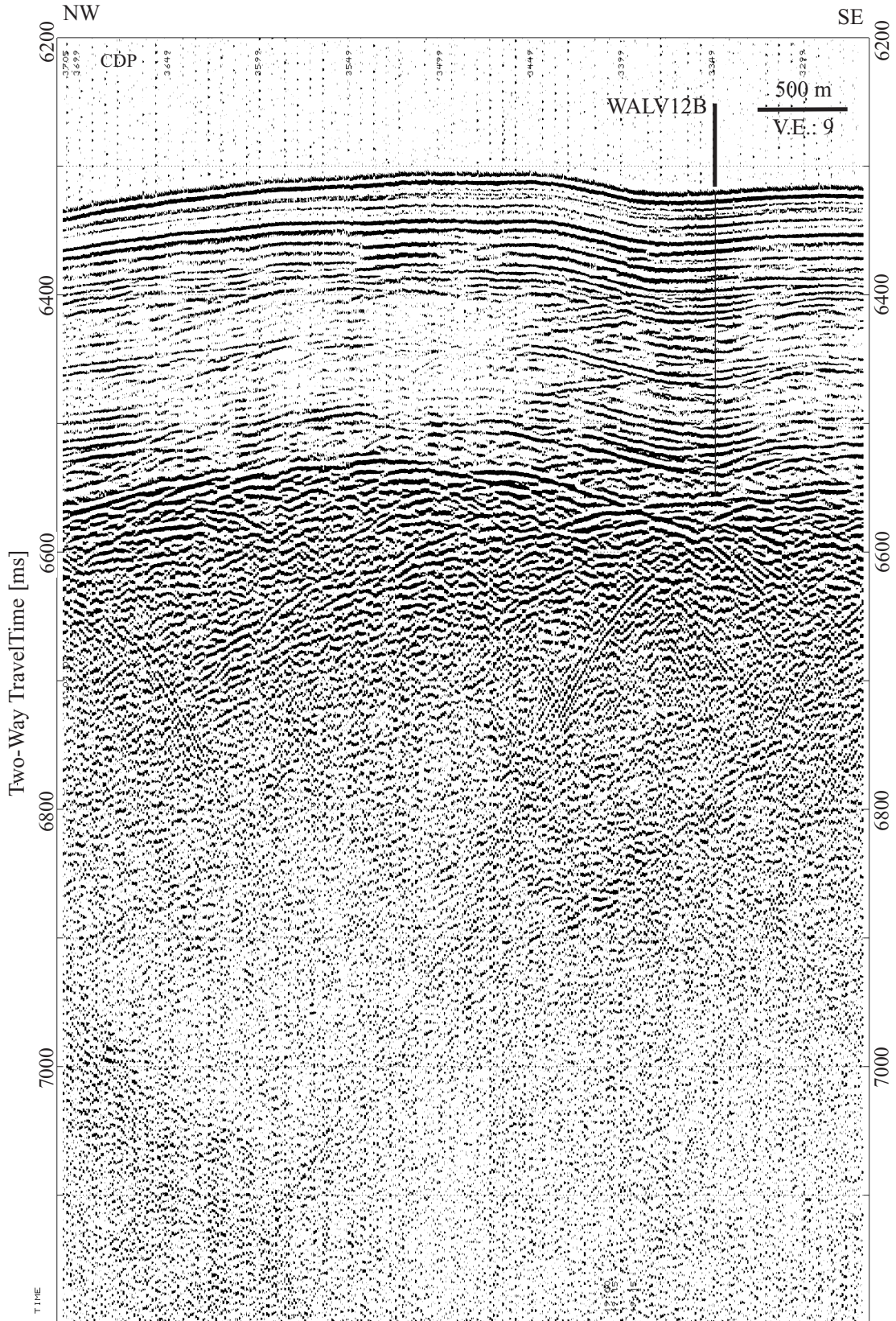
Objectives: See "Scientific Objectives."

Drilling Program: Double or triple APC to refusal; single or double XCB to target depth.

Downhole Logging Program: none.

Nature of Rock Anticipated: Calcareous ooze in the upper section, chalk in the lower section.

GeoB 01-036/ WALV 12B



Proposed Site: WALV-12C

Priority: 2

Position: 26°49.61'S, 0°48.63'E

Water Depth: 4768 m

Sediment Thickness: 270 m

Target Depth: 200 mbsf

Approved Maximum Penetration: 340 mbsf

Seismic Coverage: MCS GeoB01-036, CDP 6438.

Parasound Coverage: Geob01-036, 21.01.01, 21:45h.

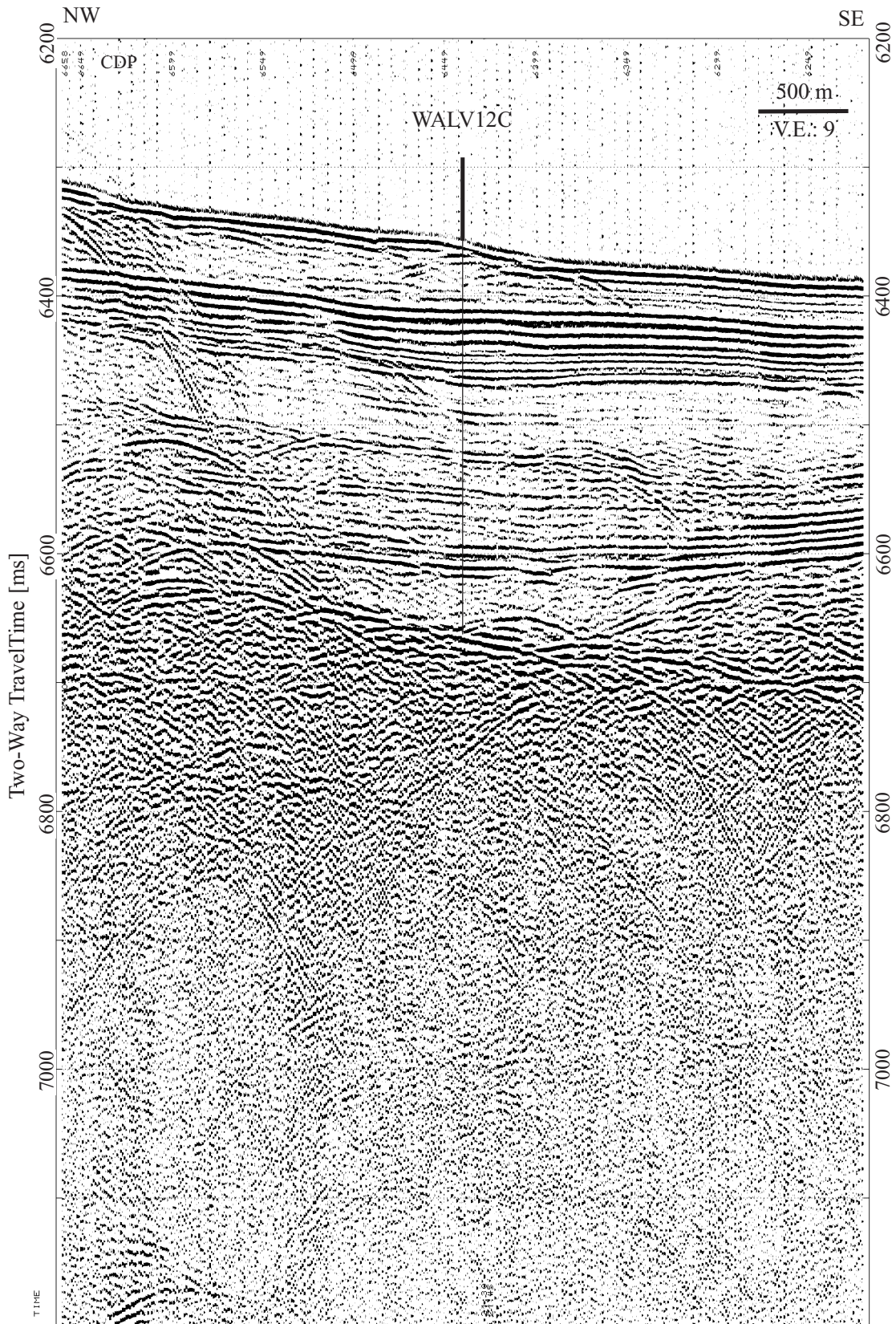
Objectives: See "Scientific Objectives."

Drilling Program: Double or triple APC to refusal; single or double XCB to target depth.

Downhole Logging Program: none.

Nature of Rock Anticipated: Calcareous ooze in the upper section, chalk in the lower section.

GeoB 01-036/ WALV 12C



Proposed Site: WALV-13B

Priority: 2

Position: 24°37.70'S, 4°40.69'E

Water Depth: 3768 m

Sediment Thickness: 432 m

Target Depth: 430 mbsf

Approved Maximum Penetration: 430 mbsf

Seismic Coverage: MCS line Geob01-029b, CDP 2890.

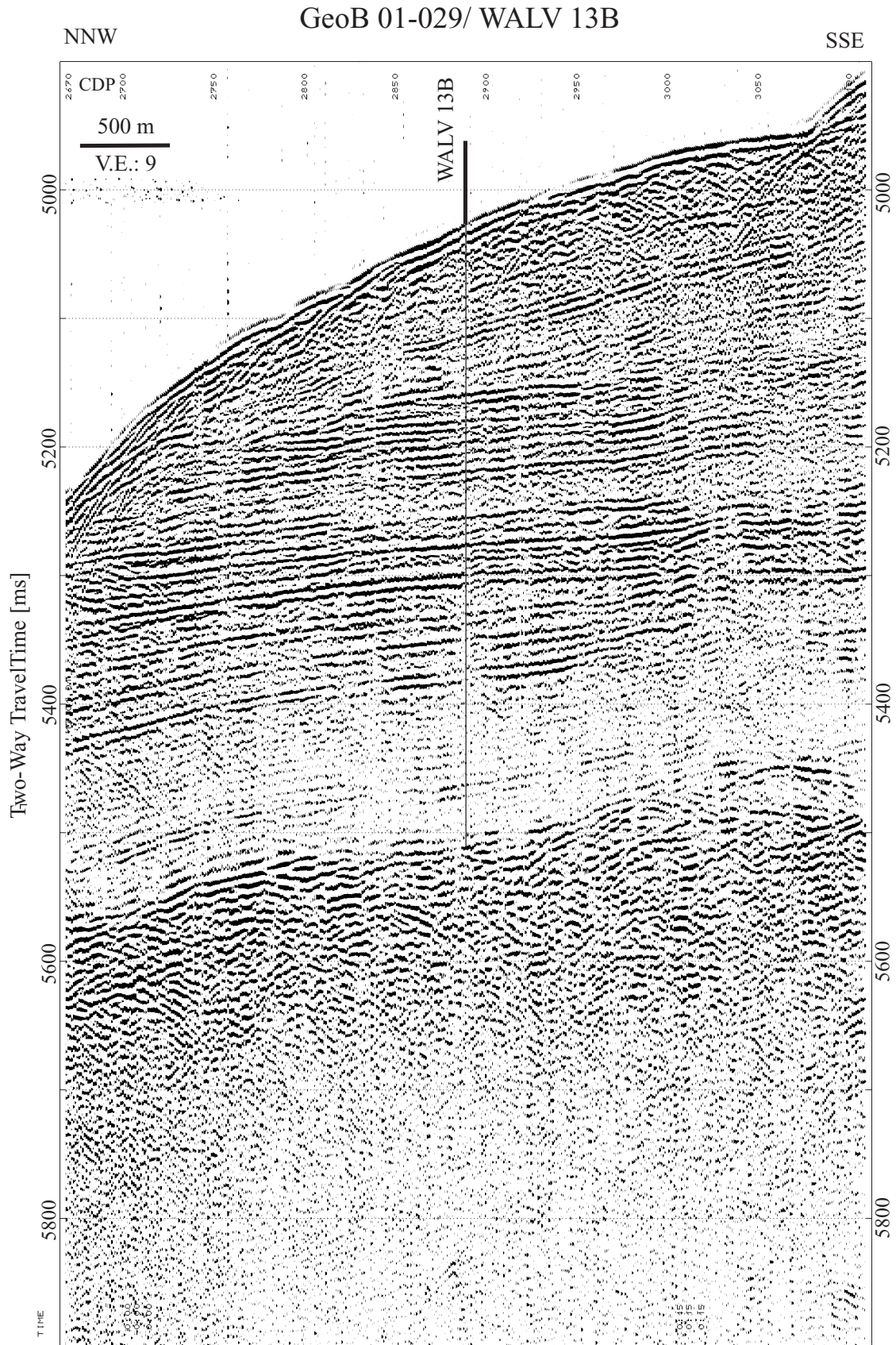
Parasound Coverage: Geob01-029, 18.01.01, 00:08h.

Objectives: See "Scientific Objectives."

Drilling Program: Double or triple APC to refusal; single or double XCB to target depth.

Downhole Logging Program: Triple-combo, FMS-sonic, WST.

Nature of Rock Anticipated: Calcareous ooze in the upper section, chalk in the lower section.



SCIENTIFIC PARTICIPANTS*

Co-Chief Scientist

Dick Kroon

Faculty of Earth Sciences
Vrije Universiteit
De Boelelaan 1085
HV 1081 Amsterdam
The Netherlands
Internet: kroo@geo.vu.nl
Work: (31) 204447261
Fax: (31) 206462457

Co-Chief Scientist

James C. Zachos

Earth Sciences Department
University of California, Santa Cruz
Earth and Marine Sciences Building
Santa Cruz CA 95064
USA
Internet: jzachos@emerald.ucsc.edu
Work: (831) 459-4644
Fax: (831) 459-3074

Staff Scientist

Peter Blum

Ocean Drilling Program
Texas A&M University
1000 Discovery Drive
College Station TX 77845-9547
USA
Internet: blum@odpemail.tamu.edu
Work: (979) 845-9299
Fax: (979) 845-0876

Inorganic Geochemist

Edmund C. Hathorne

Department of Earth Sciences
The Open University
Walton Hall
Milton Keynes MK7 6AA
United Kingdom
Internet: e.c.hathorne@open.ac.uk
Work: (44) 1908 653023
Fax: (44) 1908 655151

Inorganic Geochemist

Deborah Thomas

Geological Sciences
University of North Carolina at Chapel Hill
CB#3315, Mitchell Hall
Chapel Hill NC 27599-3315
USA
Internet: dthomas1@email.unc.edu
Work: (919) 225-7463
Fax: (919) 966-4519

Organic Geochemist

Takashi Hasegawa

Department of Earth Sciences
Kanazawa University
Kakuma-machi
Kanazawa, Ishikawa-Pref. 920-1192
Japan
Internet: jh7ujr@kenroku.kanazawa-u.ac.jp
Work: (81) 76-264-5636
Fax: (81) 76-264-5746

Paleomagnetist

Youn Soo Lee

Department of Geology
Korea Institute of Geoscience & Mineral Resources
(KIGAM)
P.O. Box 111
Yuseong Science Town, Yuseong-gu
Daejeon 305-350
Korea
Internet: lys0222@hotmail.com
Work: (82) 42-868-3036
Fax: (82) 42-861-9714

Paleontologist (foraminifers)

Daniel C. Kelly

Department of Geology and Geophysics
University of Wisconsin-Madison
1215 West Dayton Street
Madison WI 53706
USA
Internet: ckelly@geology.wisc.edu
Work: (608) 262-1698
Fax: (608) 262-0693

Paleontologist (foraminifers)

Ellen Thomas

Department of Earth and Environmental Sciences
Wesleyan University
265 Church Street
Middletown CT 06459-0139
USA
Internet: ethomas@wesleyan.edu
Work: (860) 685-2238
Fax: (860) 685-3651

Physical Properties Specialist

Rhonda Adkins

Department of Earth Sciences
James Cook University of North Queensland
Townsville QLD 4811
Australia
Internet: rhonda.adkins@jcu.edu.au
Work: (61) 7 4781 4557
Fax: (61) 7 4725 1501

*Staffing is incomplete and subject to change.

Physical Properties Specialist

Henry Vallius
Research and Development
Geological Survey of Finland
Betonimiehenkuja 4
PO Box 96
Espoo 02151
Finland
Internet: henry.vallius@gsf.fi
Work: (358) 20 550 2573
Fax: (358) 20 550 12

Sedimentologist

Dirk C. Leuschner
Institute for Geophysics and Geology
Universitaet Leipzig
Talstrasse 35
04103 Leipzig
Germany
Internet: dcleu@rz.uni-leipzig.de
Work: (49) 341-9732-909
Fax: (49) 341-9732-809

Sedimentologist

Zhifei Liu
Department of Marine Geology and Geophysics
Tongji University
1239 Siping Road
Shanghai 200092
China
Internet: lzhifei@online.sh.cn
Work: (86) 21 6598 4877
Fax: (86) 21 6598 8808

Sedimentologist

Kyger C. Lohmann
Department of Geological Sciences
University of Michigan
425 East University
Ann Arbor MI 48109-1063
USA
Internet: kacey@umich.edu
Work: (734) 763-2298
Fax: (734) 763-4690

Sedimentologist

Micah Nicolo
Department of Earth Science
Rice University
6100 Main Street
MS-126
Houston TX 77005-1892
USA
Internet: mnicolo@joiscience.org
Work: (713) 348-4880
Fax: (713) 348-5214

Sedimentologist

Christina Riesselman
Department of Geological and Environmental Sciences
Stanford University
Braun Hall, Bldg. 320
Sanford, CA 94305-2115
USA
Internet: criesselman@joiscience.org
Work: (650) 725-6830
Fax: (650) 725-0979

Sedimentologist

Stephen A. Schellenberg
Department of Geological Sciences
San Diego State University
5500 Campanile Drive
San Diego CA 92182-1020
USA
Internet: schellenberg@geology.sdsu.edu
Work: (619) 594-1039
Fax: (619) 594-4372

Stratigraphic Correlator

Ursula Röhl
Department of Geosciences
Universität Bremen
Postfach 33 04 40
Klagenfurter Strasse
28334 Bremen
Germany
Internet: uroehl@allgeo.uni-bremen.de
Work: (49) 421-2182482
Fax: (49) 421-2183116

Logging Staff Scientist

Philippe Gaillot
Laboratoire de Mesures en Forages, ISTEEM
Universite Montpellier II
Laboratoire de Tectonophysique
Place Eugene Bataillon
34095 Montpellier Cedex 5
France
Internet: gaillot@dstu.univ-montp2.fr
Work: (33) 467 149 310
Fax: (33) 467 149 308

Schlumberger Engineer

Steven Kittredge
911 Center Point Road
Carrollton GA 30117
USA
Internet: kittredge1@webster.oilfield.slb.com
Work: (281) 480-2000
Fax: (281) 480-9550

Operations Manager

Ronald M. Grout

Ocean Drilling Program
Texas A&M University
1000 Discovery Drive
College Station TX 77845-9547
USA

Internet: grout@odpemail.tamu.edu
Work: (979) 845-2144
Fax: (979) 845-2308

Laboratory Officer

Burnette W. Hamlin

Ocean Drilling Program
Texas A&M University
1000 Discovery Drive
College Station TX 77845-9547
USA

Internet: hamlin@odpemail.tamu.edu
Work: (979) 845-2496
Fax: (979) 845-0876

Assistant Laboratory Officer

Timothy Bronk

Ocean Drilling Program
Texas A&M University
1000 Discovery Drive
College Station TX 77845-9547
USA

Internet: bronk@odpemail.tamu.edu
Work: (979) 845-0879
Fax: (979) 845-0876

Marine Laboratory Specialist: Yeoperson
TBD

Ocean Drilling Program
Texas A&M University
1000 Discovery Drive
College Station TX 77845
USA

Internet:
Work:
Fax:

Marine Laboratory Specialist: Chemistry

Christopher Bennight

Ocean Drilling Program
Texas A&M University
1000 Discovery Drive
College Station TX 77845
USA

Internet: chris@slowcar.net
Work: (979) 458-1874
Fax: (979) 845-0876

Marine Laboratory Specialist: Chemistry

Walter Jones

Ocean Drilling Program
Texas A&M University
1000 Discovery Drive
College Station TX 77845
USA

Internet: jones_w@odpemail.tamu.edu
Work: (979) 845-9186
Fax: (979) 845-0876

Marine Laboratory Specialist: Core

Jason Deardorff

Ocean Drilling Program
Texas A&M University
1000 Discovery Drive
College Station TX 77845
USA

Internet: jwdeardorff@hotmail.com
Work: (979) 845-3602
Fax: (979) 845-0876

Marine Laboratory Specialist: Curator

Mads Radsted

Ocean Drilling Program
Texas A&M University
1000 Discovery Drive
College Station TX 77840
USA

Internet: radsted@odpemail.tamu.edu
Work: (979) 845-4822
Fax: (979) 845-0876

**Marine Lab Specialist: Downhole Tools/
Marine Lab Specialist: Thin Sections**

Jessica Huckemeyer

Ocean Drilling Program
Texas A&M University
1000 Discovery Drive
College Station, TX 77845
USA

Internet: huckemeyer@odpemail.tamu.edu
Work: (979) 845-4822
Fax: (979) 845-1303

Marine Lab Specialist: Paleomagnetism

Paul Teniere

Ocean Drilling Program
Texas A&M University
1000 Discovery Drive
College Station, TX 77845
USA

Internet: teniere@hotmail.com
Work: (979) 845-3602
Fax: (979) 845-0876

Marine Lab Specialist: Photographer
Leah Shannon Center

Ocean Drilling Program
Texas A&M University
1000 Discovery Drive
College Station, TX 77845
USA
Internet: housley@odpemail.tamu.edu
Work: (979) 845-2480
Fax: (979) 845-0876

Marine Laboratory Specialist: Physical
Properties

John W.P. Riley
Ocean Drilling Program
Texas A&M University
1000 Discovery Drive
College Station TX 77845
USA
Internet: riley@odpemail.tamu.edu
Work: (979) 845-3602
Fax: (979) 845-0876

Marine Laboratory Specialist: Underway
Geophysics

Johanna M. Suhonen
Ocean Drilling Program
Texas A&M University
1000 Discovery Drive
College Station TX 77845-9547
USA
Internet: suhonen@odpemail.tamu.edu
Work: (979) 845-9186
Fax: (979) 845-0876

Marine Laboratory Specialist: X-Ray
Robert M. Wheatley

Ocean Drilling Program
Texas A&M University
1000 Discovery Drive
College Station TX 77845
USA
Internet: wheatley@odpemail.tamu.edu
Work: (979)
Fax: (979) 845-0876

Marine Electronics Specialist
Jan Jurie Kotze

Ocean Drilling Program
Texas A&M University
1000 Discovery Drive
College Station TX 77845
USA
Internet: kotzej@megaweb.co.za
Work: (979) 845-3602
Fax: (979) 845-0876

Marine Electronics Specialist
Pieter Pretorius

Ocean Drilling Program
Texas A&M University
1000 Discovery Drive
College Station TX 77845-9547
USA
Internet: pretorius@odpemail.tamu.edu
Work: (979) 845-3602
Fax: (979) 845-0876

Marine Computer Specialist
John Davis

Ocean Drilling Program
Texas A&M University
1000 Discovery Drive
College Station TX 77845
USA
Internet: jdavis@odpemail.tamu.edu
Work: (979) 862-4849
Fax: (979) 458-1617

Marine Computer Specialist
Michael J. Hodge

Ocean Drilling Program
Texas A&M University
1000 Discovery Drive
College Station TX 77845-9547
USA
Internet: hodge@odpemail.tamu.edu
Work: (979) 862-4845
Fax: (979) 458-1617

ODP/TAMU Programmer
Yunyou Yao

Ocean Drilling Program
Texas A&M University
1000 Discovery Drive
College Station TX 77840
USA
Internet: yao@odpemail.tamu.edu
Work: (979) 845-3036
Fax: (979) 458-1617